Monte Carlo Methods in CT Imaging

Marc Kachelrieß

German Cancer Research Center (DKFZ)
Heidelberg, Germany
www.dkfz.de/ct

DEUTSCHES KREBSFORSCHUNGSZENTRUM
IN DER HELMHOLTZ-GEMEINSCHAFT

Clinical CT

e.g. Definition Flash dual source spiral cone-beam CT scanner, Siemens Healthcare, Forchheim, Germany.

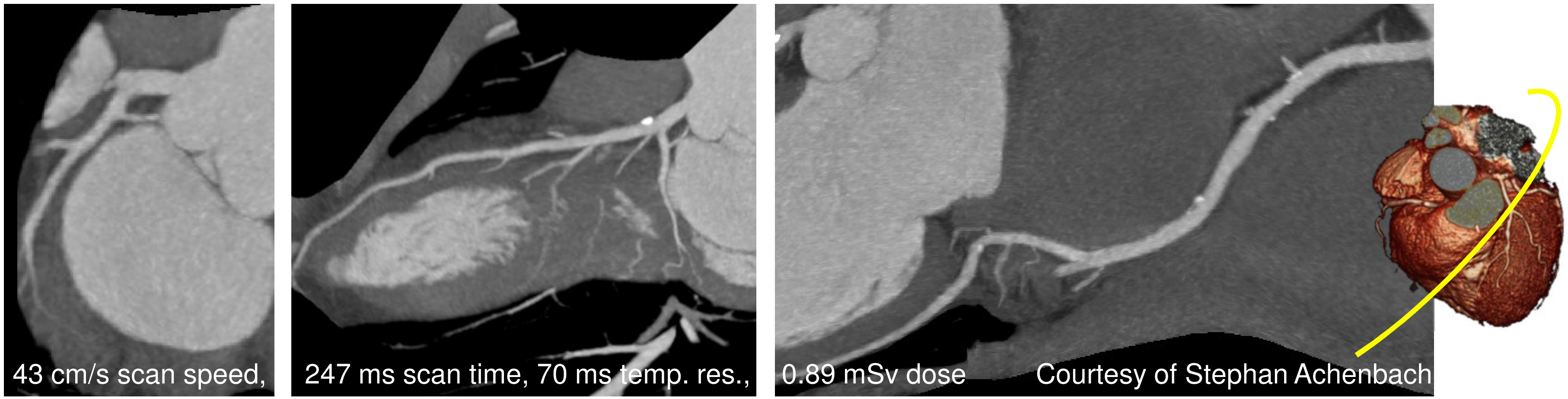

Image courtesy by Siemens Healthcare

Fixed C-Arm CT

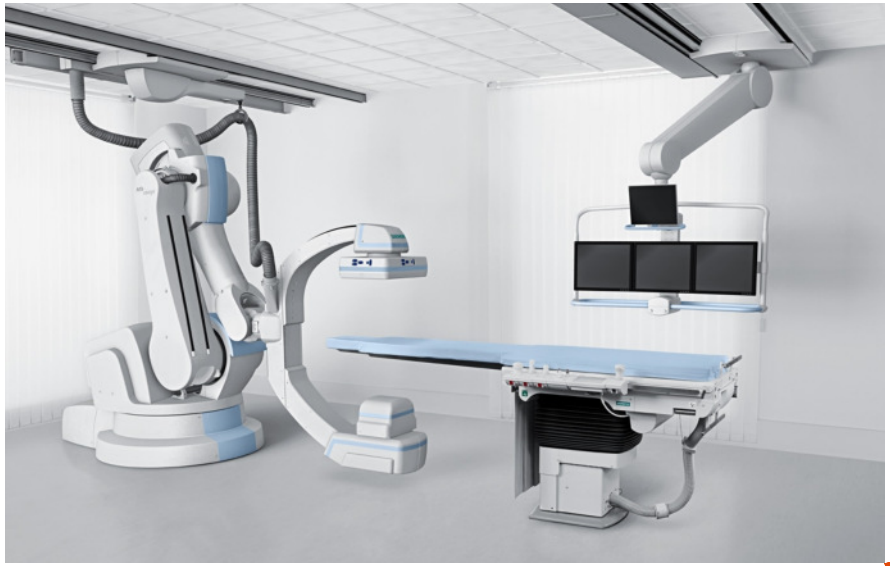

Flat detector inside

e.g. floor-mounted Artis Zeego or ceiling-mounted Artis Zee, Siemens Healthcare, Forchheim, Germany

Mobile C-Arm CT

e.g. Vision RFD 3D, Ziehm Imaging GmbH, Nürnberg, Germany

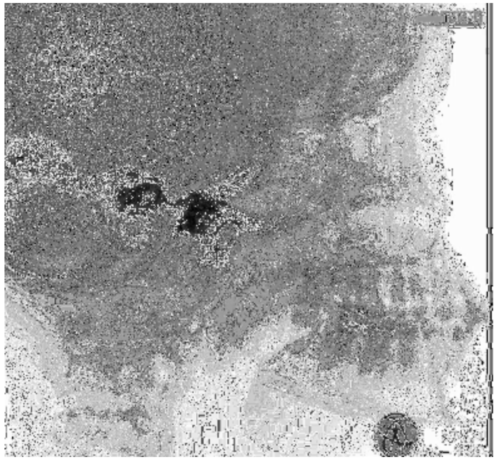

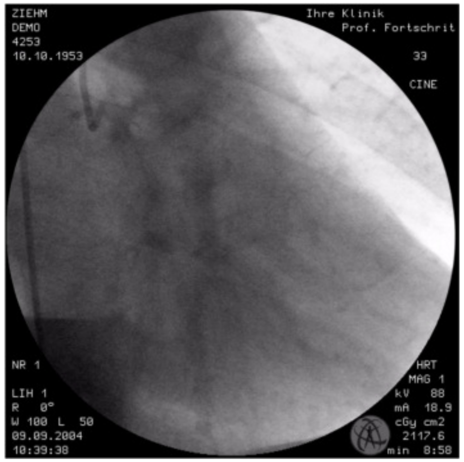

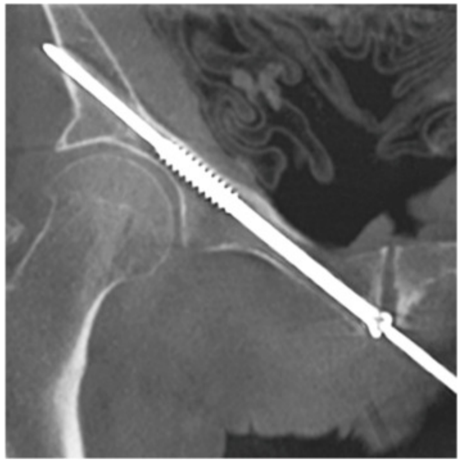

Dental Volume Tomography (DVT)

e.g. Orthophos XG 3D, Sirona Dental Systems GmbH, Bensheim, Germany

CBCT Guidance for Radiation Therapy

Flat detector inside

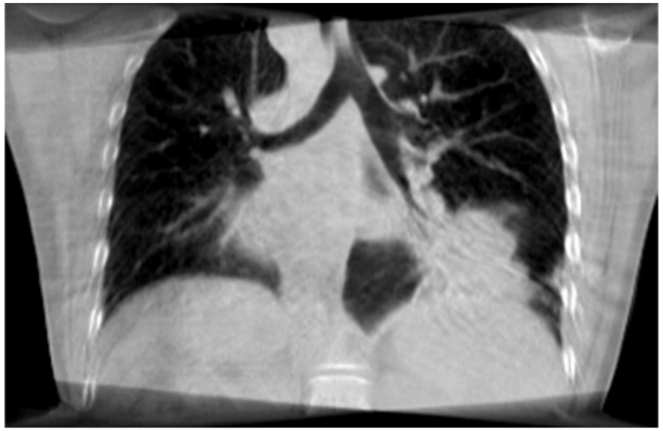

e.g. TrueBeam, Varian Medical Systems, Palo Alto, CA, USA

Image courtesy by Varian Medical Systems

Micro CT for Preclinical Research

e.g. TomoScope, CT Imaging, Erlangen, Germany

Industrial CT

Flat detector inside

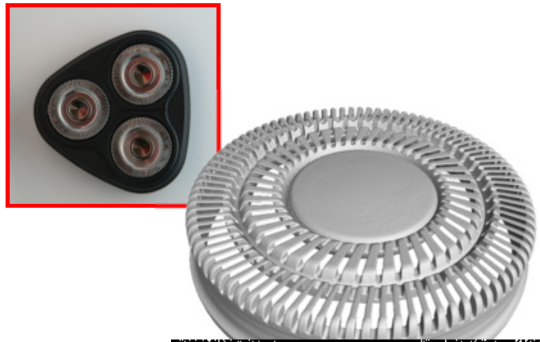

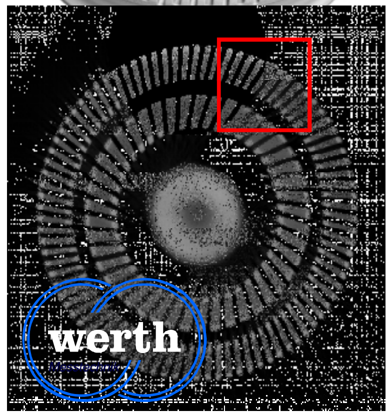

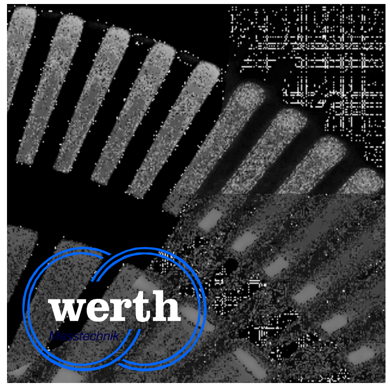

e.g. TomoScope HV 500, Werth Messtechnik, Gießen, Germany

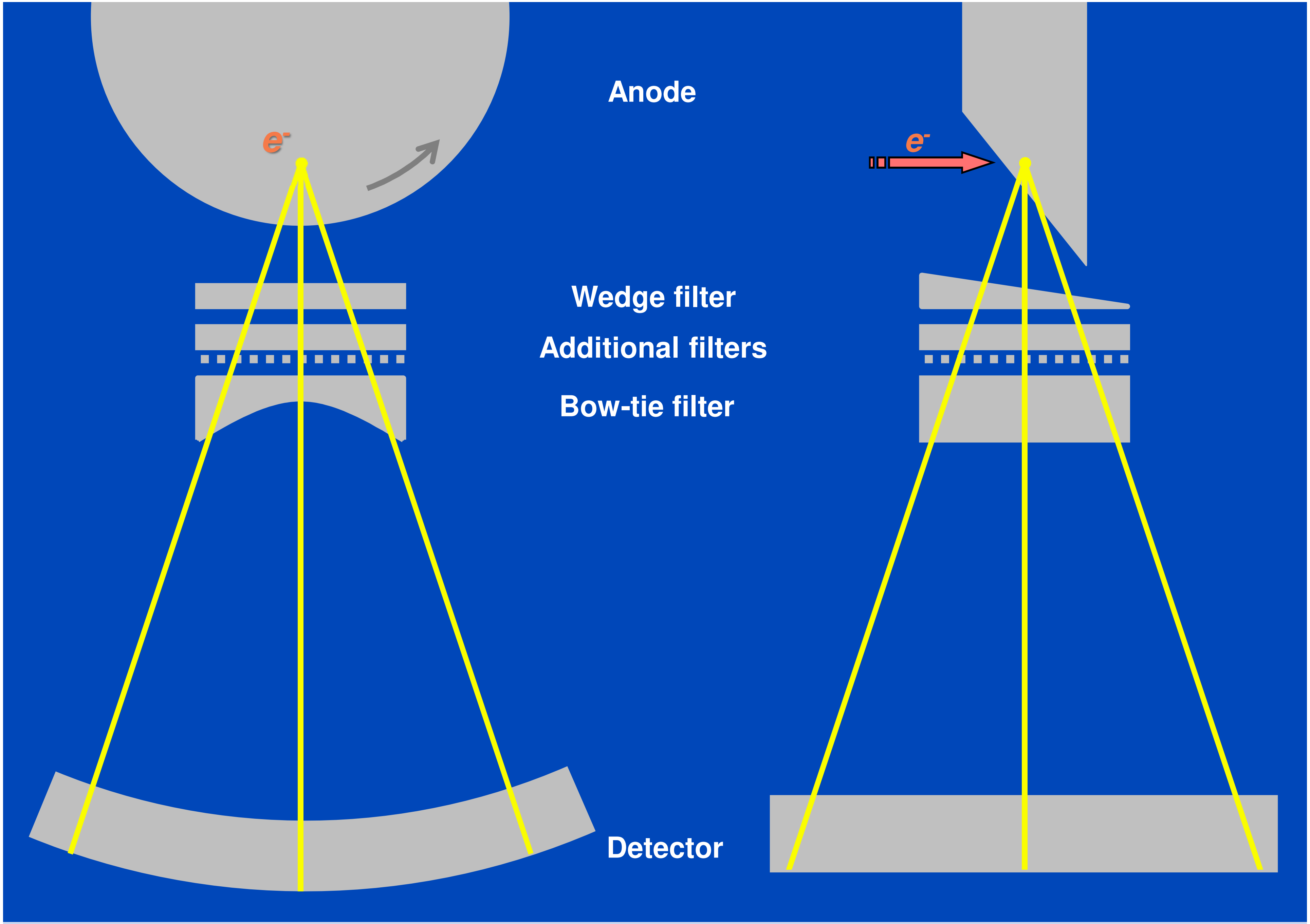

Figure not drawn to scale. Order of prefiltration may differ from scanner to scanner.

dkfz.

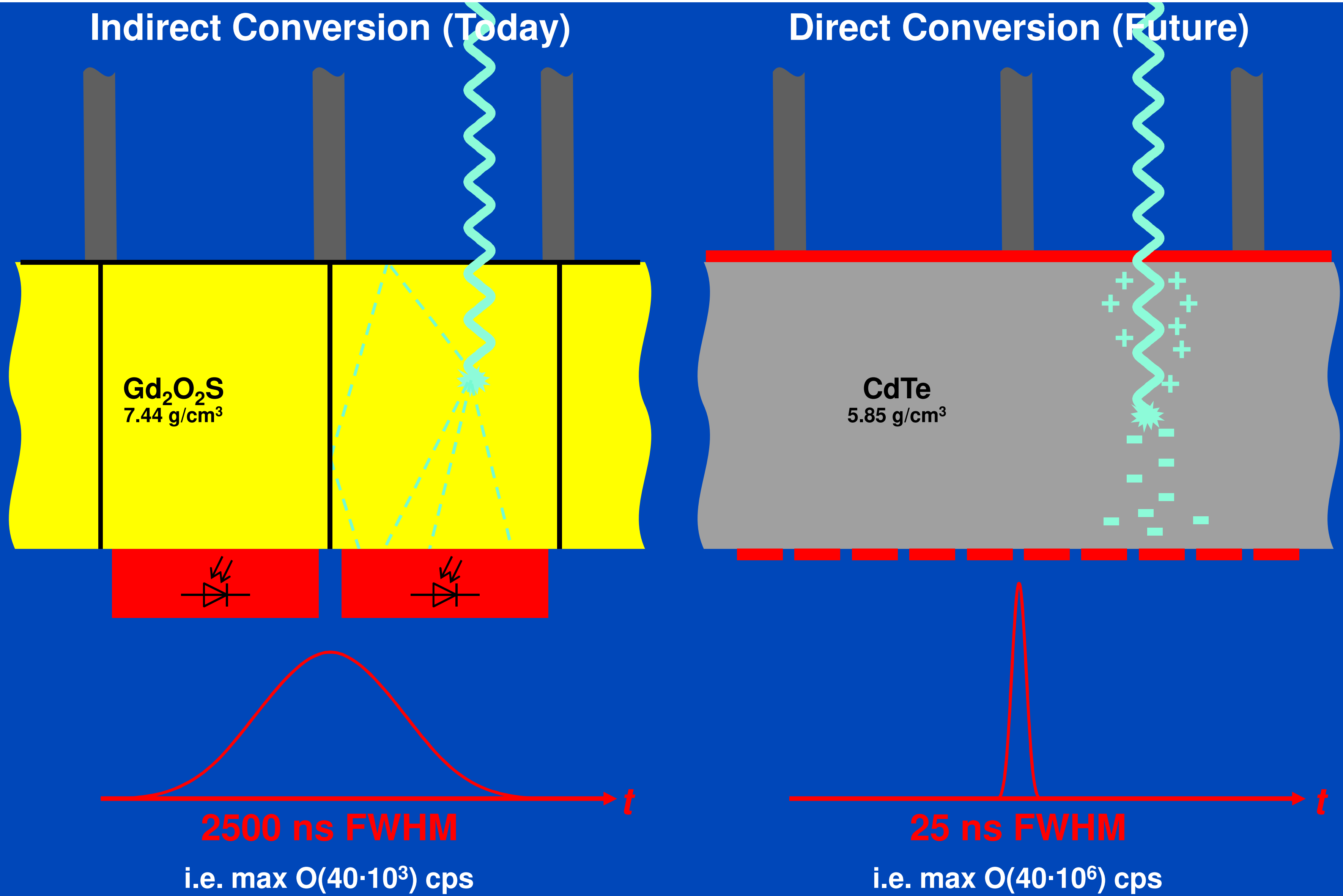

Requirements for CT: up to 10^9 x-ray photon counts per second per mm^2.
Hence, photon counting only achievable for direct converters.

Contents

Monte Carlo and/or alternatives to simulate

- X-ray spectrum
- Off-focal radiation
- Patient dose
- Scatter
- Detector properties

Most Common Monte Carlo Codes

- EGS (Electron Gamma Shower)
  - Development of the original EGS code ended with version EGS4
  - EGSnrc: maintained by the Ionization Radiation Standards Group Canada
  - EGS5: maintained by KEK, Japan
- FLUKA (FLUktuierende KAskade)
  - Development by INFN (National Institute for Nuclear Physics, Italy) & CERN
- Geant4 (Geometry and tracking)
  - Development and maintanance by international Geant collaboration
  - GATE is Geant4 for emission tomography
- MARS
  - Development by FermiLab
- MCNP (Monte Carlo N-Particle Transport Code)
  - Developed by Los Alamos National Laboratory
  - Variants: MCNPX, MCNP5, MCNP6
- PENELOPE
- …

Particular Needs of X-Ray Imaging and CT

- CT often requires raytracing through voxel volumes.
- Typical CT applications do not require to track all events.
- CT interactions are Rayleigh scatter, photo effect and Compton scatter.
- CT energies are restricted to the range from 10 keV to 150 keV (clinical) or up to 600 keV (industrial).
- Speed is of importance if patient-dependent photon trajectories need to be calculated.
- Thus, a home-made Monte Carlo code is typically of better performance than Geant4 et al.

Monte Carlo Acceleration Techniques (Variance Reduction) for X-Ray Imaging and CT

- Sample first interaction point
- Avoid photon termination due to photo effect
- Use virtual photons that do particle splitting at interaction points
- Position-depedent importance sampling (optimizes NSplit)
- Forced detection
- Woodcock tracking
- Cutoff energy and interaction number

X-Ray Spectra

X-Ray Spectra

- Facts
  - Wide range of tube voltages
  - Different target materials and anode angles
  - Transmission vs. reflection targets
  - Emitted vs. detected $w_{\mathrm{det}}(E) \propto E^{01}\, w_{\mathrm{emit}}(E)\,(1 - e^{-\mu_{\mathrm{D}}(E)d_{\mathrm{D}}})$
  - Different spectrum for each detector pixel $w(E) = w_L(E)$
- Why need to know?
  - Data preprocessing
  - Beam hardening correction
  - Scatter correction
  - Dose estimation
  - ...

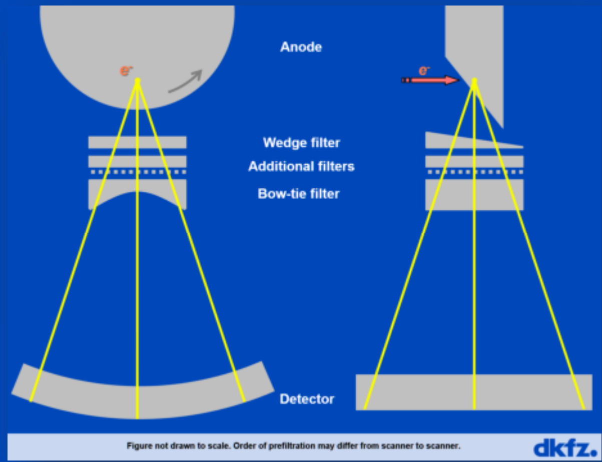

$$q(L) = -\ln \int dE\, w_L(E) e^{-\int dL\, \mu(\boldsymbol{r}, E)}$$

$$= -\ln \int dE\, w_L(E) e^{-p_1\psi_1(E) - p_2\psi_2(E)}$$

Spectrum Models

- Empirical and semiempirical models for spectrum generation are available and very useful
- Not all types of anodes are handled, however
- Not all tube voltages are considered
- Not all target materials are available
- Off-focal radiation is not considered
- Tucker & Co. …

Semiempirical model for generating tungsten target x-ray spectra

Douglas M. Tucker
Department of Biomedical Engineering, School of Engineering, University of Alabama at Birmingham, Birmingham, Alabama 35294

Gary T. Barnes and Dev P. Chakraborty[a)]
Department of Radiology, University of Alabama Hospitals and Clinics, University of Alabama at Birmingham, Birmingham, Alabama 35294

(Received 11 December 1989; accepted for publication 30 August 1990)

A semiempirical model for generating tungsten target x-ray spectra is presented. This model extends earlier work in two significant areas. First, both bremsstrahlung and characteristic x-ray production are assumed to occur at varying depths within the target. Second, optimal parameters for the model were determined from experimental spectra utilizing nonlinear least-squares techniques. As a result, good agreement is obtained between calculated and measured x-ray tube spectra and output for different target angles and a wide range of x-ray tube potentials. Such is not the case with previously published models.

I. INTRODUCTION

The x-ray spectrum is fundamental to the x-ray imaging process and it is often useful to be able to predict accurately diagnostic x-ray spectra. The earliest theoretical model of thick target bremsstrahlung spectra is the well-known expression develped by Kulenkampff[1] and Kramers[2]

$$E\,N(E)\,dE = \text{const}\; Z(T-E)\,dE\,, \quad (1)$$

of emitting a photon. Most electron deflections … nuclei are elastic. In a small number of incidences, … will be emitted. For an electron of kinetic energy … nucleus of charge Ze, the differential cross section $d\sigma_{\text{rad}}$ for the emission of a photon between E and $E+dE$ is given by[10]

$$d\sigma_{\text{rad}} = \sigma_0 Z^2 B\,\frac{T+m_0c^2}{T}\,\frac{dE}{E}\,, \quad (2)$$

Tungsten anode spectral model using interpolating cubic splines: Unfiltered x-ray spectra from 20 kV to 640 kV

Andrew M. Hernandez
Biomedical Engineering Graduate Group, University of California Davis, Sacramento, California 95817

John M. Boone[a)]
Departments of Radiology and Biomedical Engineering, Biomedical Engineering Graduate Group, University of California Davis, Sacramento, California 95817

(Received 20 August 2013; revised 17 January 2014; accepted for publication 31 January 2014; published 7 March 2014)

Purpose: Monte Carlo methods were used to generate lightly filtered high resolution x-ray spectra spanning from 20 kV to 640 kV.
Methods: X-ray spectra were simulated for a conventional tungsten anode. The Monte Carlo N-Particle eXtended radiation transport code (MCNPX 2.6.0) was used to produce 35 spectra over the tube potential range from 20 kV to 640 kV, and cubic spline interpolation procedures were used to create piecewise polynomials characterizing the photon fluence per energy bin as a function of x-ray tube potential. Using these basis spectra and the cubic spline interpolation, 621 spectra were generated at 1 kV intervals from 20 to 640 kV. The tungsten anode spectral model using interpolating cubic splines (TASMICS) produces minimally filtered (0.8 mm Be) x-ray spectra with 1 keV energy resolution. The TASMICS spectra were compared mathematically with other, previously reported spectra.
Results: Using paired *t*-test analyses, no statistically significant difference (i.e., $p > 0.05$) was observed between compared spectra over energy bins above 1% of peak bremsstrahlung fluence. For all energy bins, the correlation of determination (R^2) demonstrated good correlation for all spectral comparisons. The mean overall difference (MOD) and mean absolute difference (MAD) were com-

Spectrum Estimation using Attenuation Measurements

- Measure absorbers of different thicknesses and materials
- Ill-posed problem, thus add prior knowledge
- Reproduction of spectrum in most cases not important (but everyone believes so).

IOP Publishing | Institute of Physics and Engineering in Medicine

Physics in Medicine & Biolo

Phys. Med. Biol. 60 (2015) 339–357

doi:10.1088/0031-9155/60/1/3

An indirect transmission measurement-based spectrum estimation method for computed tomography

Wei Zhao[1], Kai Niu[1], Sebastian Schafer[2] and Kevin Royalty[2]

[1] Department of Medical Physics, U
Avenue, Madison, WI 53705, USA
[2] Siemens Medical Solutions, USA I

E-mail: wzhao49@wisc.edu

Received 26 July 2014, revised 11 N
Accepted for publication 14 Novemb
Published 12 December 2014

Abstract

The characteristics of an x-ray
and related tasks. In practice, d
difficult to directly measure the

TML ABSTRACT + LINKS

JOURNAL OF APPLIED PHYSICS 97, 124701 (2005)

A robust method of x-ray source spectrum estimation from transmission measurements: Demonstrated on computer simulated, scatter-free transmission data

Emil Y. Sidky,[a)] Lifeng Yu, Xiaochuan Pan, Yu Zou, and Michael Vannier
University of Chicago Department of Radiology 5841 S. Maryland Avenue, Chicago, Illinois 60637

(Received 6 December 2004; accepted 19 April 2005; published online 16 June 2005)

Knowledge of the x-ray spectrum in diagnostic imaging is important for dose calculations, correction for beam-hardening artifacts, and dual-energy computed tomography. One way to determine the x-ray source spectrum is to estimate it from transmission data of a known phantom. Although such an approach is experimentally simple, spectrum estimation from transmission data is

X-ray spectrum estimation for accurate attenuation simulation

Carsten Leinweber, Joscha Maier, and Marc Kachelrieß[a)]
German Cancer Research Center (DKFZ), Heidelberg, BW, Germany

(Received 12 January 2017; revised 3 September 2017; accepted for publication 15 September 2017; published 28 October 2017)

Purpose: To estimate detected x-ray spectra from transmission measurements of known attenuators that allow to accurately simulate the transmission in unknown attenuators.
Methods: Starting from the established spectrum estimation method using the truncated singular value decomposition (TSVD) we extended the algorithm by incorporating prior knowledge about the statistical nature of the transmission data and about high-frequency spectral components like characteristic peaks. Thereby our proposed approach requires only minimal prior knowledge, namely the energy positions of characteristic peaks or k-edges, which are typically well-known. This ensures that the final spectrum is not biased towards a given prior spectrum which is often observed in other

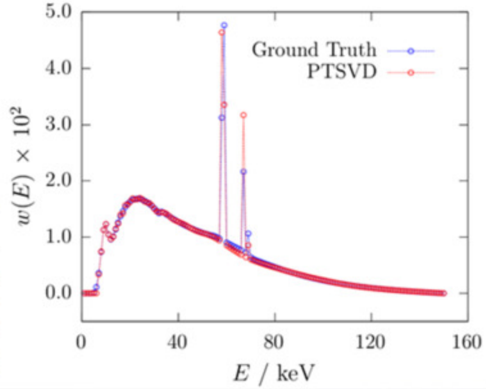

Measurement of Detected Spectrum using a PCD

Counts vs. Threshold level

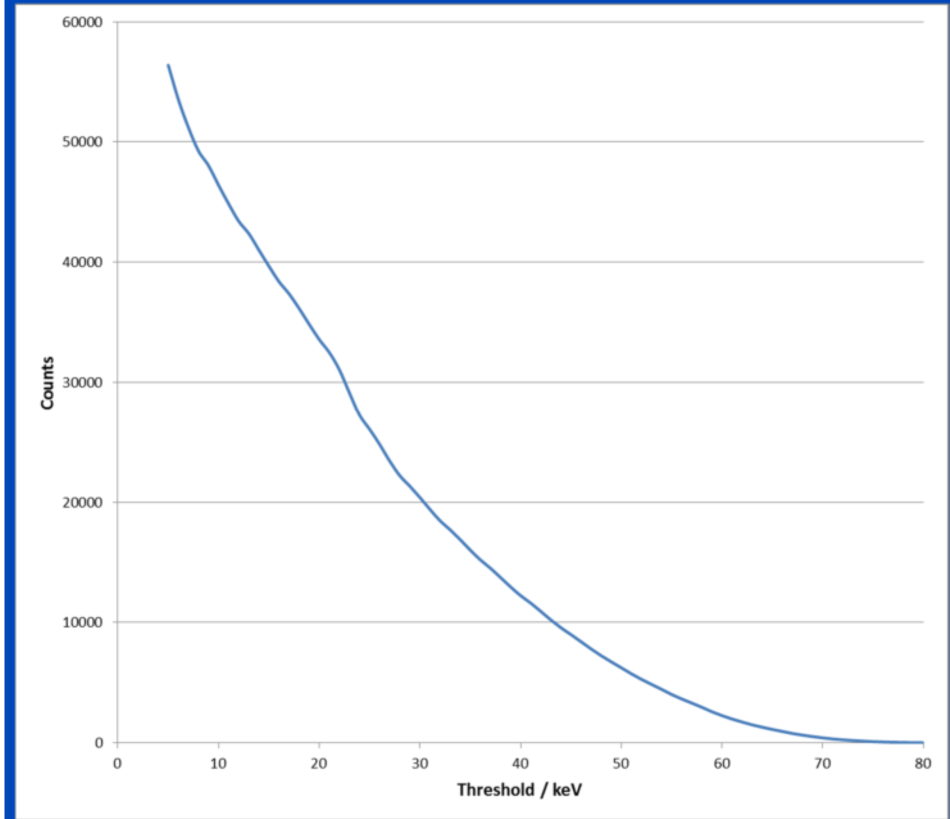

Spectrum (derivative)

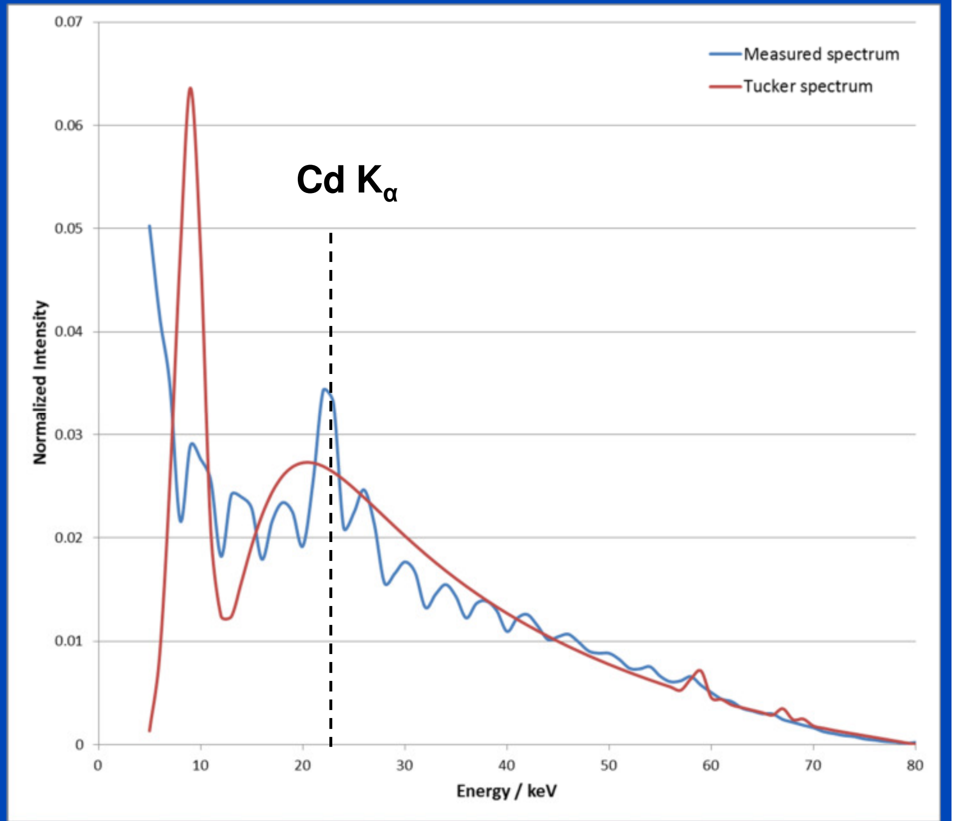

Estimation of Off-Focal Radiation by MC Simulation of the X-Ray Tube

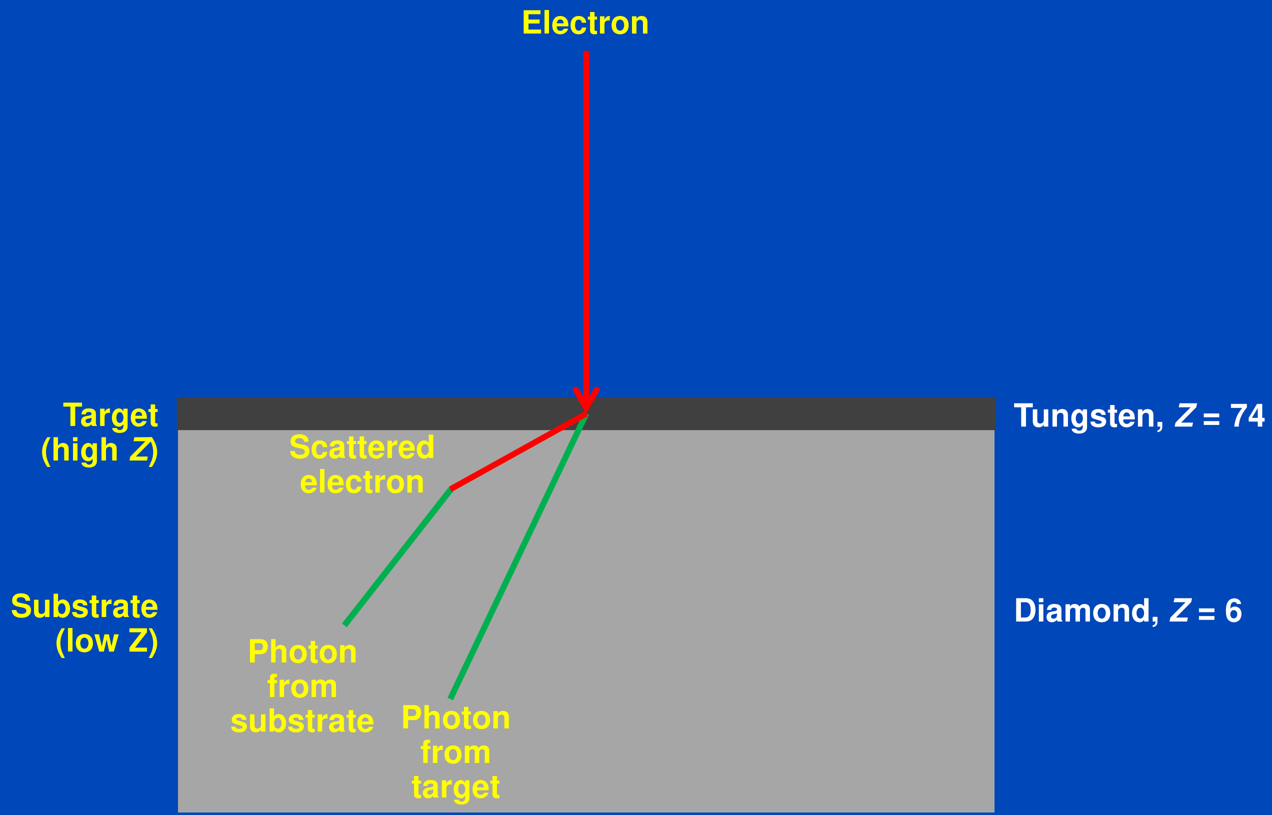

Estimation of the X-Ray Spectrum

- Monte-Carlo simulation of single electron tracks through target[1]
- Target configuration of the industrial CT system

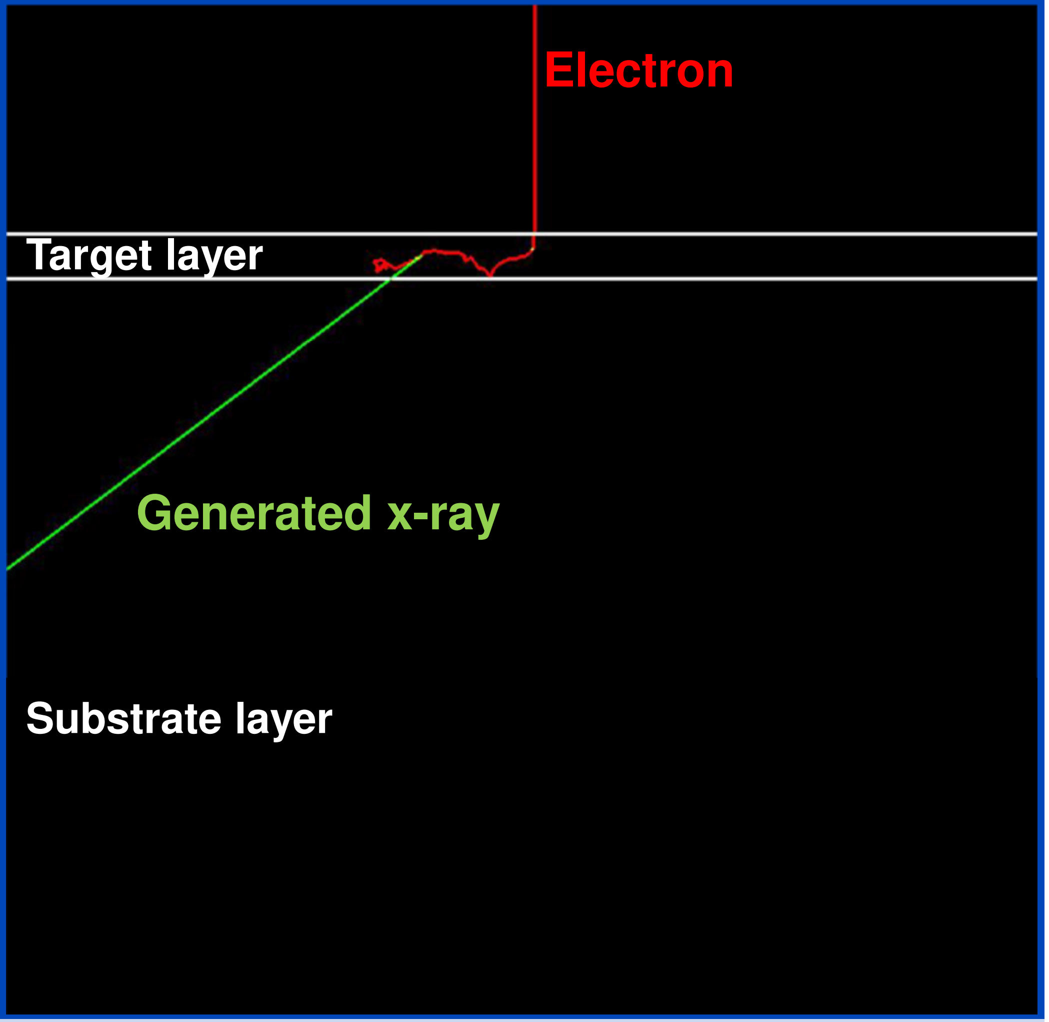

[1]S. Agostinelli et al, "Geant4—a simulation toolkit", Nucl. Instrum. Meth. A. 506(3), 250-303 (2003)

dkfz.

Estimation of the X-Ray Spectrum

- Monte-Carlo simulation of single electron tracks through target[1]
- Target configuration of the industrial CT system

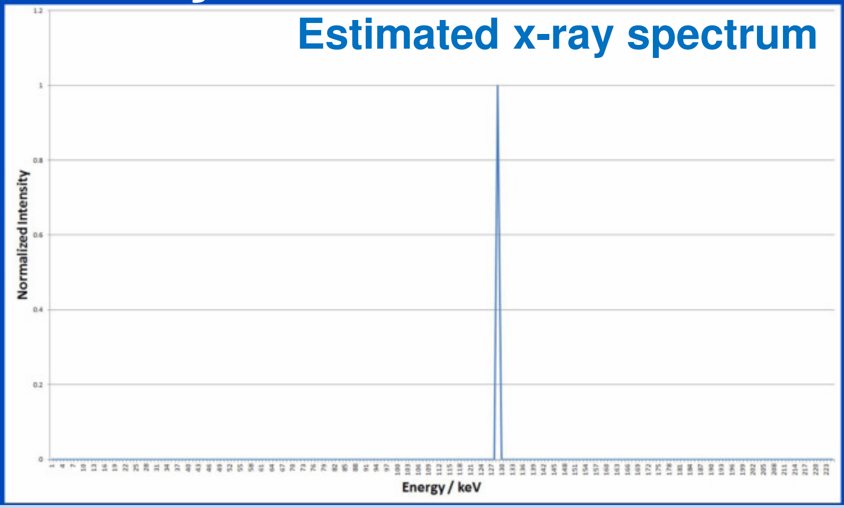

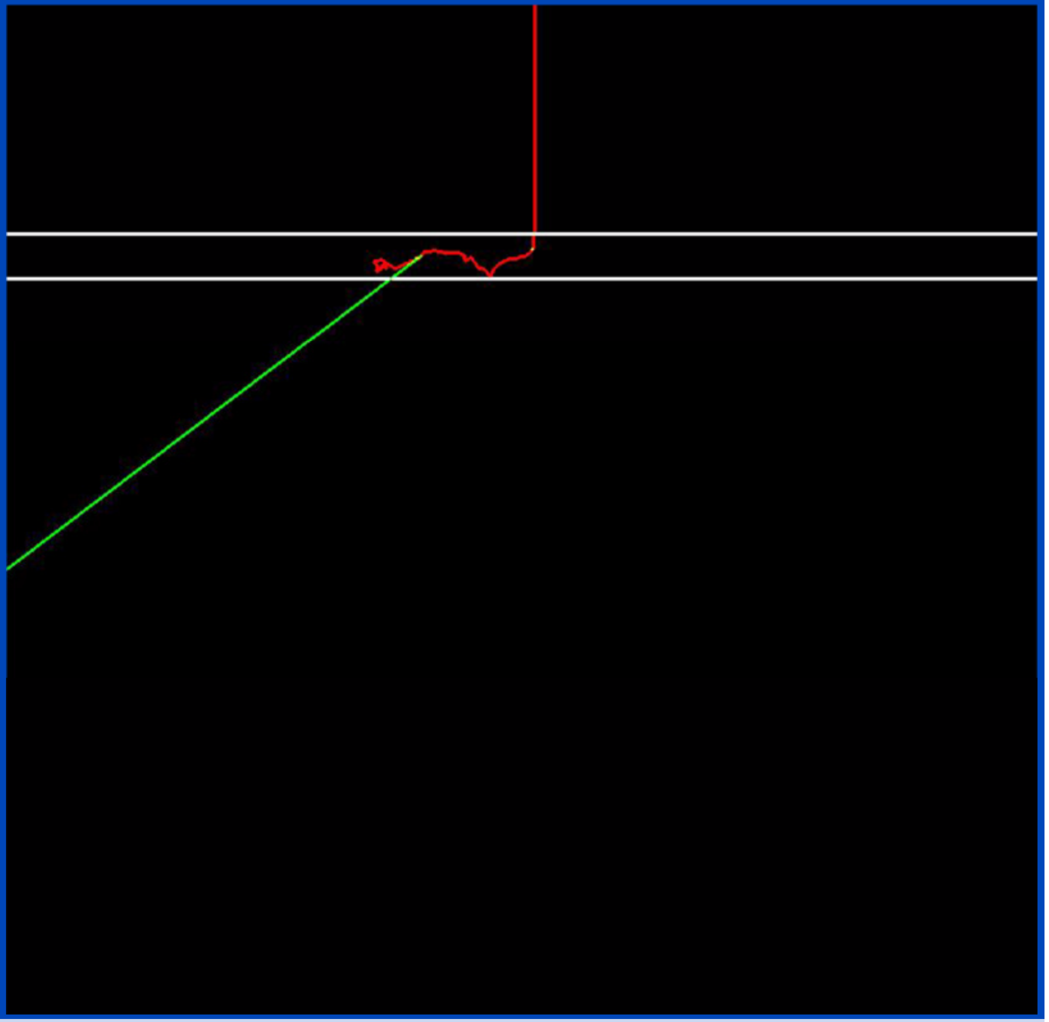

Geant4 Monte Carlo computation time: O(1 day)

Comparison of X-Ray Spectra

No Prefilter

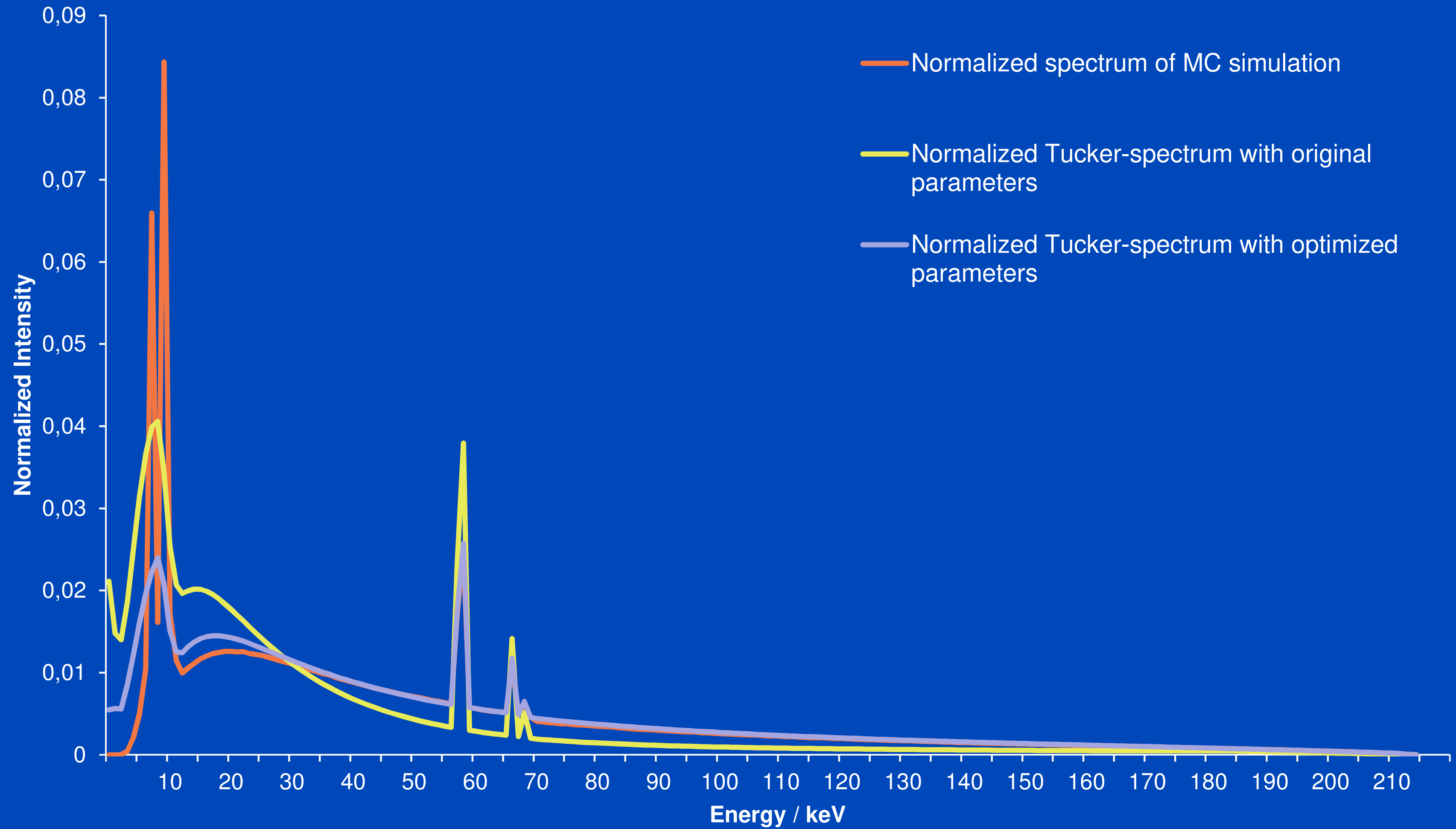

Parameters to modify: Tucker internal such as the parametrization of the Bremsstrahlung cross section and the mean energy loss per distance of electrons

dkfz.

Comparison of X-Ray Spectra

0.5 mm Sn-Prefilter

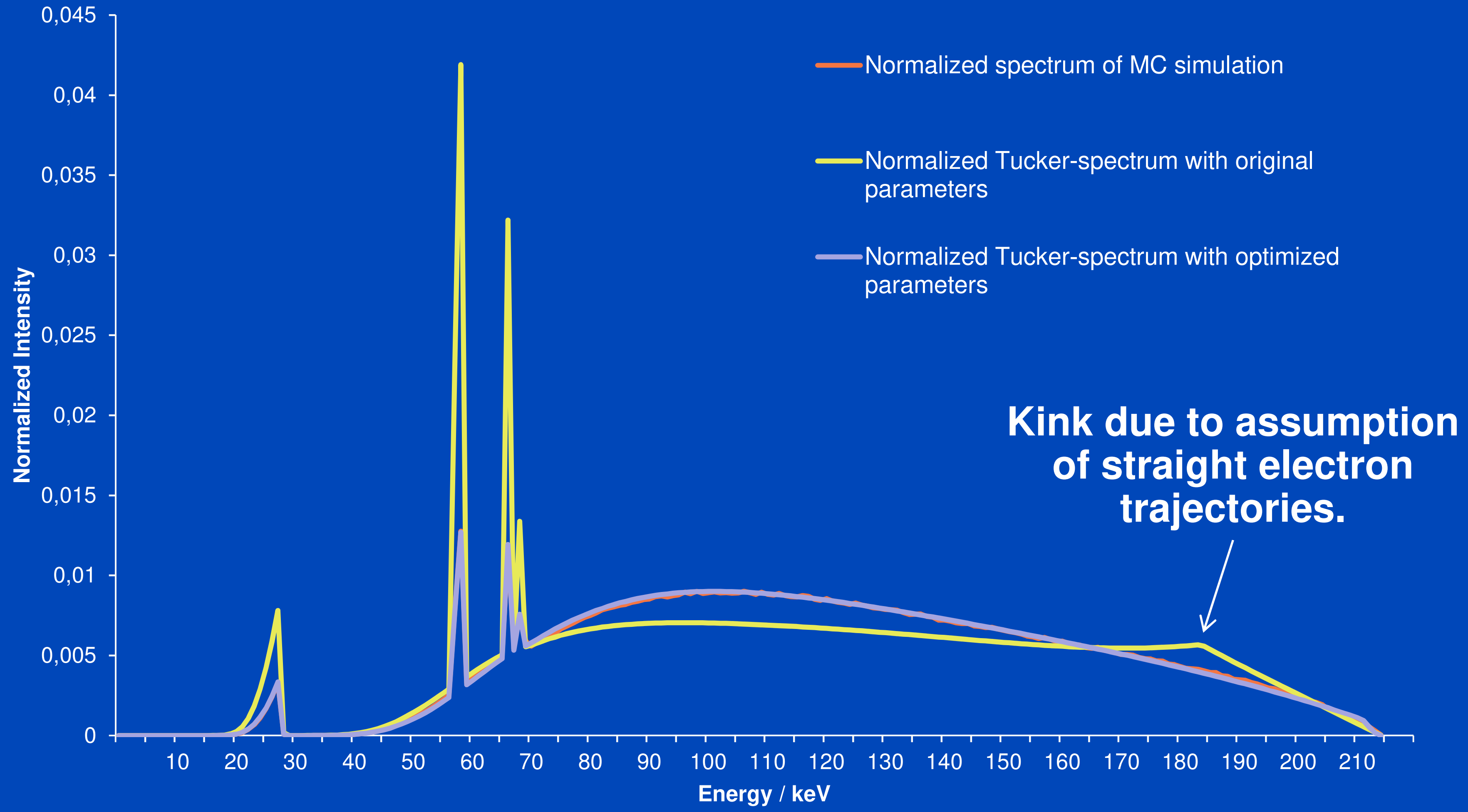

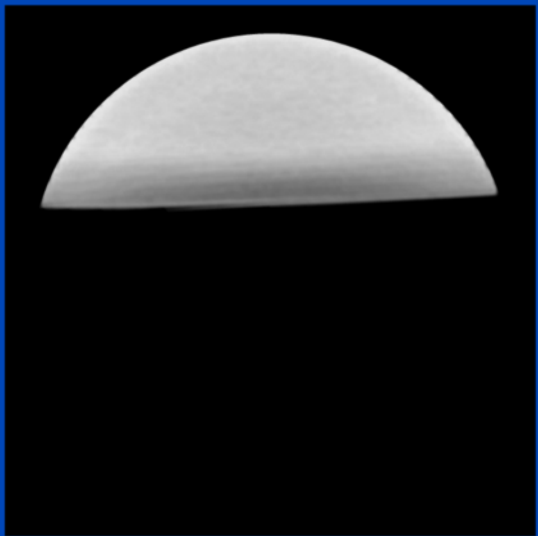

+

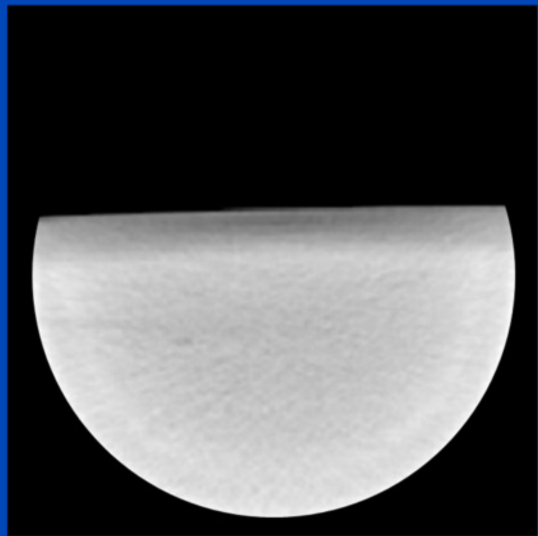

? =

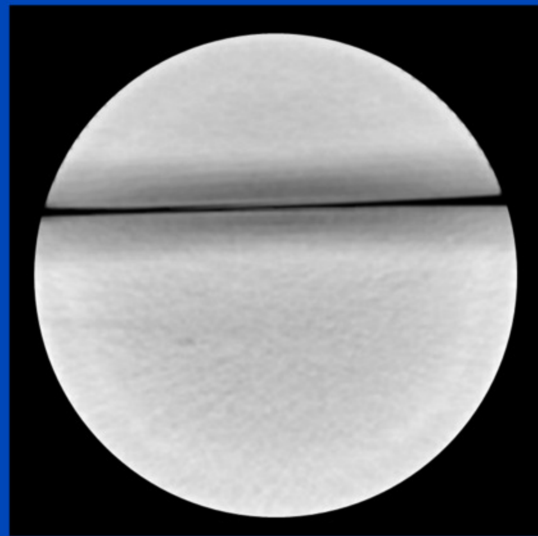

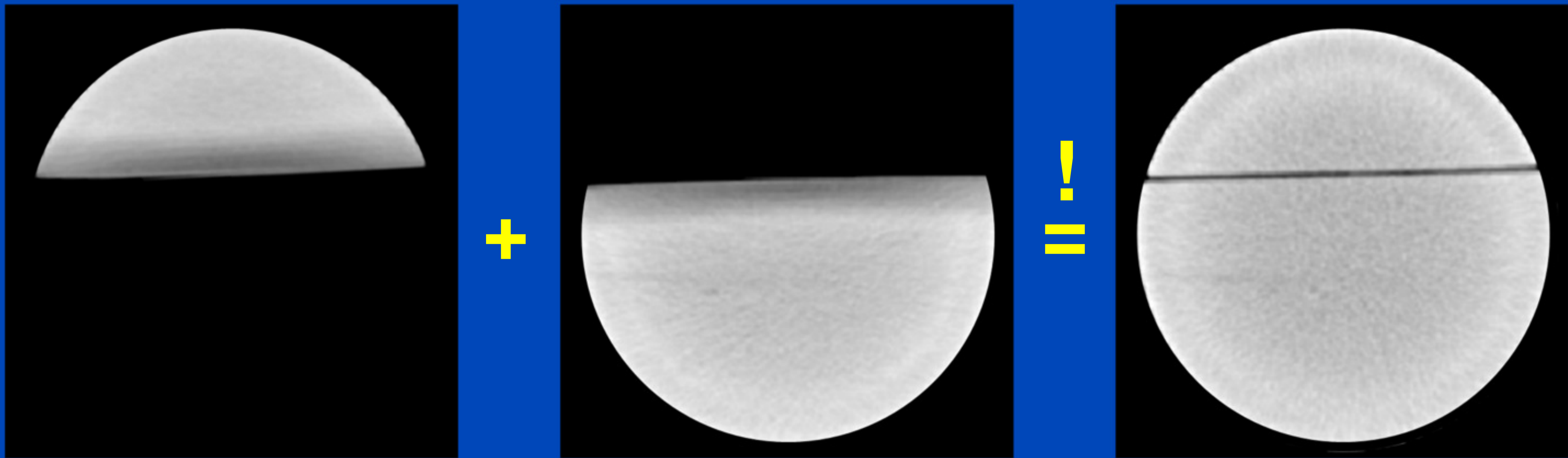

Off-Focal Radiation

Off-Focal Radiation

- Contribution of off-focal x-rays to the acquired projection data
- Intensities that correspond to high intersection lengths appear too bright
  → Underestimation of the component's attenuation

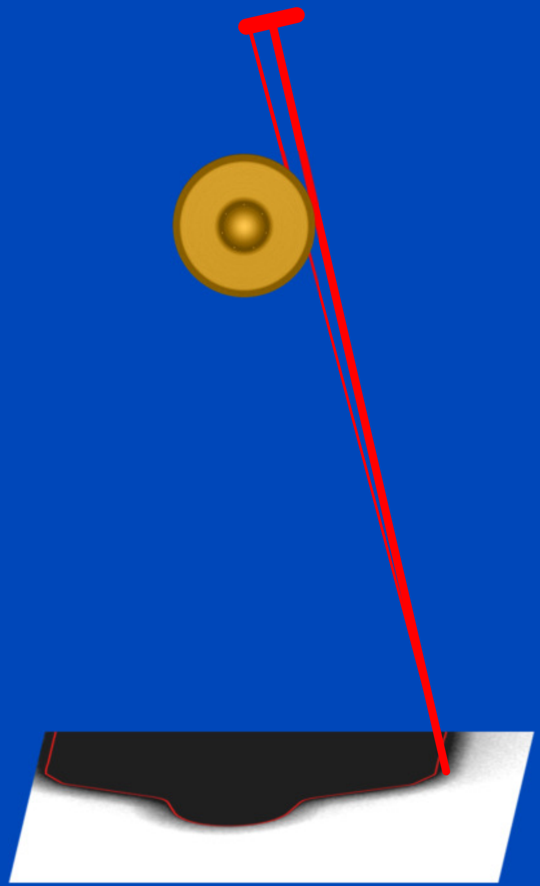

Measured intensities, window level #1

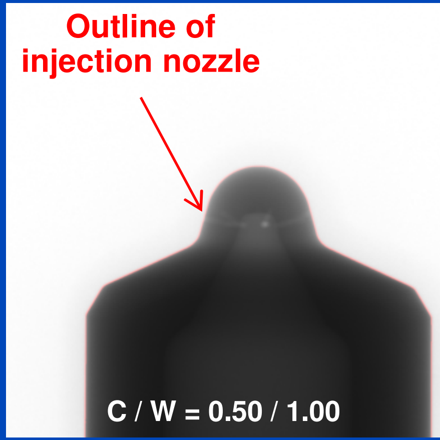

Measured intensities, window level #2

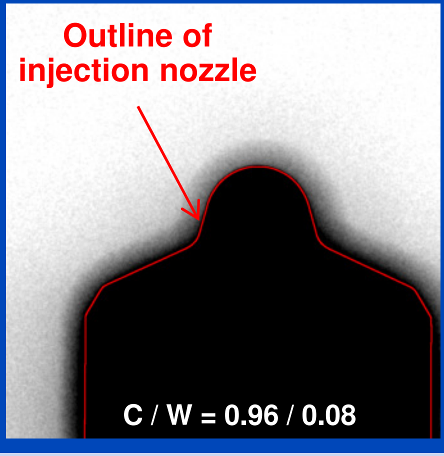

Off-Focal Radiation

- Contribution of off-focal x-rays to the acquired projection data
- Intensities that correspond to high intersection lengths appear too bright
  → Underestimation of the component's attenuation

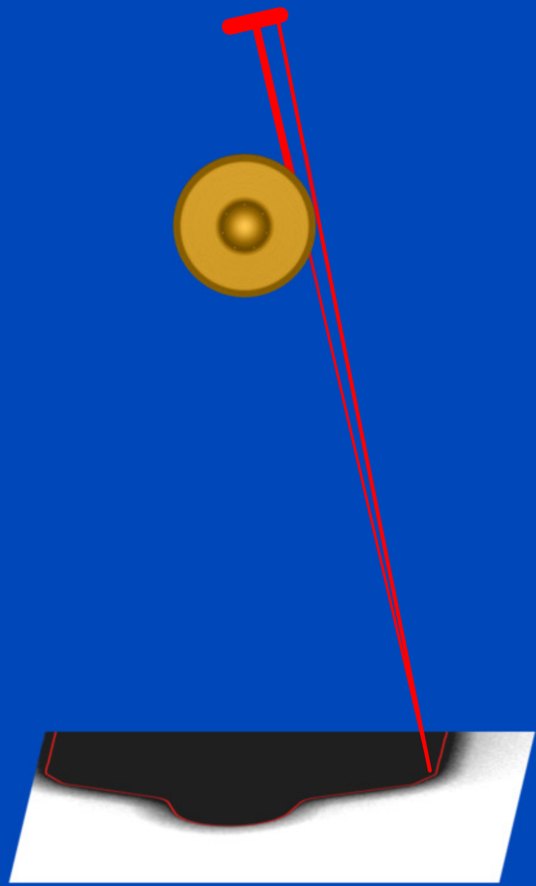

Measured intensities, window level #1

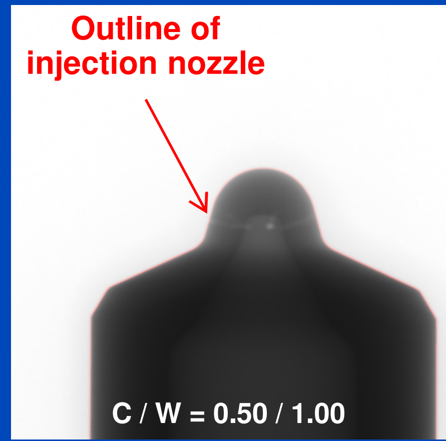

Measured intensities, window level #2

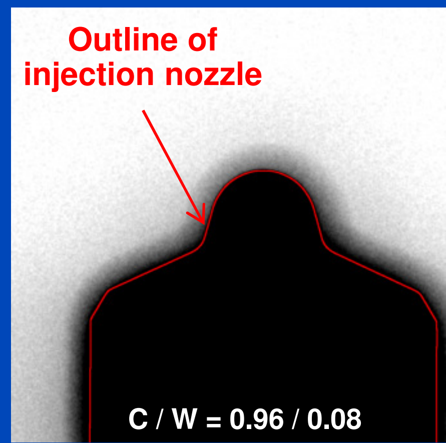

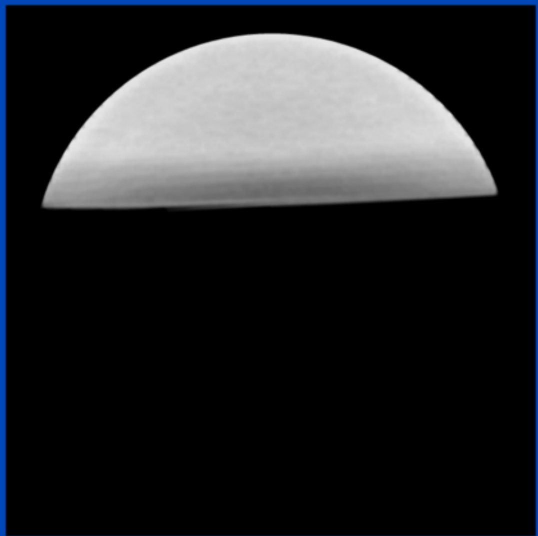

+

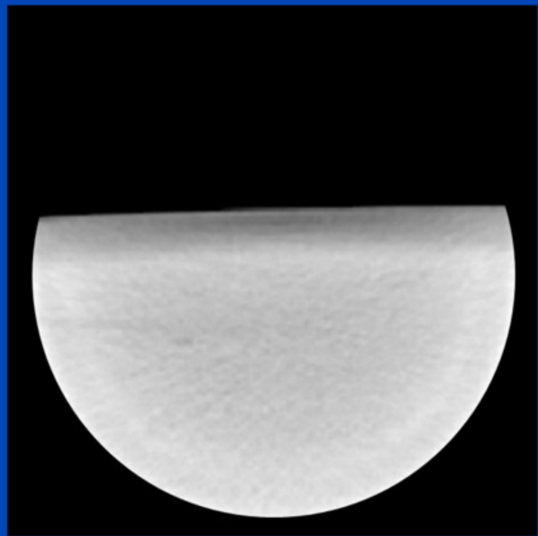

? =

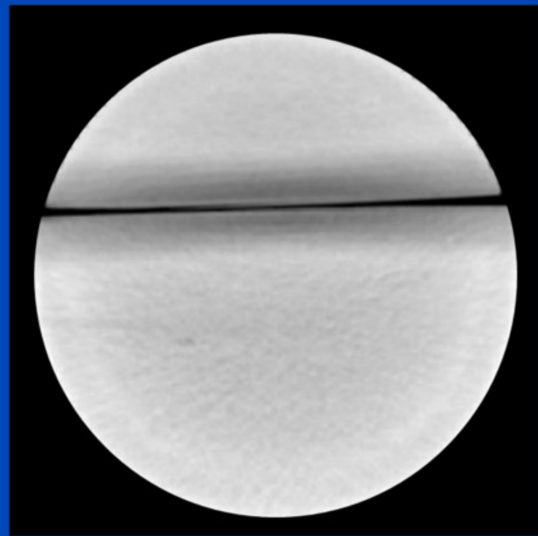

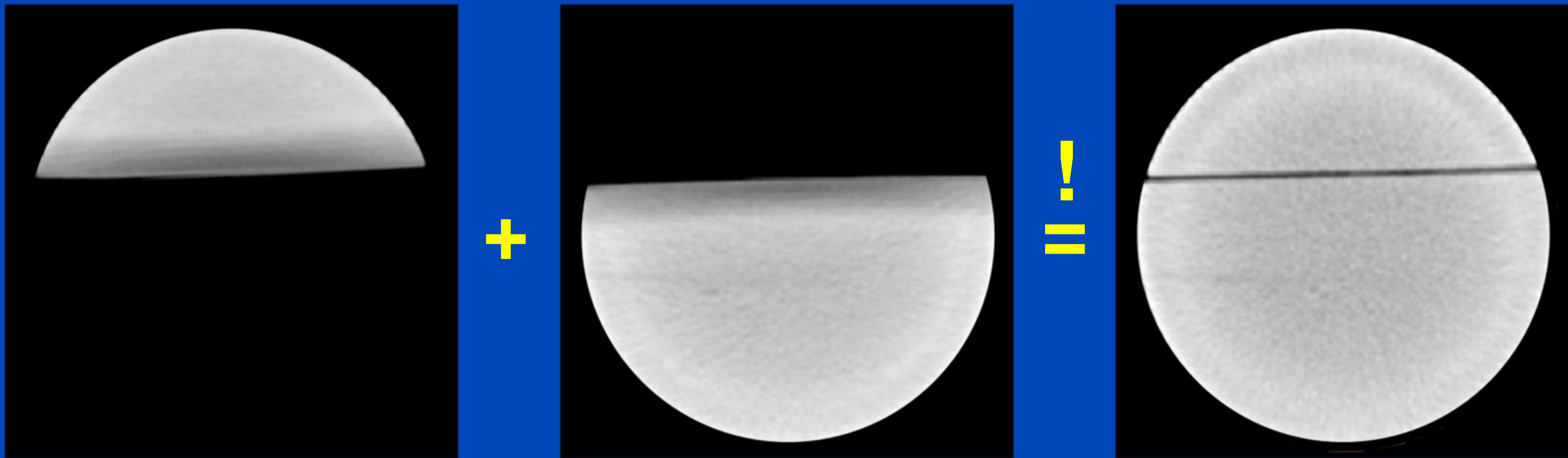

Measuring Off-Focal Shape

- Measurement of a lead slit
- Evaluation of line profiles within the acquired projections
- Calculation of the spatial distribution of the focal spot from the line profile
- Simulation of off-focal radiation by convolving the projections with a kernel that represents the focal spot distribution

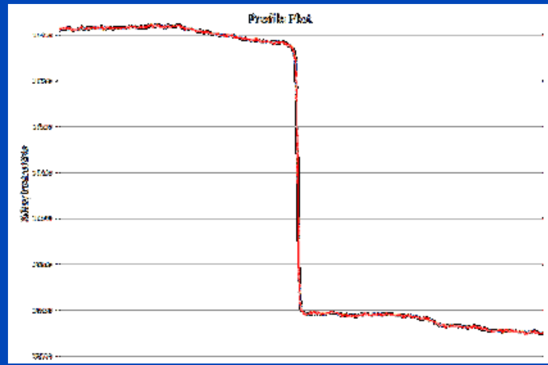

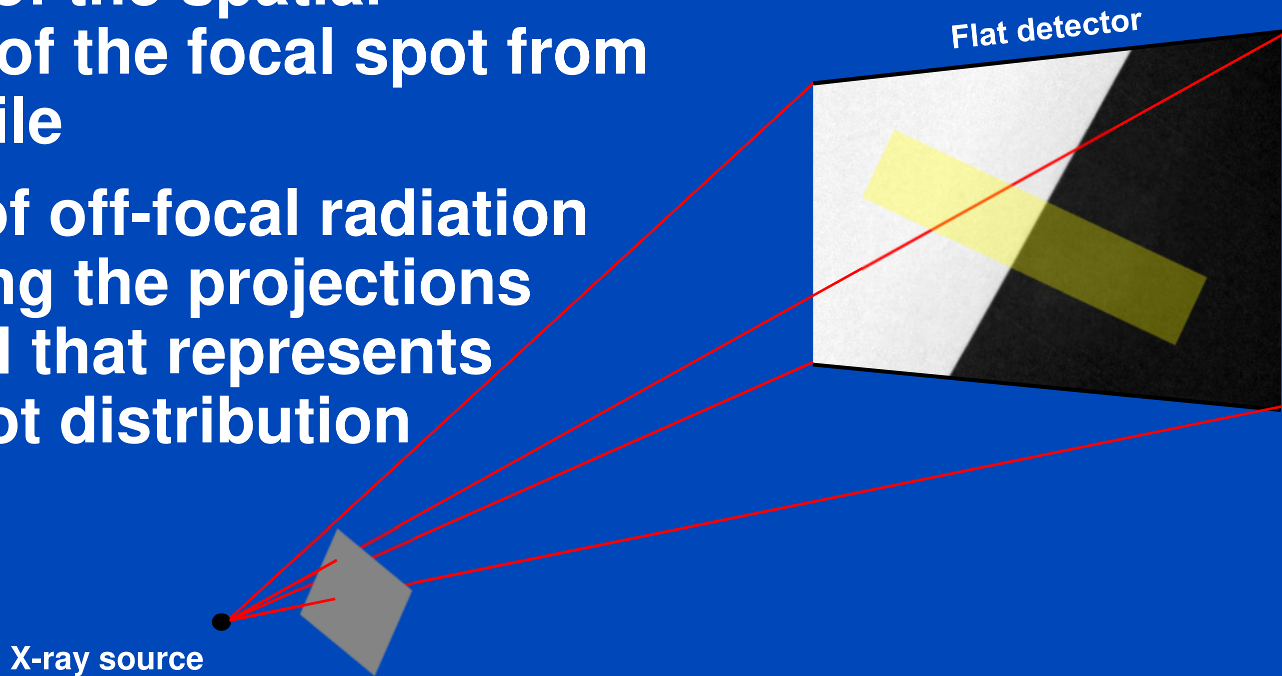

dkfz.

Estimation of Off-Focal Radiation by MC Simulation of the X-Ray Tube

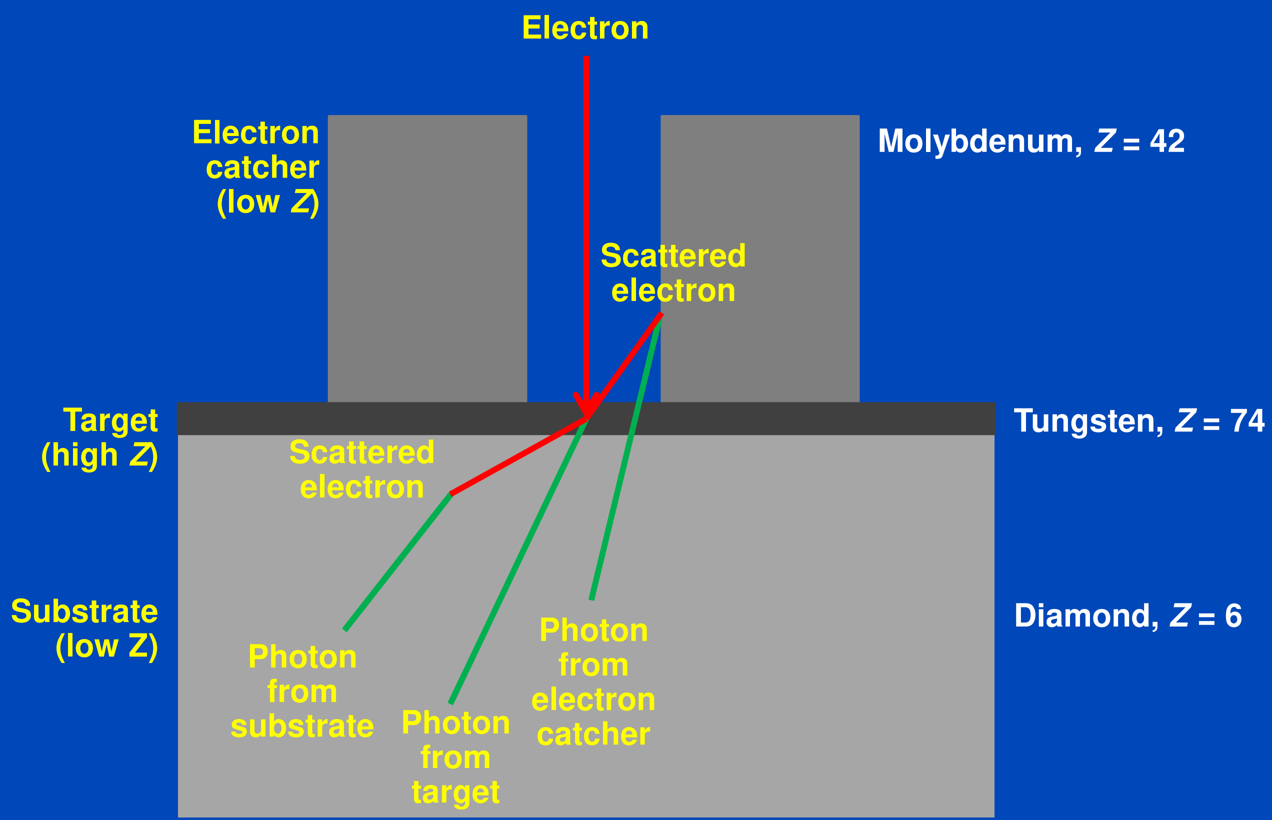

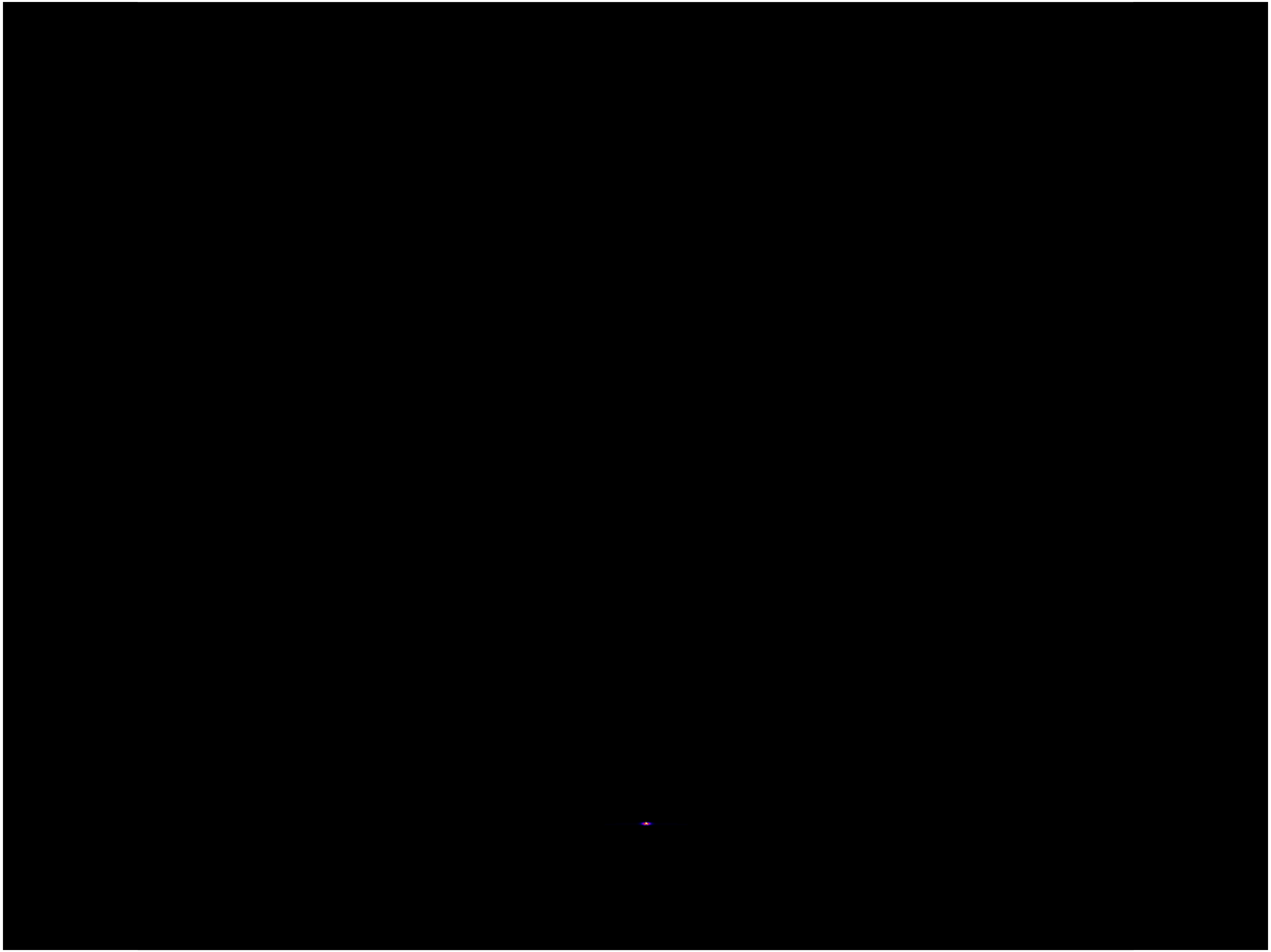

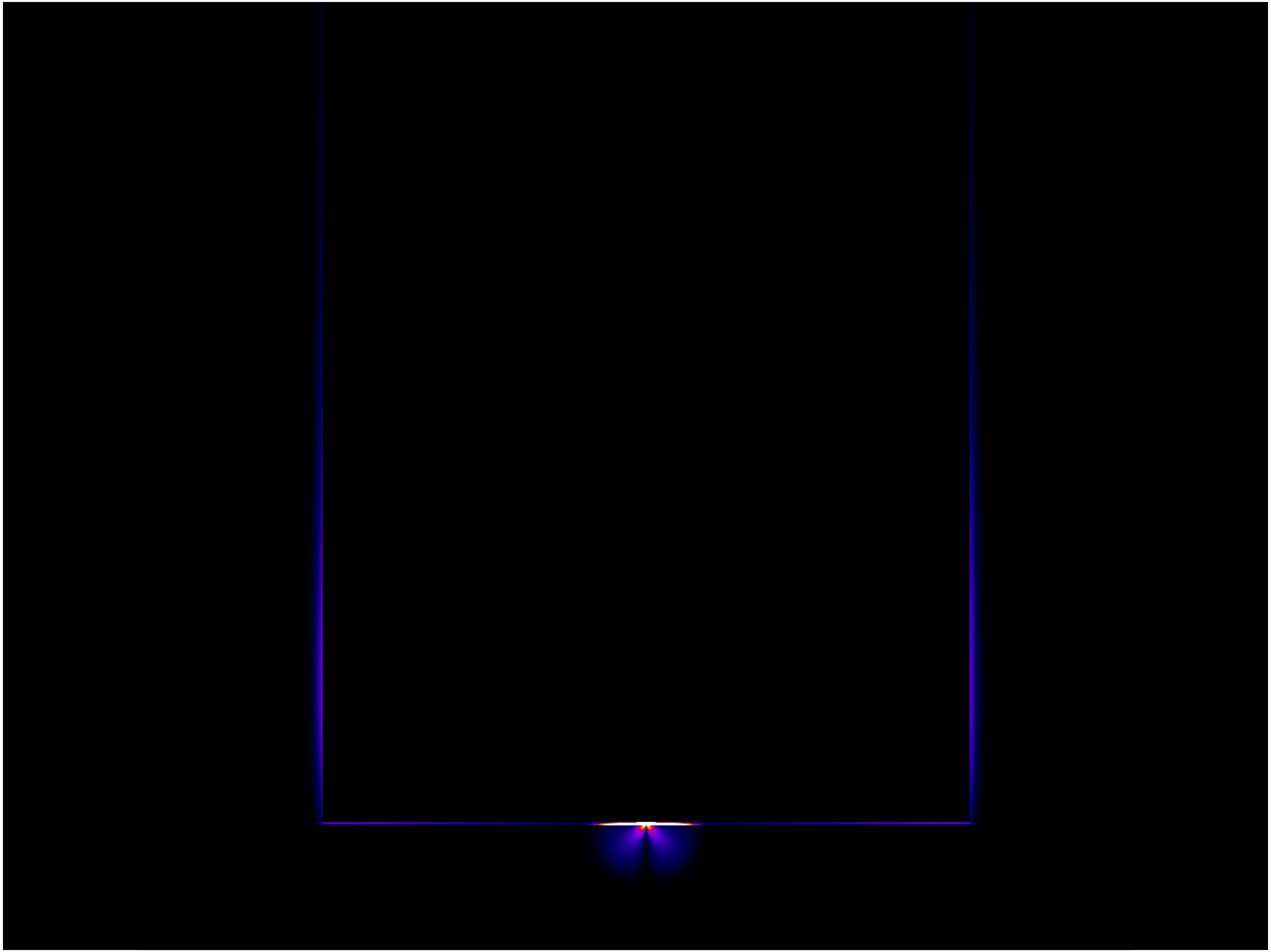

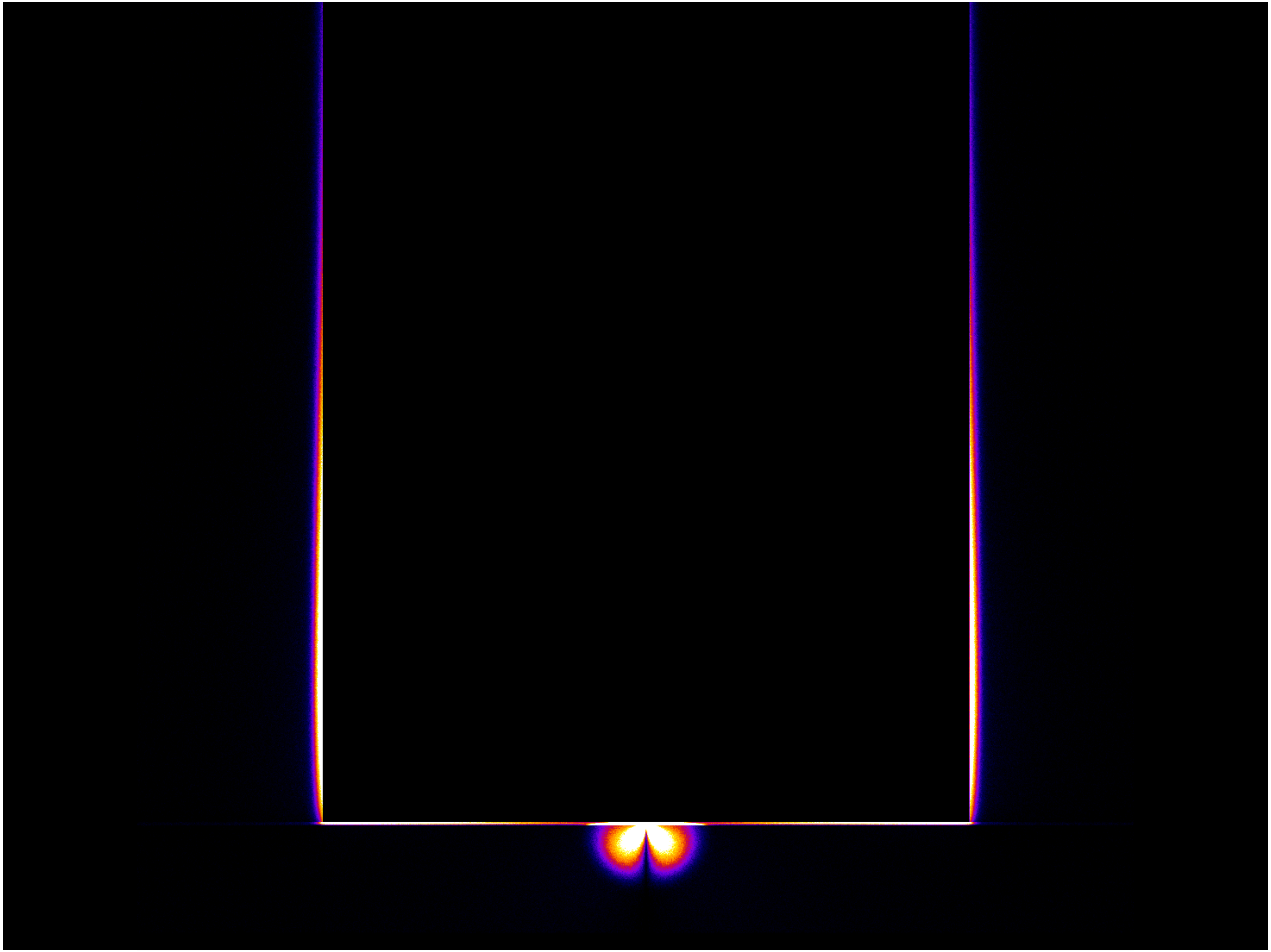

Off-Focal Radiation of a Micro Focus Transmission Source

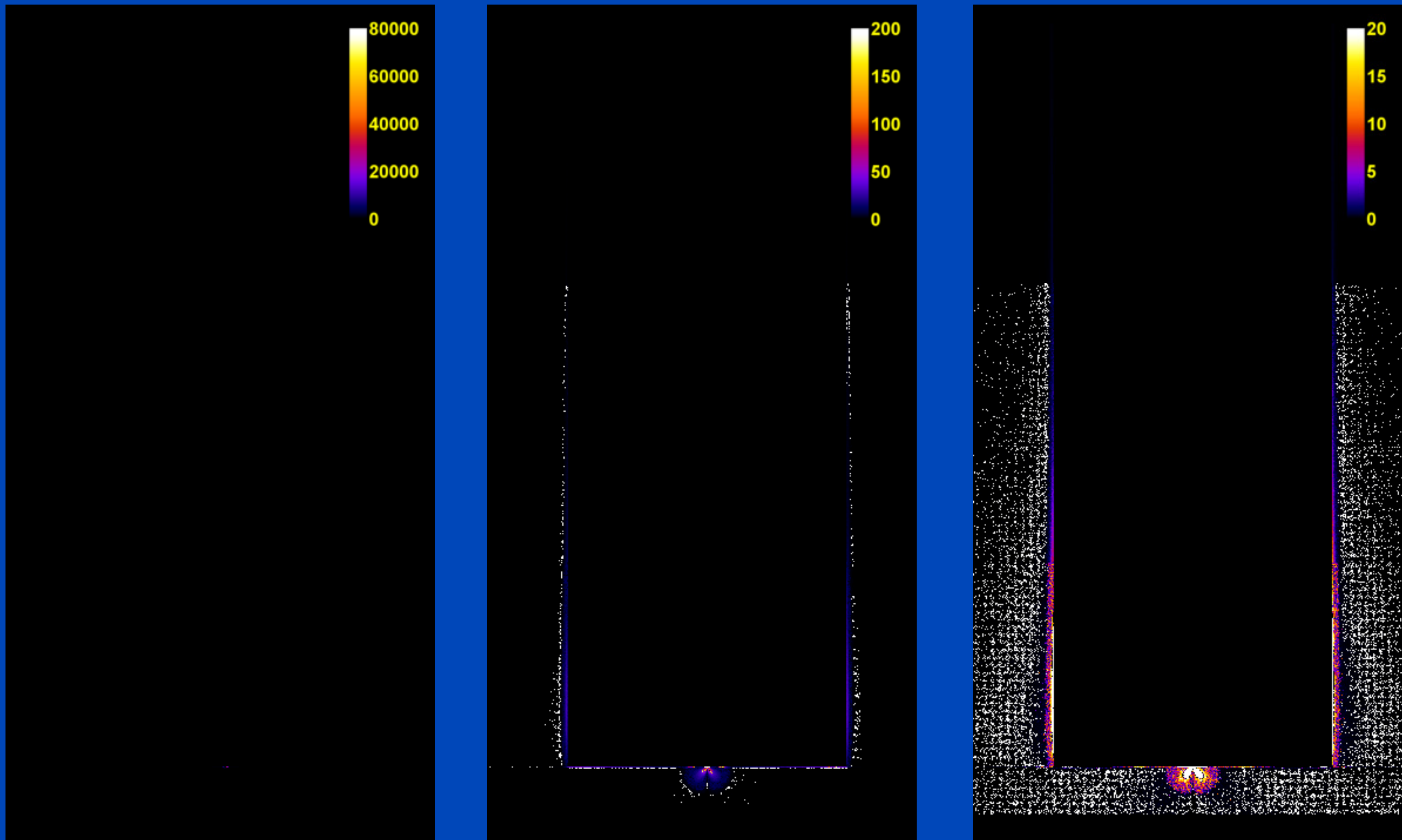

The three images are identical up to their window center and width. We simulated a needle beam of electrons.

Spectral Distribution of On- and Off-Focal Radiation

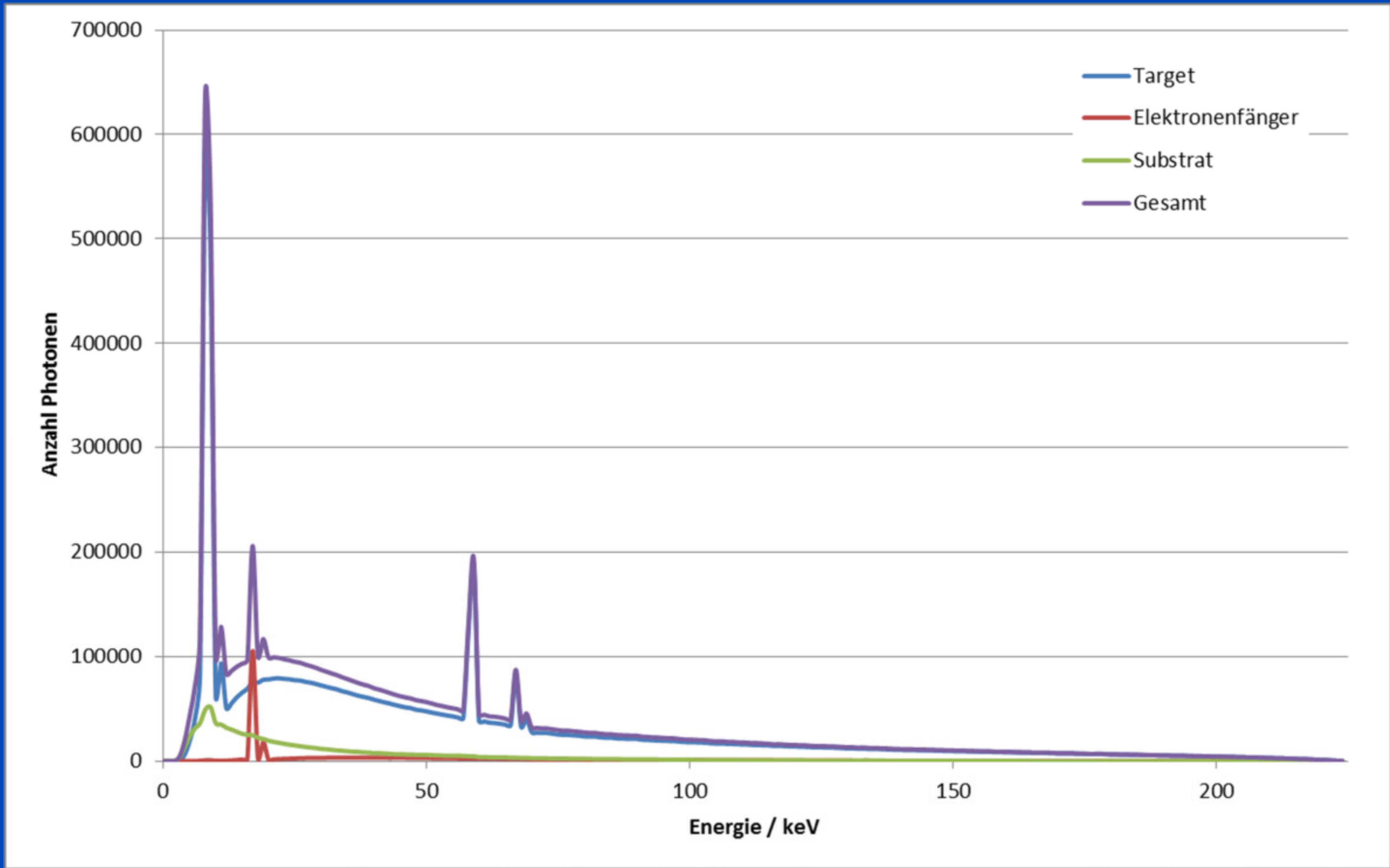

Patient Dose

MC Estimation of Dose Distribution

- Useful to study dose reduction techniques
  - Tube current modulation
  - Prefiltration and shaped filtration
  - Tube voltage settings
  - …
- Mainly used to estimate patient dose
  - Risk assessment requires segmentation of the organs (difficult)
  - Often semiantropomorphic patient models take over
  - The infamous k-factors that convert DLP into D_{eff} are derived this way, e.g. k_{chest} = 0.014 mSv/mGy/cm
  - …

MC Dose Simulation for a 360° Scan

Patient

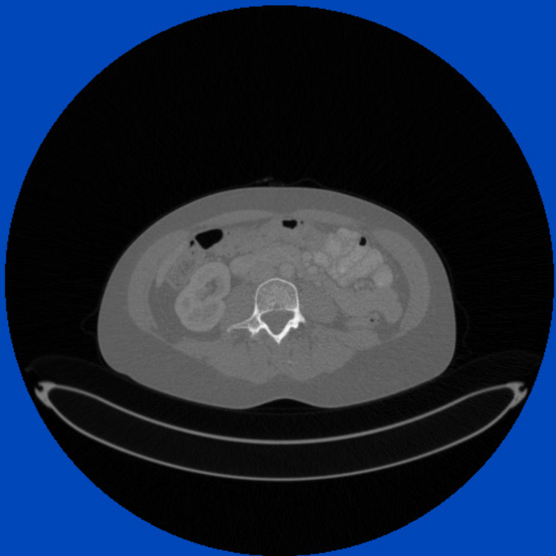

Dose per Projection

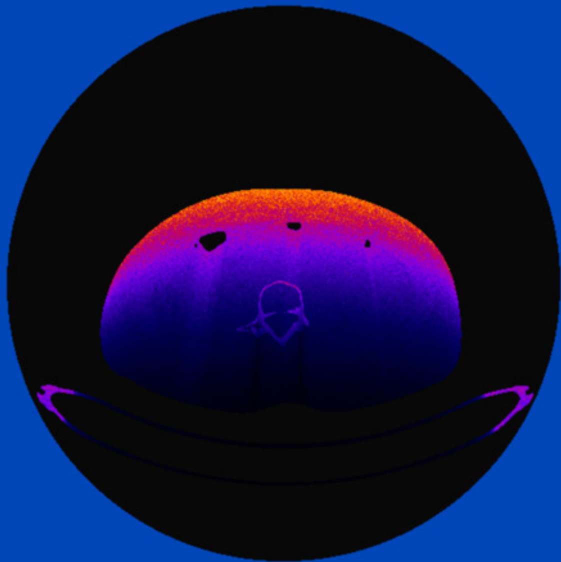

Cumulative Dose

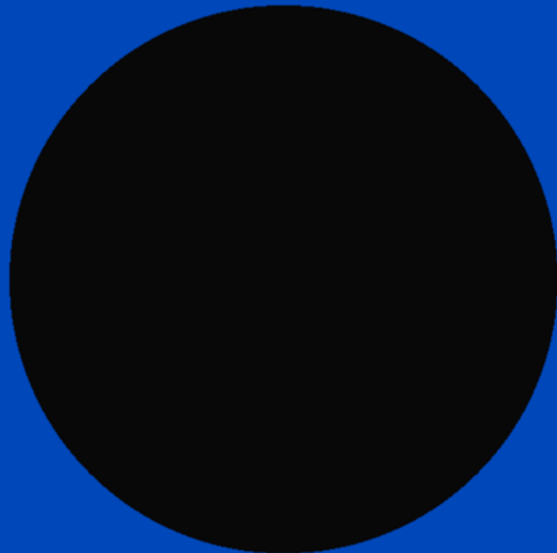

Influence of Bowtie Filter

- Commercial CT-scanners are usually equipped with a bowtie filter in order to optimize the patient dose distribution.
- Monte-Carlo dose calculations or statistical reconstruction algorithms require exact knowledge of the bowtie filter.
- The shape as well as the composition of the bowtie filter is usually not disclosed by the CT vendors.

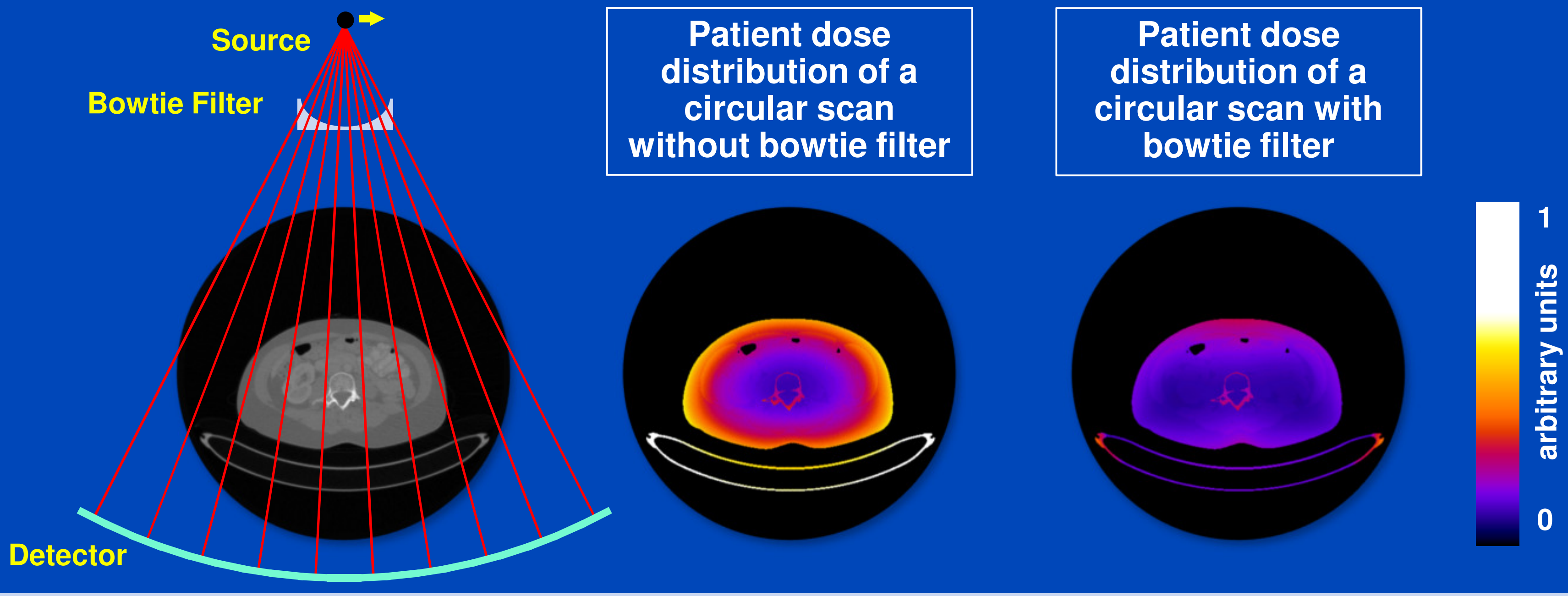

dkfz.

Automatic Exposure Control (AEC)
(z-dependent + angular dependent tube current modulation)

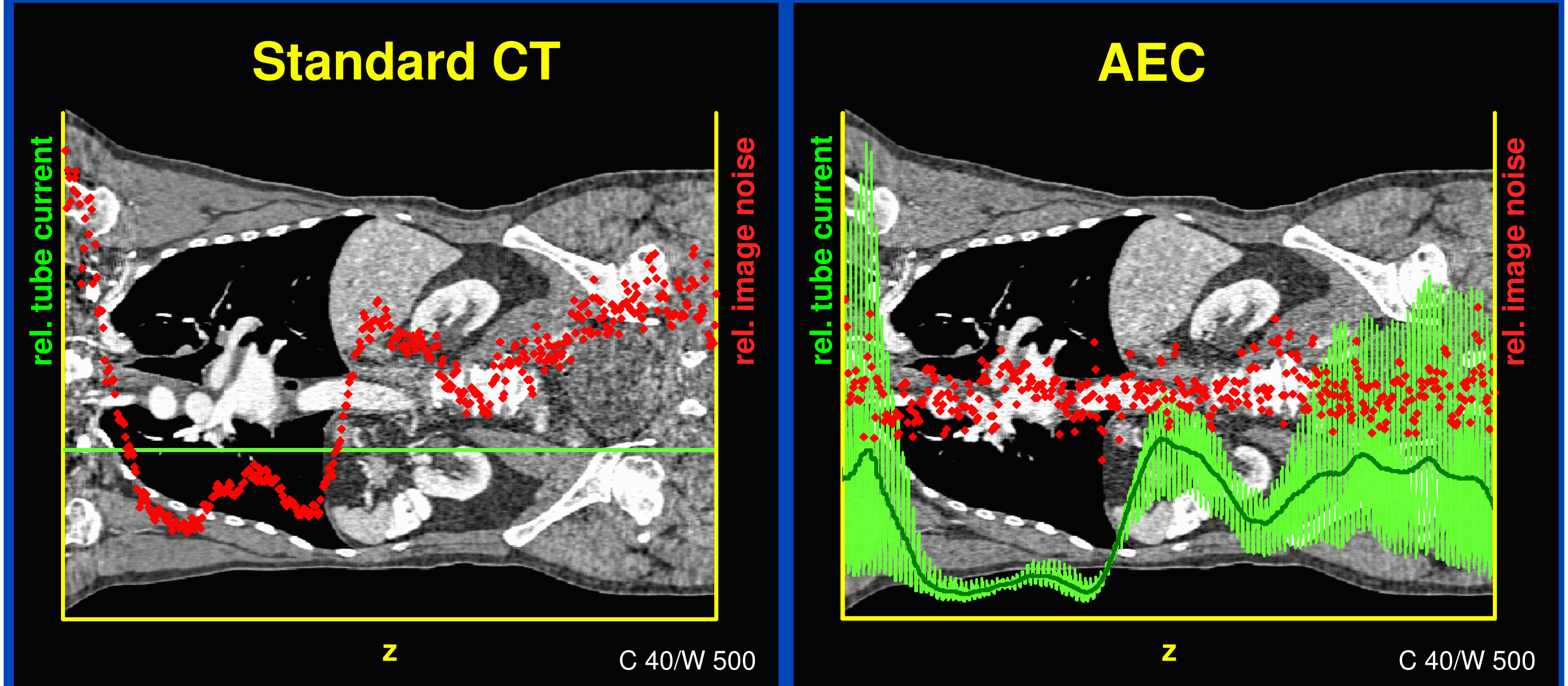

34% mAs reduction with AEC at constant image quality for that specific case

Dose Modulation: DOM, TCM, AEC, …

- Better dose usage
- ECG pulsing
- Avoiding organs of risc
- Specification of image quality $\sigma(z)$

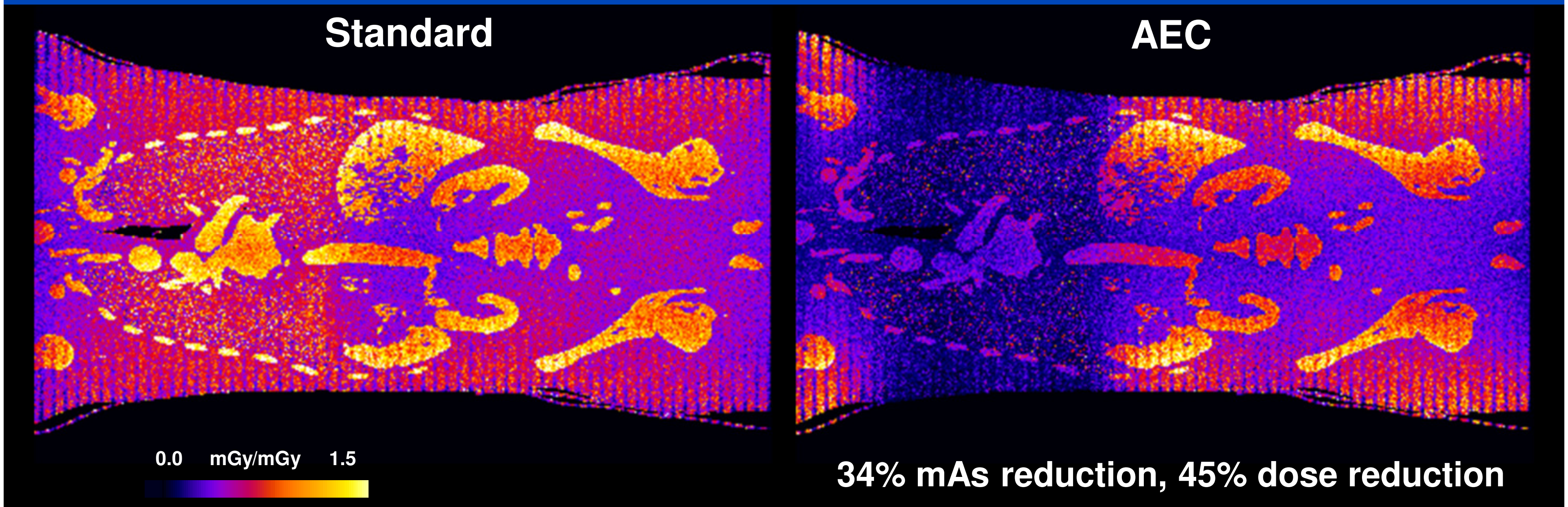

Siemens X-Care

- X-Care: organ-based dose modulation mode can selectively limit the radiation exposure of sensitive organs, for instance, the breast or the eyes.
- Hence, the radiation intensity is reduced when the patient is irradiated in the front.

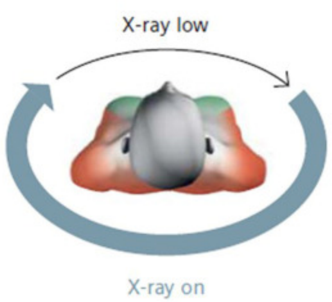

Illustration of the X-CARE principle.

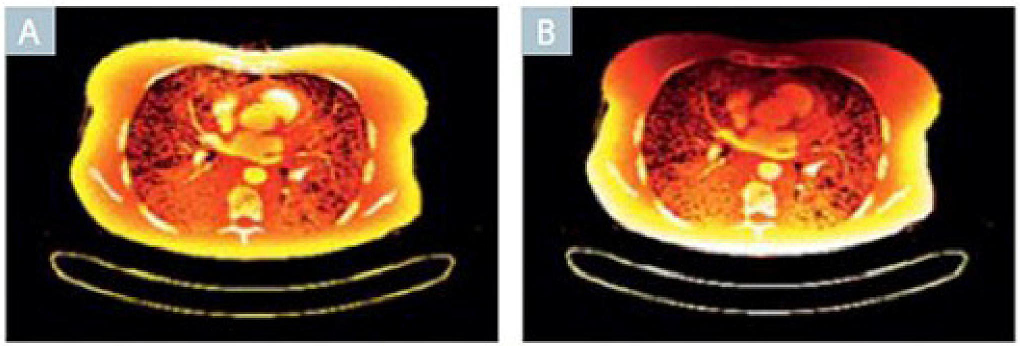

A: Radiation doses without X-CARE and B: with X-CARE. Darker areas indicate lower absorbed dose.

Scatter

Scatter

μ: Linear attenuation coefficient

d: Intersection length

$I_{\rm p}$: Primray intensity

$I_{\rm s}$: Scatter intensity

$I_{\rm ps}$: Measured intensity (primary and scatter)

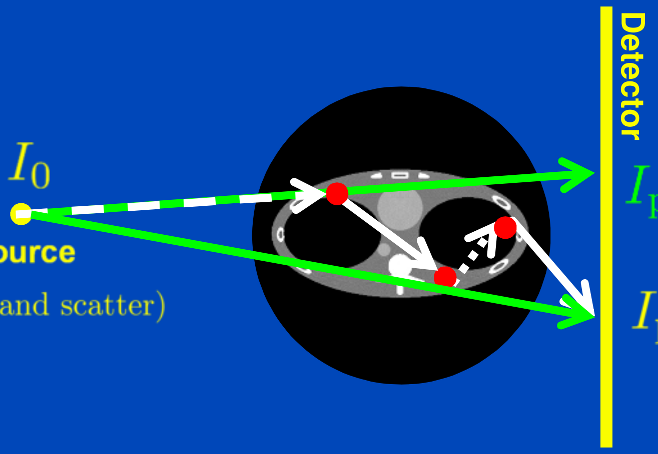

$$I_{\rm p} = I_0 \cdot e^{-\mu \cdot d}$$

$$I_{\rm ps} = I_{\rm p} + I_{\rm s}$$

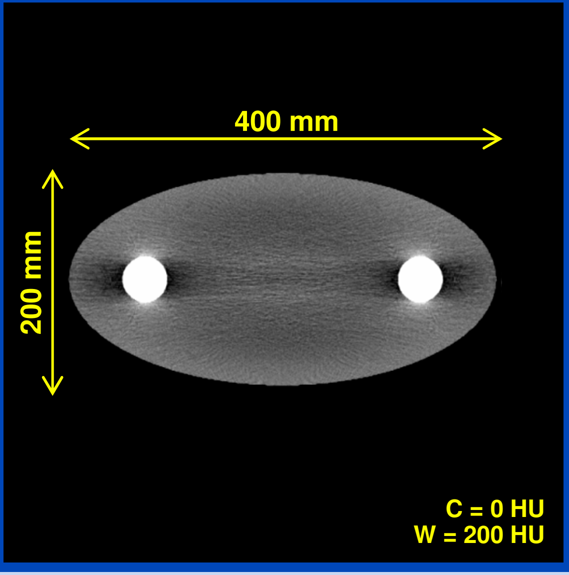

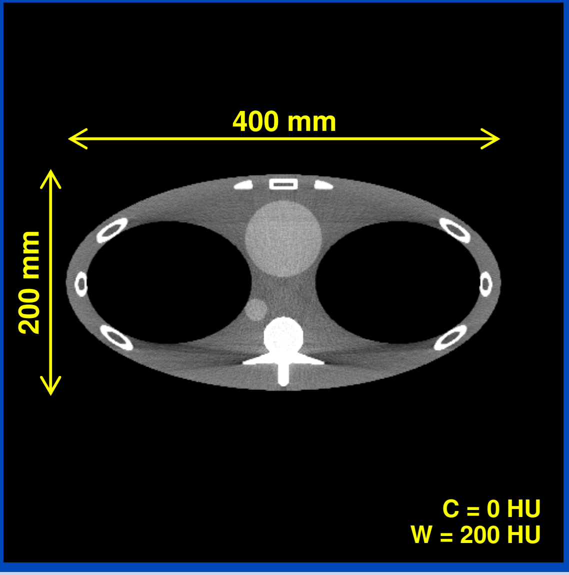

Scatter Artifact Reduction

- Several algorithmic methods found in the literature:
  - Monte Carlo-based (slow but good)
  - Convolution-based (fast, but not accurate)
  - Simple subtraction methods (even faster, but even less accurate)
  - …
- Hardware-based methods
  - Anti scatter grid
  - Beam blockers
  - Primary modulators
  - …
- Nice two-part review paper
  - Rührnschopf and Klingenbeck, Med. Phys., 38(7), 4296 –4311, 2011.
  - Rührnschopf and Klingenbeck, Med. Phys., 38(9), 5186– 5199, 2011.

Kernel-Based Scatter Estimation

3D Point Spread Scatter Kernels

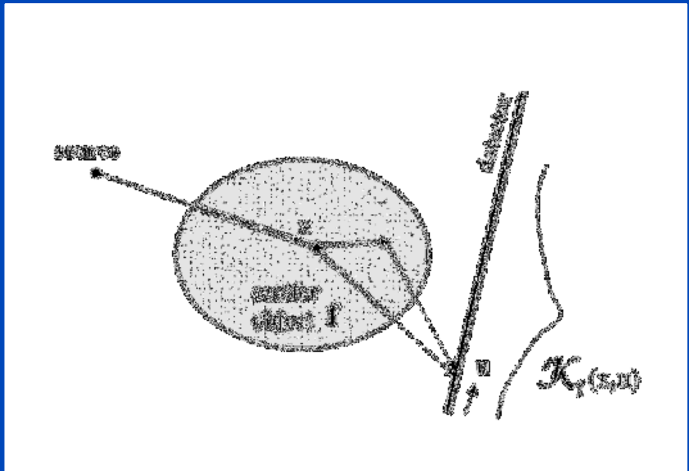

$$I_\mathrm{s}(\boldsymbol{u}) = \int \Phi(I_\mathrm{ps}(\boldsymbol{x}))\, K_{\boldsymbol{f}}(\boldsymbol{x},\boldsymbol{u})d\boldsymbol{x}$$

High complexity due to 3D integration

2D Beam Spread Scatter Kernels

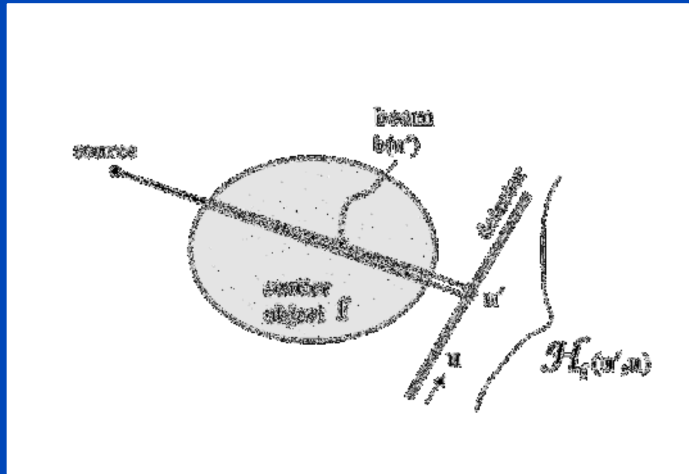

$$I_\mathrm{s}(\boldsymbol{u}) = \int \Phi(I_\mathrm{ps}(\boldsymbol{u}'))\, H_{\boldsymbol{f}}(\boldsymbol{u}',\boldsymbol{u})d\boldsymbol{u}'$$

Reduced complexity due to 2D integration

Scatter intensity I_s is expressed as an integral transform of the scatter potential $\Phi(I_{ps})$ (I_{ps}: Measured intensity) multiplied by a scatter kernel K_f respectively H_f.
In general K and H may depend on may parameters f, e.g. detector coordinates, tube voltage, projection angle, object, scatter geometry, …

Kernel-Based Scatter Estimation

- **Approximation of the scatter distribution $I_{\mathrm{s,\ est}}$ as an integral transform of the scatter source term $T(p)$ and a scatter propagation kernel $G(\boldsymbol{u}, \boldsymbol{u}', \boldsymbol{c})$:**

$$\begin{aligned} I_{\mathrm{s,\ est}}(\boldsymbol{u}) &= \int T(p)(\boldsymbol{u}')G(\boldsymbol{u}, \boldsymbol{u}', \boldsymbol{c})d\boldsymbol{u}' \\ &\approx T(p)(\boldsymbol{u}) * G(\boldsymbol{u}, \boldsymbol{c}) \end{aligned}$$

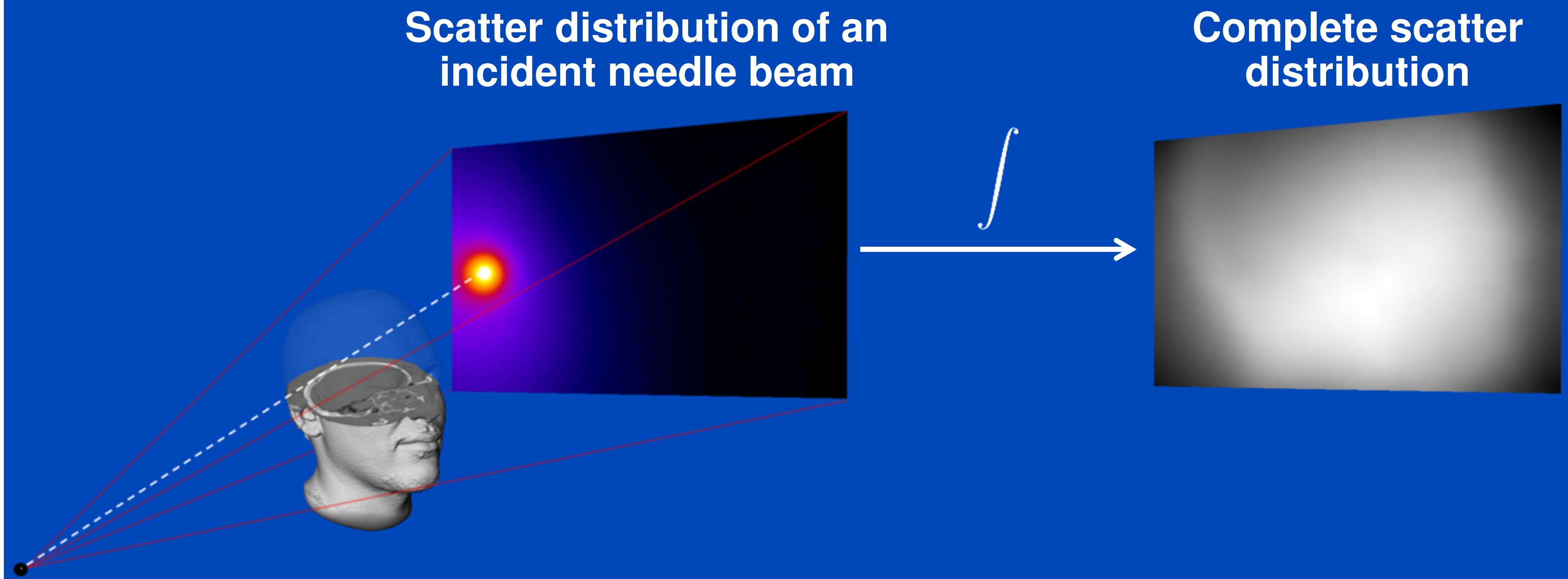

PEP

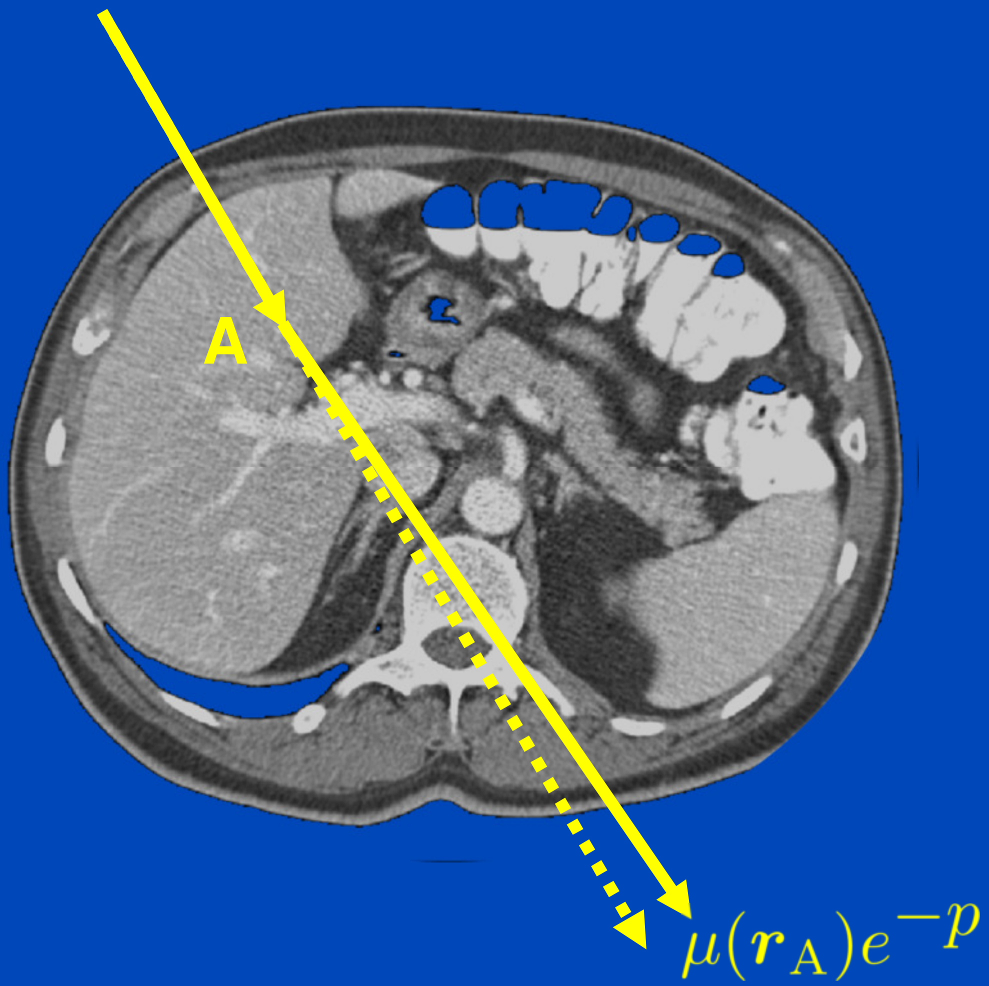

PEP

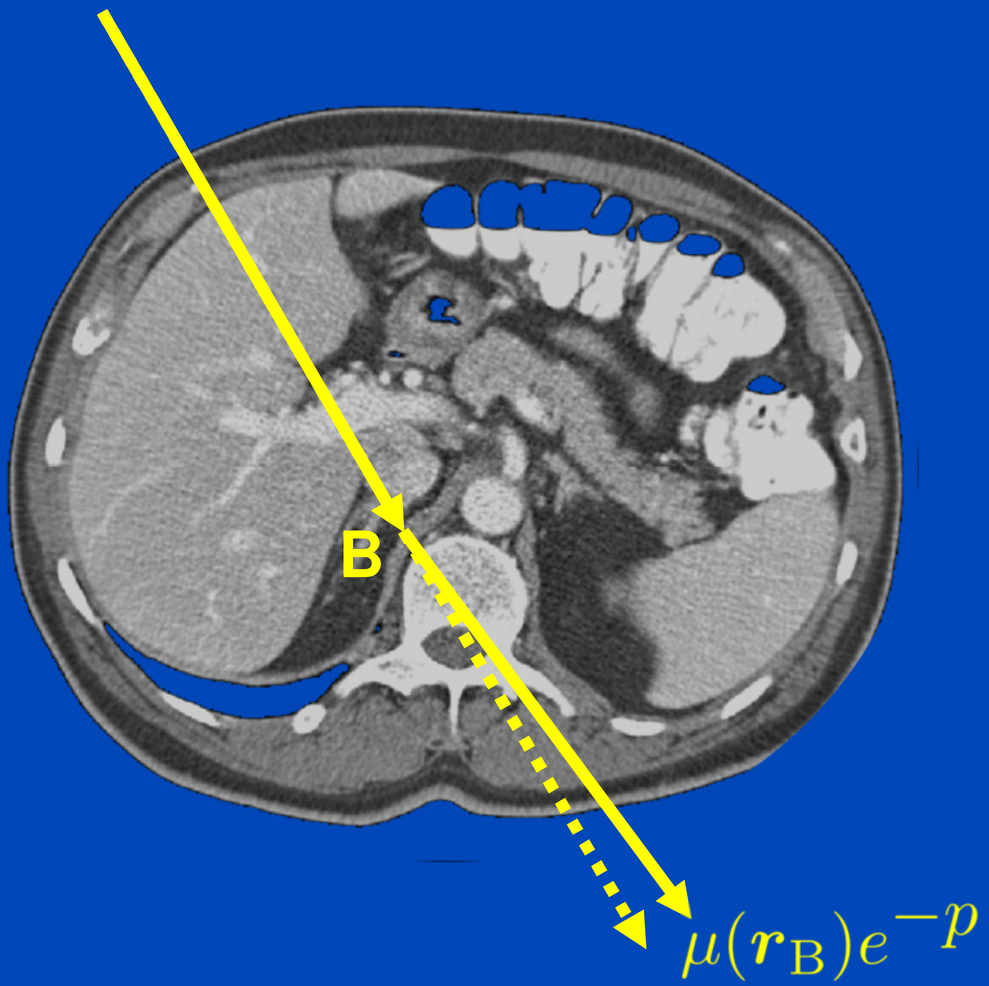

dkfz.

PEP

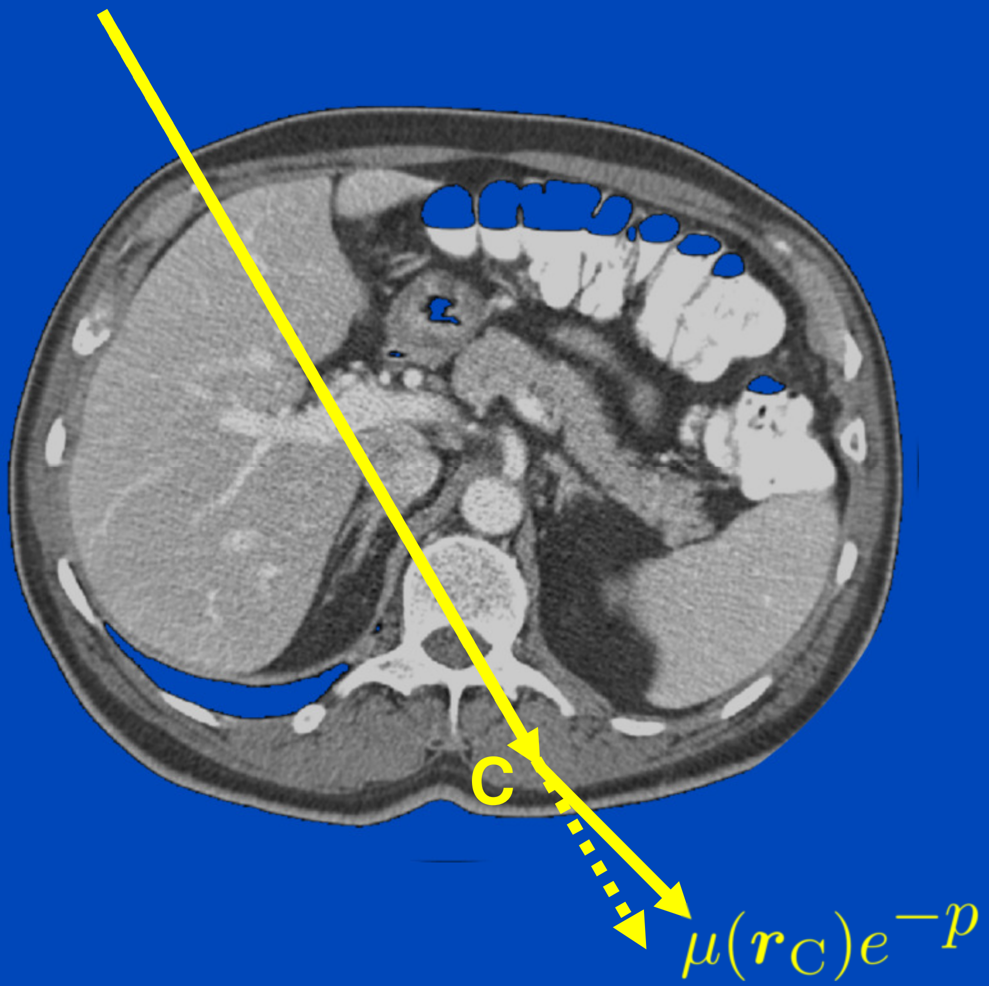

PEP

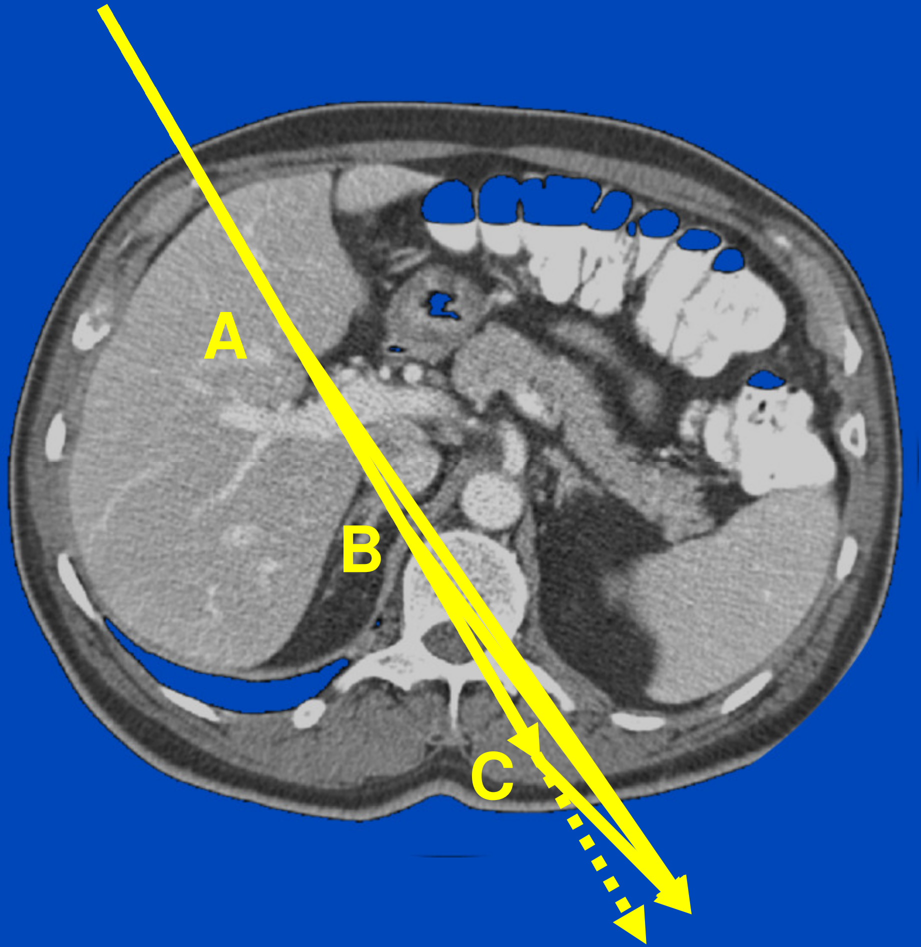

$$\big(\mu(\boldsymbol{r}_\mathrm{A})+\mu(\boldsymbol{r}_\mathrm{B})+\mu(\boldsymbol{r}_\mathrm{C})\big)e^{-p}=p\,e^{-p}$$

Kernel-Based Scatter Estimation

- 3D vs. 2D kernels
- Shift variant vs. shift invariant kernels
- Accuracy
- Speed

Monte-Carlo-Based Scatter Estimation

- Gold standard
- Accurate
- Slow

Scatter Estimation

Monte Carlo-based

Measured intensities (primary plus scatter)

Reconstruction

Simulation of physical photon paths based on density and material distribution

Physical effects:
Photo effect
Compton scattering
Rayleigh scattering

Monte Carlo-based scatter estimate $\hat{I}_{\mathrm{s}}^{\mathrm{MC}}$

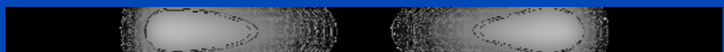

Patient-specific, many computations

Convolution-based

Measured intensities (primary plus scatter)

$$\hat{I}_{\mathrm{s}}^{\mathrm{CB}}(\boldsymbol{c}) = \Phi\big(I_{\mathrm{ps}}, \boldsymbol{c}\big) * K(\boldsymbol{c})$$

Convolution of the scatter potential Φ with scatter kernel K

I_{ps}: Primary plus scatter intensity

c (vector): Open coefficients

We used the convolution-based method of Ohnesorge et al.*

Convolution-based scatter estimate $\hat{I}_{\mathrm{s}}^{\mathrm{CB}}$

Not patient-specific, few computations

* Ohnesorge et al., Efficient scatter correction algorithm for third and fourth generation CT scanners, Eur. Radiol., 9, 563-569 (1999).

Hybrid Scatter Correction

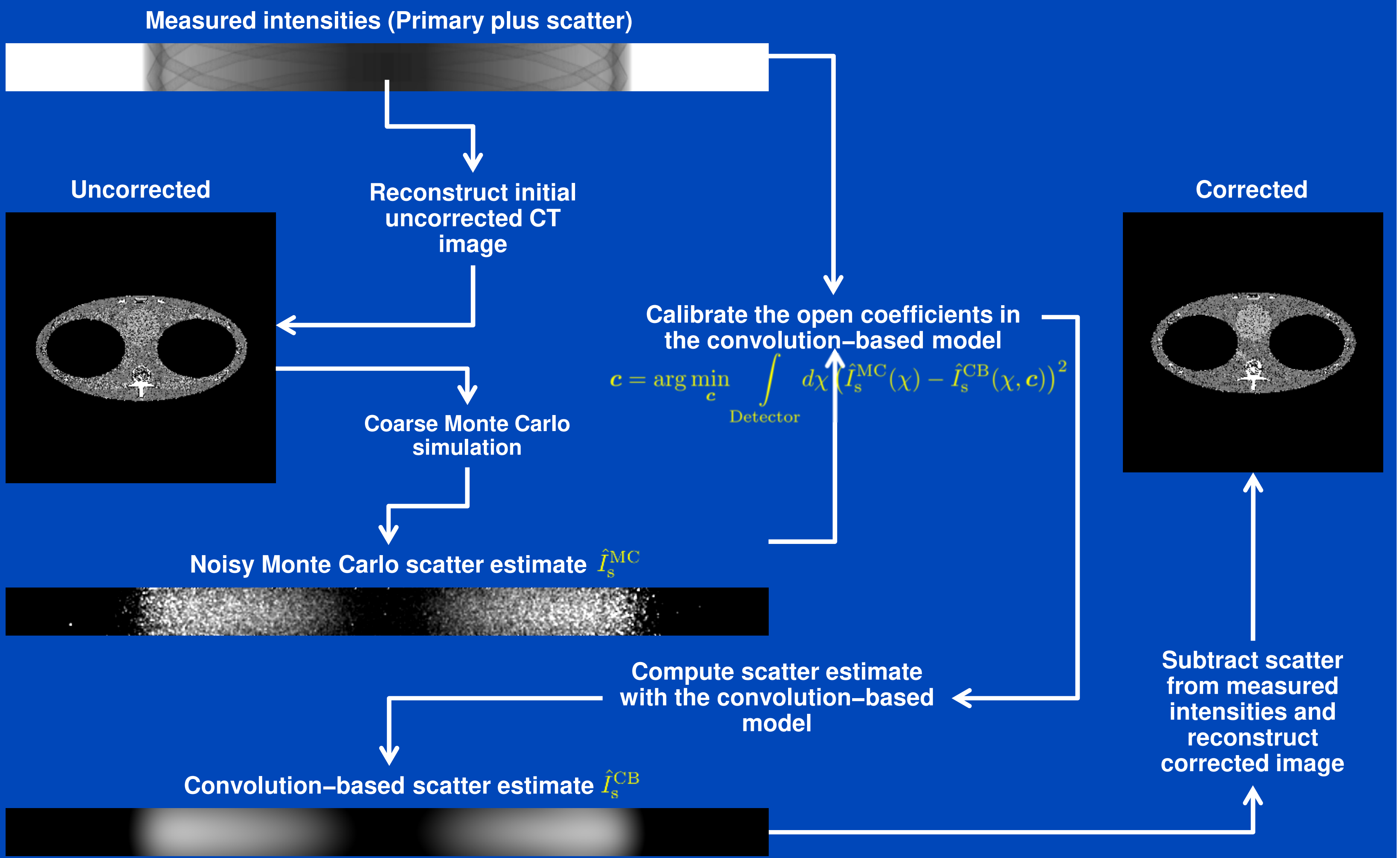

M. Baer and M. Kachelrieß. Hybrid scatter correction for CT imaging.
Phys. Med. Biol. 57(21):6849-6867, October 2012.

Scatter Correction Approaches in CT

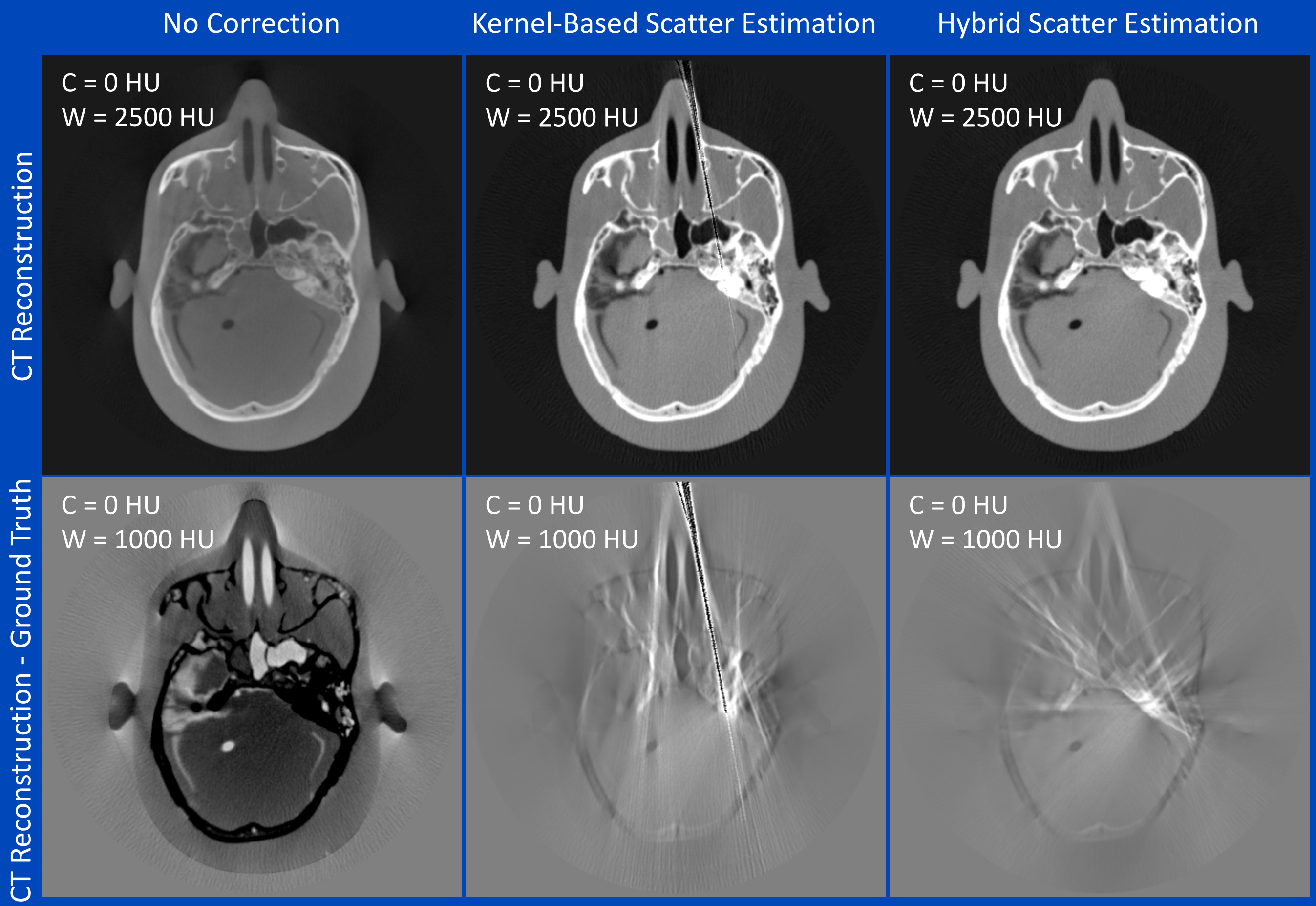

Detector: Efficiency

Motivation

- **Häufig wird die Detektoreffizienz wie folgt simuliert:**

$$\eta(E_\gamma) = 1 - e^{-\mu(E_\gamma)\cdot L} \quad \textbf{bzw.} \quad \eta(E_\gamma) = 1 - e^{-\mu_{\mathrm{tr}}(E_\gamma)\cdot L}$$

- **Oft ausreichend.**
- **Jedoch keine gute Übereinstimmung mit Monte-Carlo Simulationen**
- **Genaueres Modell für bessere Übereinstimmung**

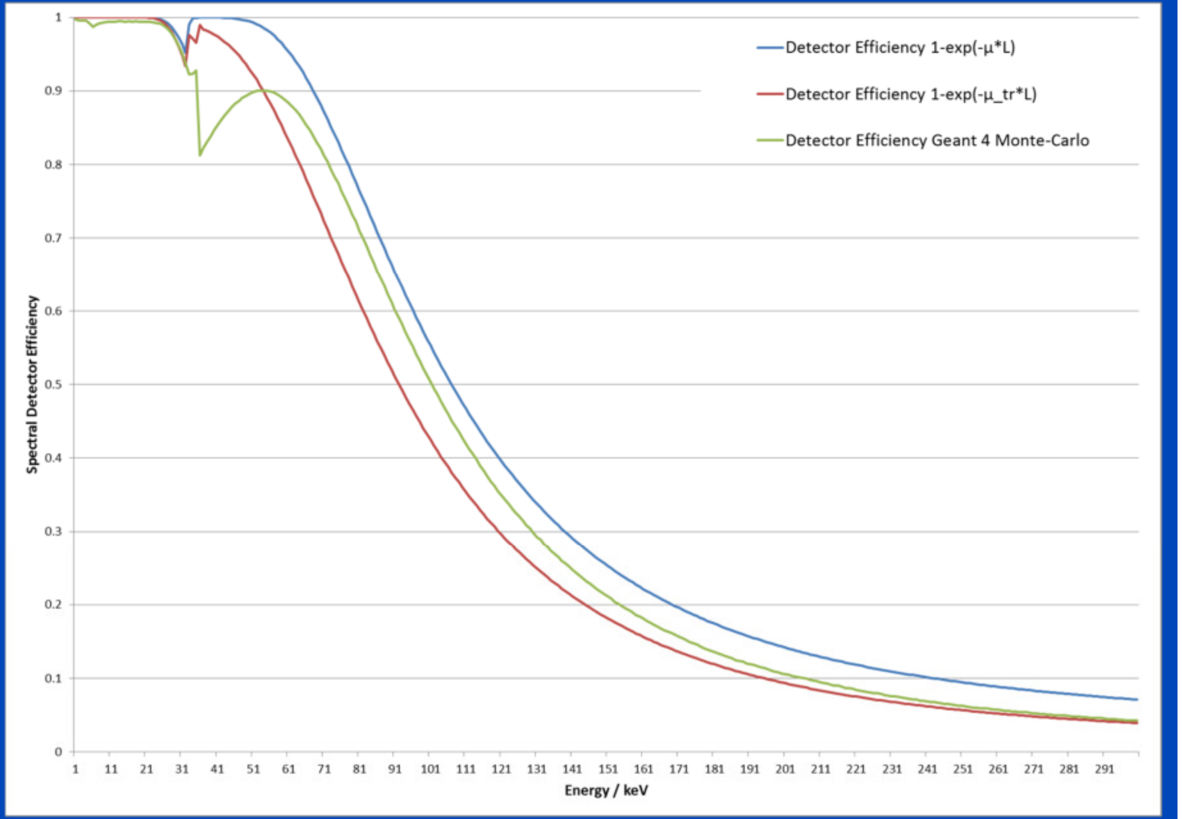

Mögliche Wechselwirkungen

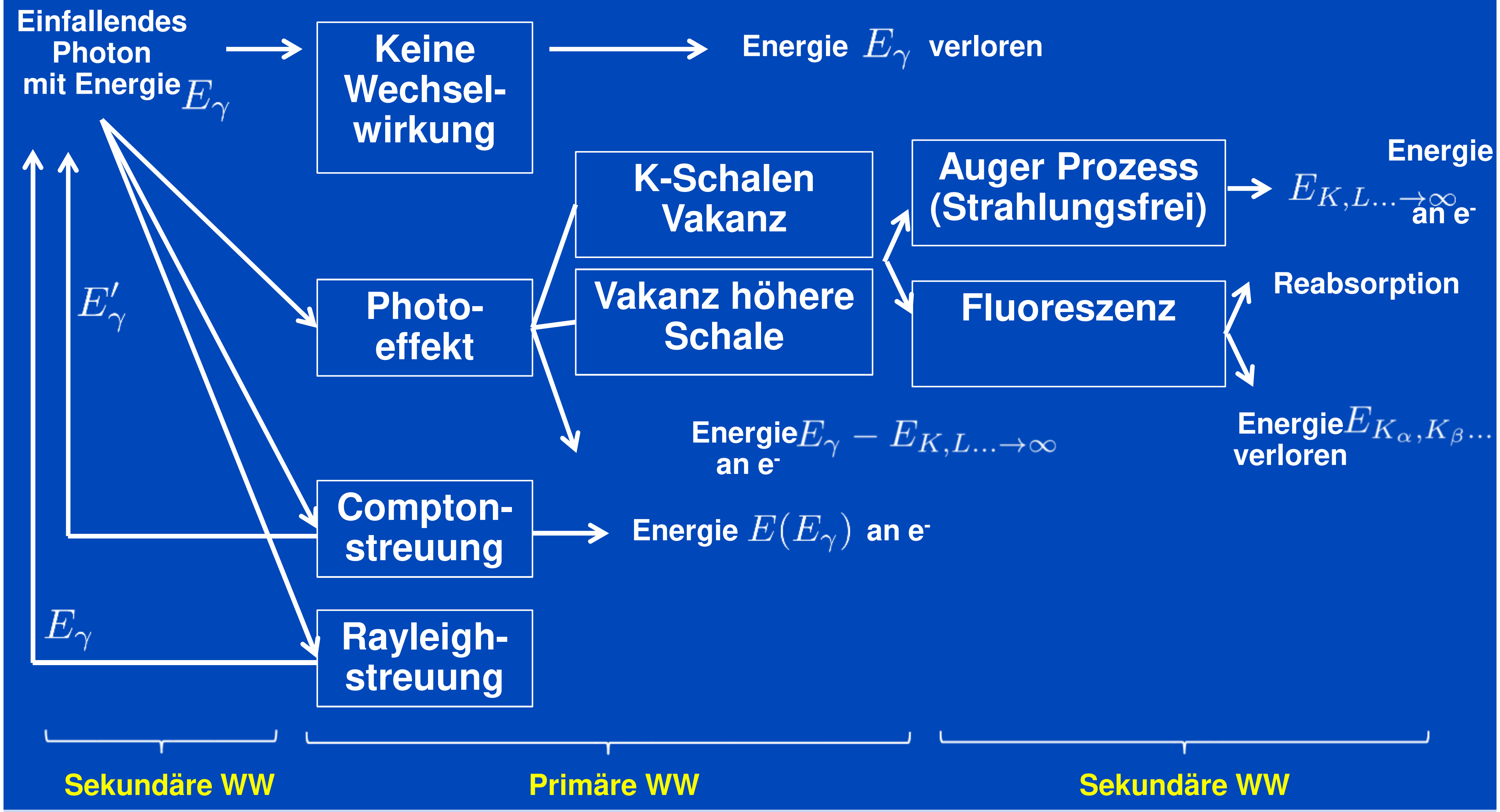

Detektoreffizienz

- Die Detektoreffizienz $\eta(E_\gamma)$ gibt den Anteil der einfallenden Energie zu der im Detektor absorbierten Energie an

$$\eta(E_\gamma) = \frac{E_{\text{in}}}{E_{\text{dep}}}$$

- Diese lässt sich wie folgt berechnen:

$$\eta(E_\gamma) = \frac{E_\gamma}{\int_{E=0}^{\infty} dE\, E\, w_{\text{dep}}(E)}$$

wobei $w_{\text{dep}}(E)$ die Wahrscheinlichkeitsdichte für eine Energiedeposition ist.

- Im Folgenden wird die Wahrscheinlichkeitsdichte wie folgt approximiert:

$$w_{\text{dep}}(E) = w_{\text{prim}}(E) + w_{\text{sec}}(E)$$

Detektoreffizienz
Vereinfachungen

- Keine Mehrfachstreuung
- Sekundärphotonen (Fluoreszenz- oder gestreute Photonen) übertragen ihre komplette Energie bei einer weiteren Wechselwirkung an das Szintillatormaterial
- Die komplette an das Szintillatormaterial übertragene Energie wird detektiert
- Linearer Zusammenhang zwischen Energie und optischen Photonen
- Photoeffekt:
  - Energie die auf Elektronen übertragen wird, wird komplett und lokal deponiert
  - Energieverlust nur durch K_α / K_β Escape. (L, M Fluoreszenzphotonen haben sehr geringe Reichweite und werden wieder absorbiert)

Wahrscheinlichkeitsdichte

Primäre Wechselwirkung

$$w_{\text{prim}}(E) = \int_{r=0}^{\infty} dr\, w_{\text{photo}}(r,E)\delta(E-E_\gamma)\left[1-\Theta(E-E_K)\,p_K\left(p_{K_\alpha}\frac{E_{K_\alpha}}{E_\gamma}+p_{K_\beta}\frac{E_{K_\beta}}{E_\gamma}\right)\right]$$
$$+\int_{r=0}^{\infty} dr\, w_{\text{compton}}(r,E)\delta(E-E_\gamma)\int_{\theta=0}^{\pi} d\theta\,\frac{d\sigma_{\text{compton}}}{d\theta}\left(1-\frac{1}{1+\frac{E}{m_e c^2}(1-\cos(\theta))}\right)$$

$w_{\text{photo}}(r,E)$ = Wahrscheinlichkeitsdichte für WW mittels Photoeffekt in Tiefe r

$w_{\text{compton}}(r,E)$ = Wahrscheinlichkeitsdichte für WW mittels Compton-Streuung in Tiefe r

δ = Delta-Funktion

Θ = Heaviside-Funktion

p_K = Wahrscheinlichkeit für Anregung der K-Schale

p_{K_α} = Wahrscheinlichkeit für Emission K_α Photon $(L \rightarrow K)$

p_{K_β} = Wahrscheinlichkeit für Emission K_β Photon $(M \rightarrow K)$

$\frac{d\sigma}{d\theta}_{\text{compton}}$ = Differentieller Wirkungsquerschnitt für Compton-Streuung

$E-\frac{E}{1+\frac{E}{m_e c^2}(1-\cos(\theta))}$ = Energie des Compton-Elektrons

Wahrscheinlichkeitsdichte

Sekundäre Wechselwirkung

$$w_{\text{sec}}(E) = \int_{r=0}^{\infty} dr\, w_{\text{photo}}(r,E) \int_{\theta=0}^{\pi} d\theta\, \frac{d\sigma_{\text{photo}}}{d\theta}\, \delta(E-E_\gamma)$$
$$\left[\Theta(E-E_K)\, p_K \left(p_{K_\alpha}\, w_{\text{int}}(r,\theta,E_{K_\alpha}) \frac{E_{K_\alpha}}{E_\gamma} + p_{K_\beta}\, w_{\text{int}}(r,\theta,E_{K_\beta}) \frac{E_{K_\beta}}{E_\gamma}\right)\right]$$
$$+ \int_{r=0}^{\infty} dr\, w_{\text{compton}}(r,E)\delta(E-E_\gamma) \int_{\theta=0}^{\pi} d\theta\, w_{\text{int}}(r,\theta,E') \frac{d\sigma_{\text{compton}}}{d\theta} \left(\frac{1}{1+\frac{E}{m_e c^2}(1-\cos(\theta))}\right)$$
$$+ \int_{r=0}^{\infty} dr\, w_{\text{rayleigh}}(r,E)\delta(E-E_\gamma) \int_{\theta=0}^{\pi} d\theta\, w_{\text{int}}(r,\theta,E) \frac{d\sigma_{\text{rayleigh}}}{d\theta}$$

$$w_{\text{rayleigh}}(r) = \text{Wahrscheinlichkeitsdichte für WW mittels Rayleigh-Streuung in Tiefe } r$$
$$w_{\text{int}}(r,\theta,E) = \text{Wahrscheinlichkeitsdichte für Wechselwirkung}$$
$$\frac{d\sigma}{d\theta}_{\text{rayleigh}} = \text{Differentieller Wirkungsquerschnitt für Rayleigh-Streuung}$$
$$\frac{E}{1+\frac{E}{m_e c^2}(1-\cos(\theta))} = \text{Energie des Compton-Photons}$$

Wahrscheinlichkeit für Wechselwirkung

- **Wahrscheinlichkeit für eine Wechselwirkung zwischen r und $r + dr$ für ein Photon mit Energie E :**

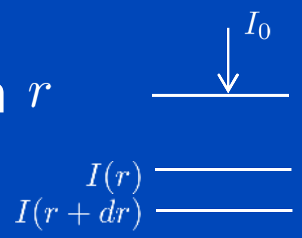

$$
\begin{aligned}
w_{\text{int}}(r,E)dr &= \frac{I(r,E) - I(r+dr,E)}{I_0(E)} \\
&= e^{-\int_0^r \mu(r',E)dr'} - e^{-\int_0^{r+dr} \mu(r',E)dr'} \\
&= e^{-\int_0^r \mu(r',E)dr'} - e^{-\int_0^r \mu(r',E)dr'} \cdot e^{-\int_r^{r+dr} \mu(r',E)dr'} \\
&= e^{-\int_0^r \mu(r',E)dr'} \cdot \left[1 - e^{-\int_r^{r+dr} \mu(r',E)dr'}\right] \\
&= e^{-\int_0^r \mu(r',E)dr'} \cdot \left[1 - e^{-M(r+dr,E)-M(r,E)}\right] \\
&= e^{-\int_0^r \mu(r',E)dr'} \cdot \left[1 - e^{-\frac{M(r+dr,E)-M(r,E)}{dr}dr}\right] \\
&= e^{-\int_0^r \mu(r',E)dr'} \cdot \left[1 - e^{-\mu(r,E)dr}\right] \\
&= e^{-\int_0^r \mu(r',E)dr'} \cdot [1 - 1 + \mu(r,E)dr] \\
&= e^{-\int_0^r \mu(r',E)dr'} \cdot \mu(r,E)dr
\end{aligned}
$$

Wahrscheinlichkeitsdichte

Wechselwirkung der einzelnen Effekte

- Wahrscheinlichkeitsdichte für eine Wechselwirkung mittels Photoeffekt:

$$\begin{aligned} w(r,E)_{\text{photo}} &= w_{\text{int}}(r,E)p_{\text{photo}}(r,E) \\ &= w_{\text{int}}(r,E)\frac{\mu_{\text{photo}}(r,E)}{\mu(r,E)} \end{aligned}$$

- Wahrscheinlichkeitsdichte für eine Wechselwirkung mittels Compton Streuung:

$$\begin{aligned} w(r,E)_{\text{compton}} &= w_{\text{int}}(r,E)p_{\text{compton}}(r,E) \\ &= w_{\text{int}}(r,E)\frac{\mu_{\text{compton}}(r,E)}{\mu(r,E)} \end{aligned}$$

- Wahrscheinlichkeitsdichte für eine Wechselwirkung mittels Rayleigh Streuung:

$$\begin{aligned} w(r,E)_{\text{rayleigh}} &= w_{\text{int}}(r,E)p_{\text{rayleigh}}(r,E) \\ &= w_{\text{int}}(r,E)\frac{\mu_{\text{rayleigh}}(r,E)}{\mu(r,E)} \end{aligned}$$

Wahrscheinlichkeit für Fluoreszenz

- Die Wahrscheinlichkeit, dass beim Photo-Effekt ein Elektron aus der K-Schale angeregt wird, kann wie folgt approximiert werden:

$$p_K = \frac{\mu(E_K + \epsilon) - \mu(E_K - \epsilon)}{\mu(E_K - \epsilon)}$$

- Die Wahrscheinlichkeiten für K-alpha Emission p_{K_α} und K-beta Emission p_{K_β} sind tabelliert.

Berechnung der Detektoreffizienz

- **Die Detektoreffizienz ist gegeben durch:**

$$\eta(E_\gamma) = \frac{E_\gamma}{\int_{E=0}^{\infty} dE\, E\, w_{\text{dep}}(E)} \approx \frac{E_\gamma}{\int_{E=0}^{\infty} dE\, E\, w_{\text{prim}}(E) + w_{\text{sec}}(E)}$$

- **Für jede Energie wird die Detektoreffizienz durch numerische Integration der Gleichungen für w_{prim} und w_{sec} berechnet**

Ergebnisse

0.3 mm CsI Szintillator

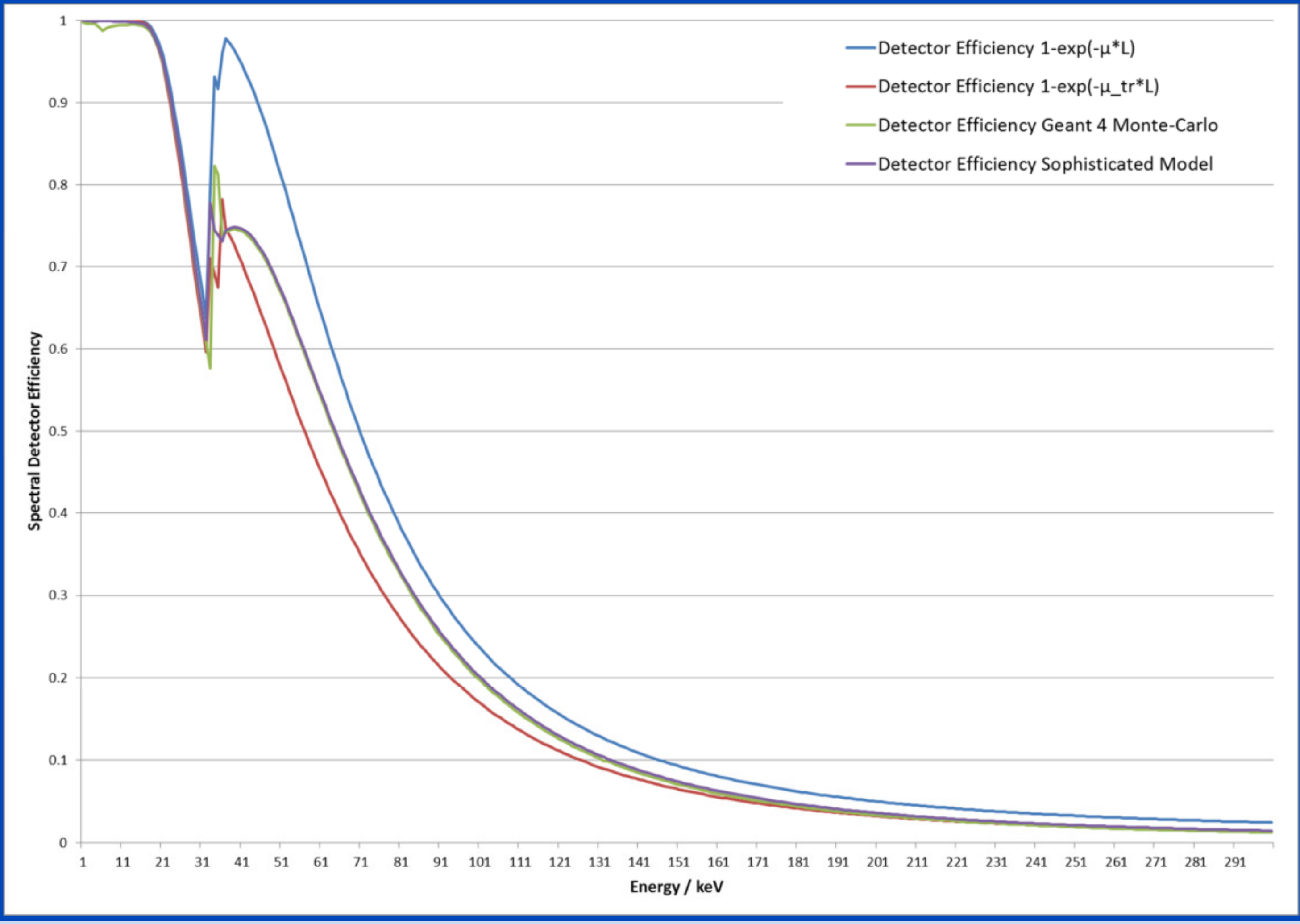

Ergebnisse

0.6 mm CsI Szintillator

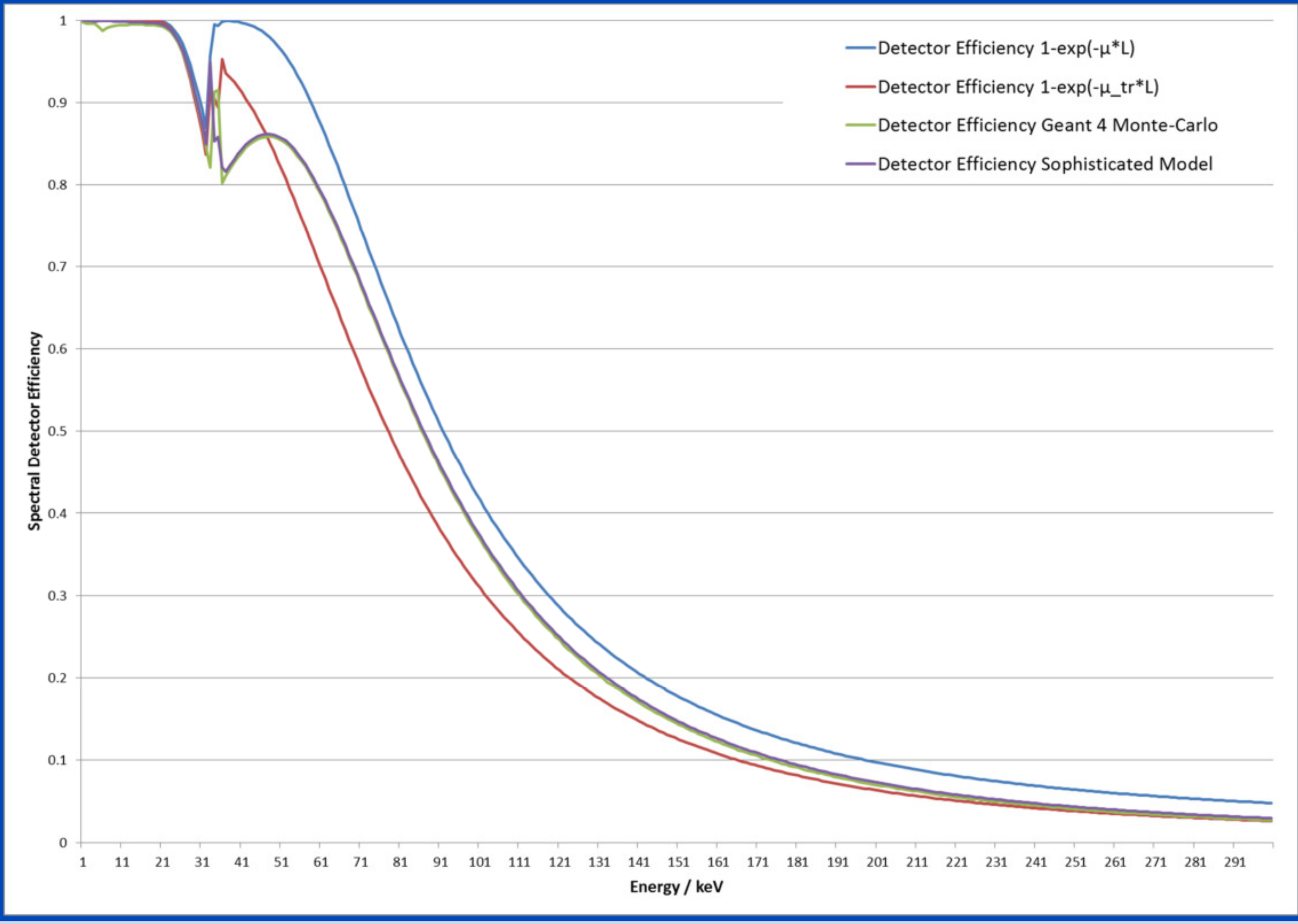

Ergebnisse

0.9 mm CsI Szintillator

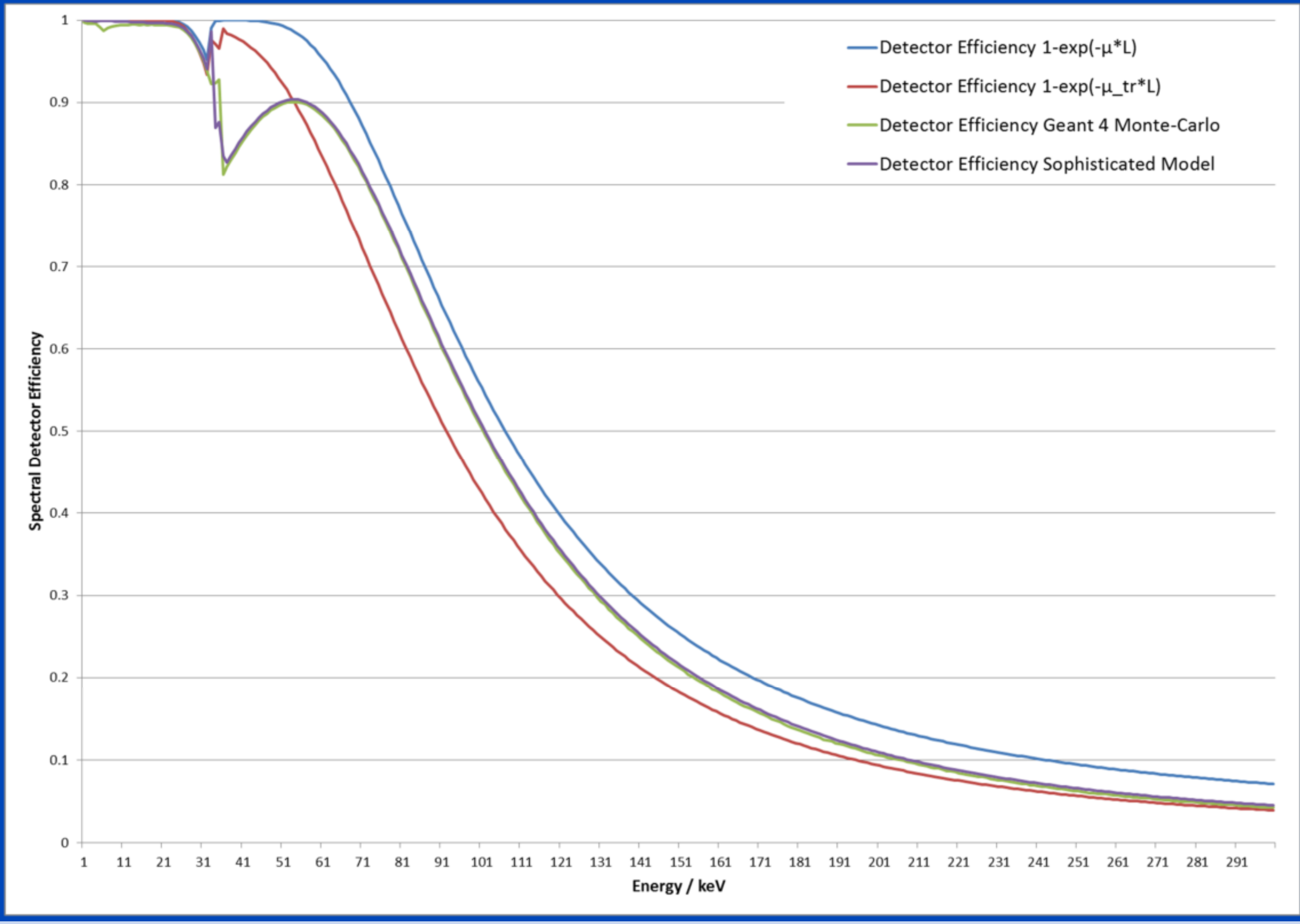

Ergebnisse

1.2 mm CsI Szintillator

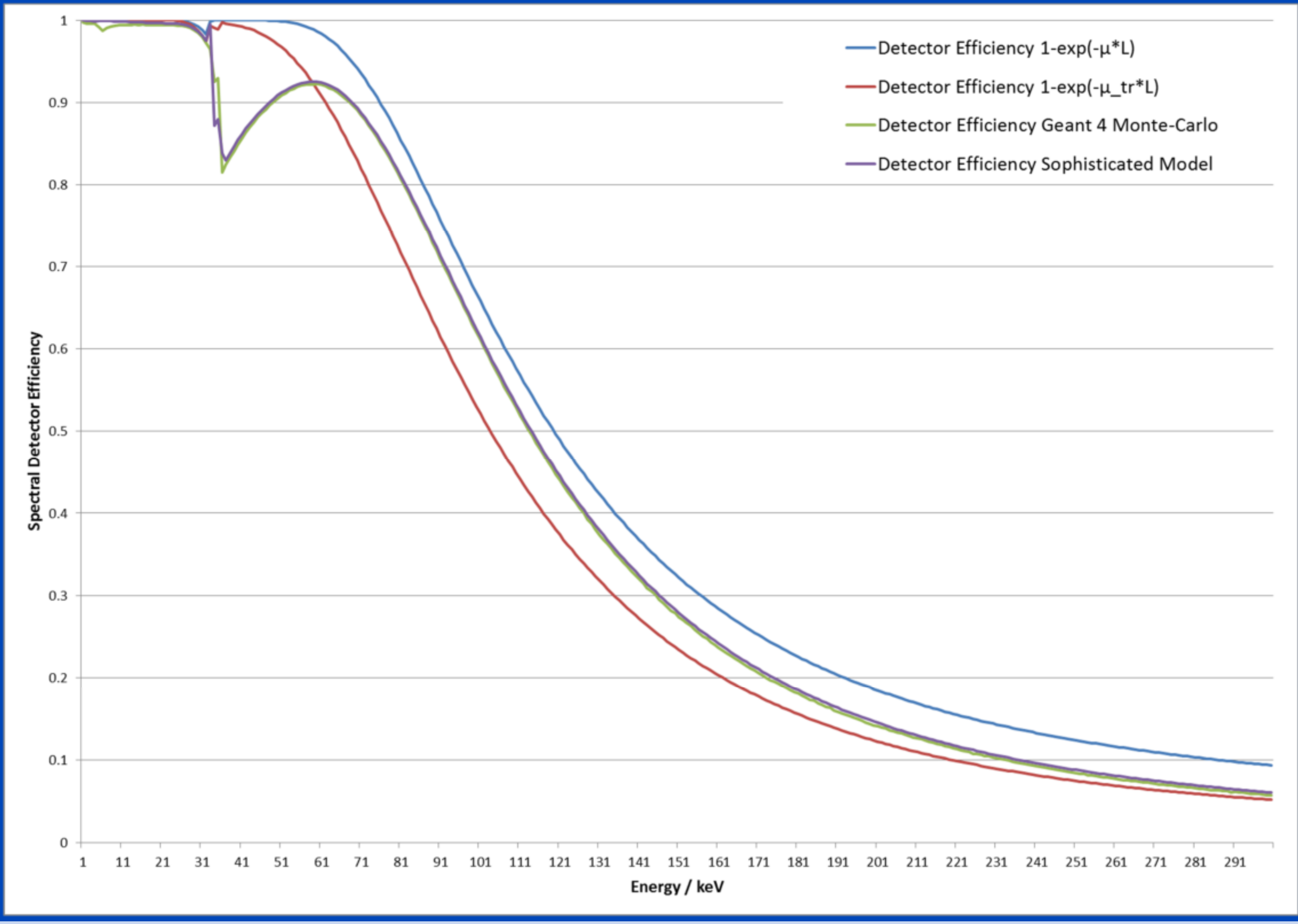

Detector: Photon Counting

Future, Photon Counting (≥ 2020)?

Macro

12	12	12	12
12	12	12	12
12	12	12	12
12	12	12	12

Chess

12	34	12	34
34	12	34	12
12	34	12	34
34	12	34	12

4×4 subpixels of 225 µm size = 0.9 mm pixels
(0.5 mm at isocenter)

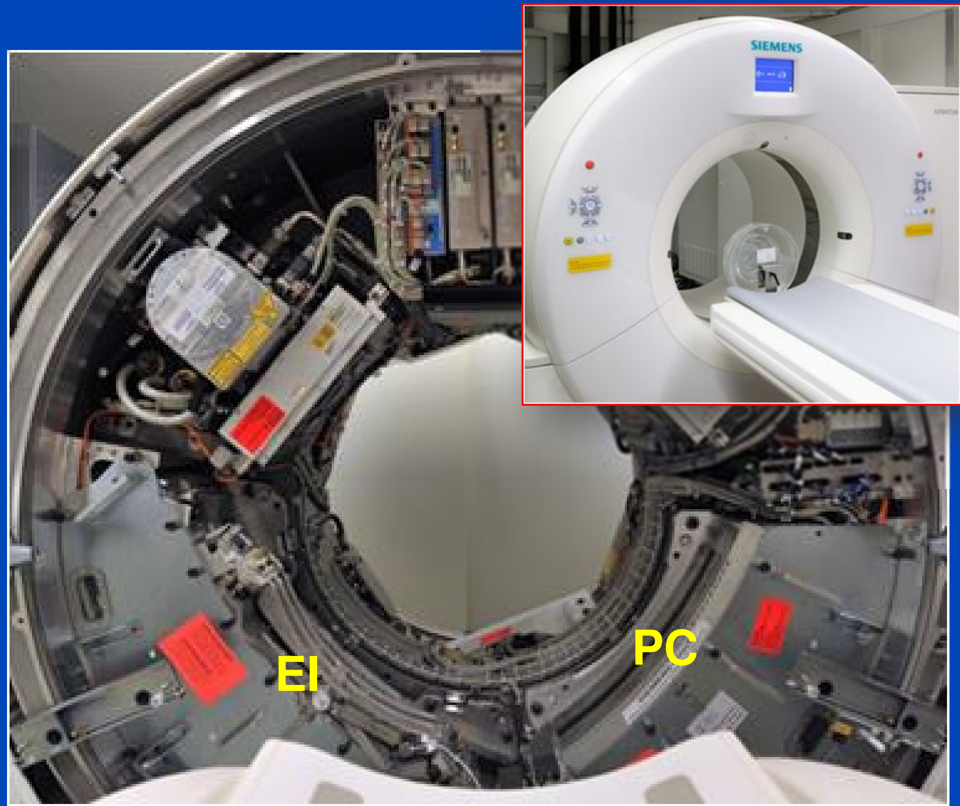

This photon-counting whole-body CT prototype, installed at the Mayo Clinic and at the NIH, is a DSCT system. However, it is restricted to run in single source mode. The second source is used for data completion and for comparisons with EI detectors.

Readout Modes of the Siemens CounT

Macro Mode
1×2 readouts
16 mm z-coverage

12	12	12	12
12	12	12	12
12	12	12	12
12	12	12	12

Chess Mode
2×2 readouts
16 mm z-coverage

12	34	12	34
34	12	34	12
12	34	12	34
34	12	34	12

Sharp Mode
5×1 readouts
12 mm z-coverage

1	1	1	1
1	1	1	1
1	1	1	1
1	1	1	1

2	2	2	2
2	2	2	2
2	2	2	2
2	2	2	2

UHR Mode
4×2 readouts
8 mm z-coverage

12	12	12	12
12	12	12	12
12	12	12	12
12	12	12	12

No FFS on thread B (photon counting detector).
4×4 subpixels of 225 µm size = 0.9 mm pixels (0.5 mm at isocenter).
The whole detector consists of 128×1920 subpixels = 32×480 macro pixels.

First Peer Reviewed Publication on CounT from NIH February 2016

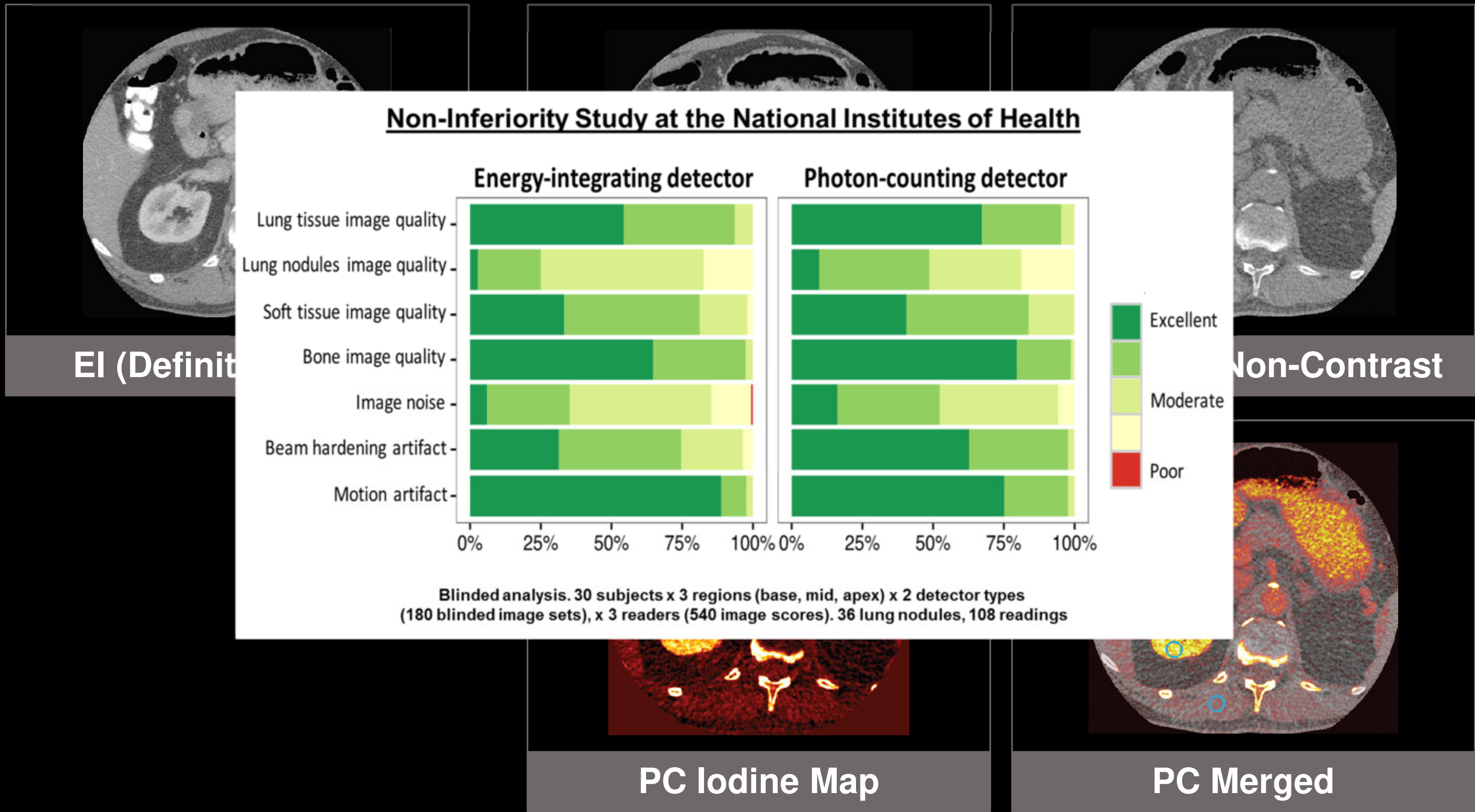

Courtesy of National Institutes of Health, Berthesda, USA

Pourmorteza A et al., Abdominal Imaging with Contrast-enhanced Photon-counting CT: First Human Experience. Radiology. 2016 Apr;279(1):239-45

Photon Events

- Detection process in the sensor
- Photoelectric effect (e.g. 80 keV)

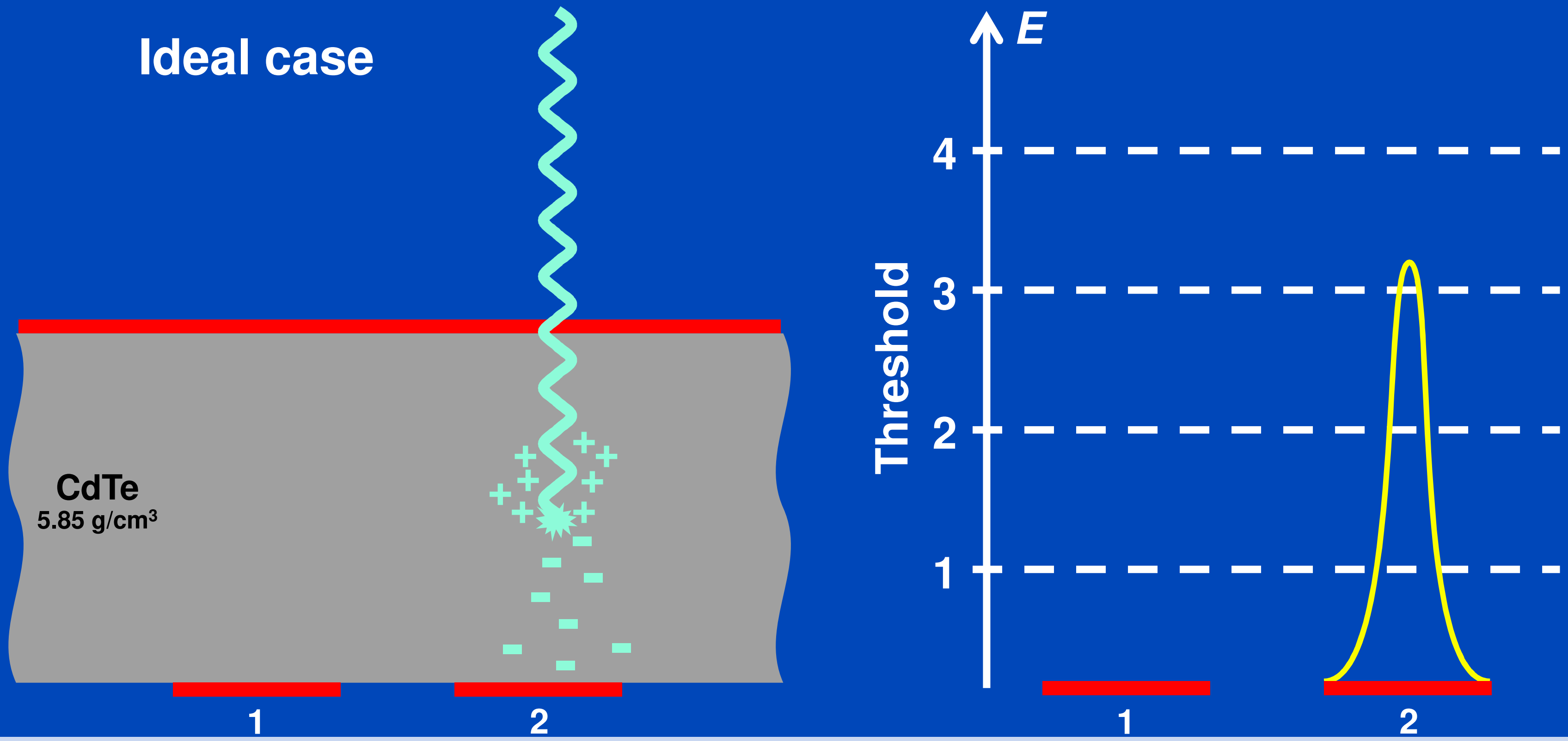

Photon Events

- Detection process in the sensor
- Compton scattering or K-fluorescence (e.g. 80 keV)

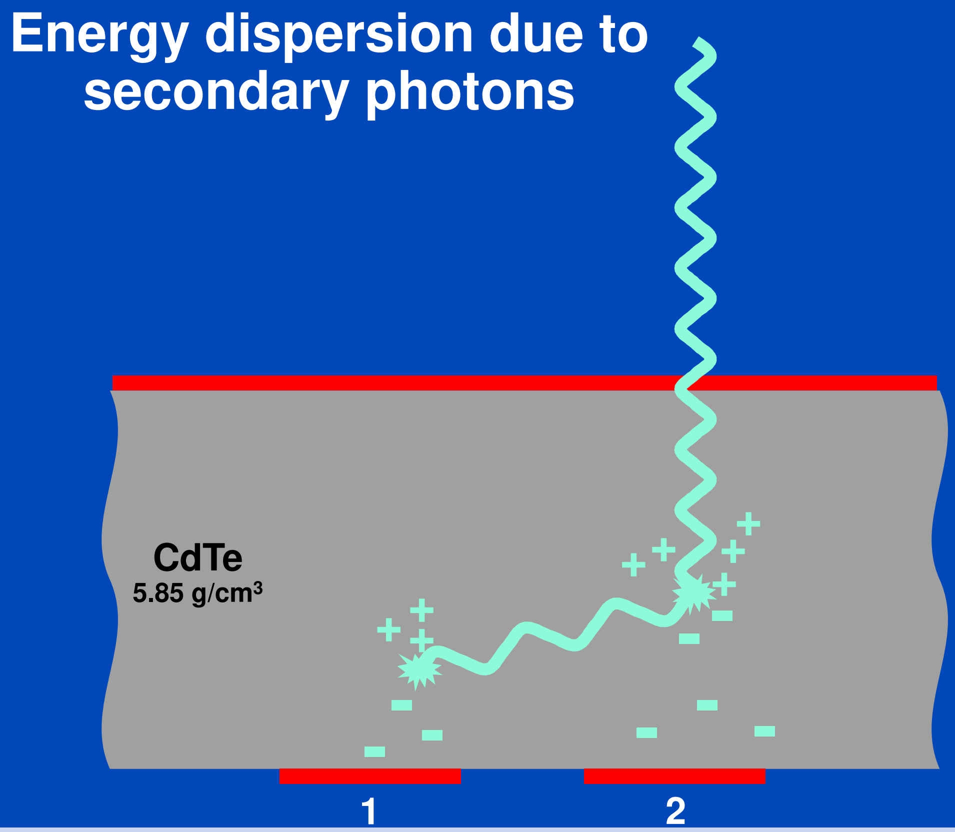

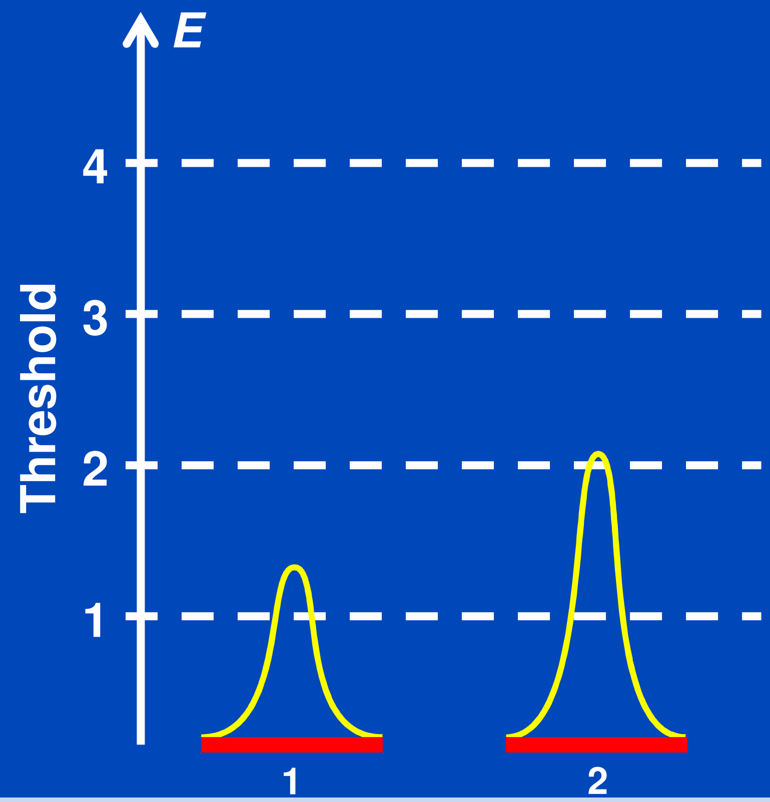

Photon Events

- Detection process in the sensor
- Photoelectric effect (e.g. 80 keV)

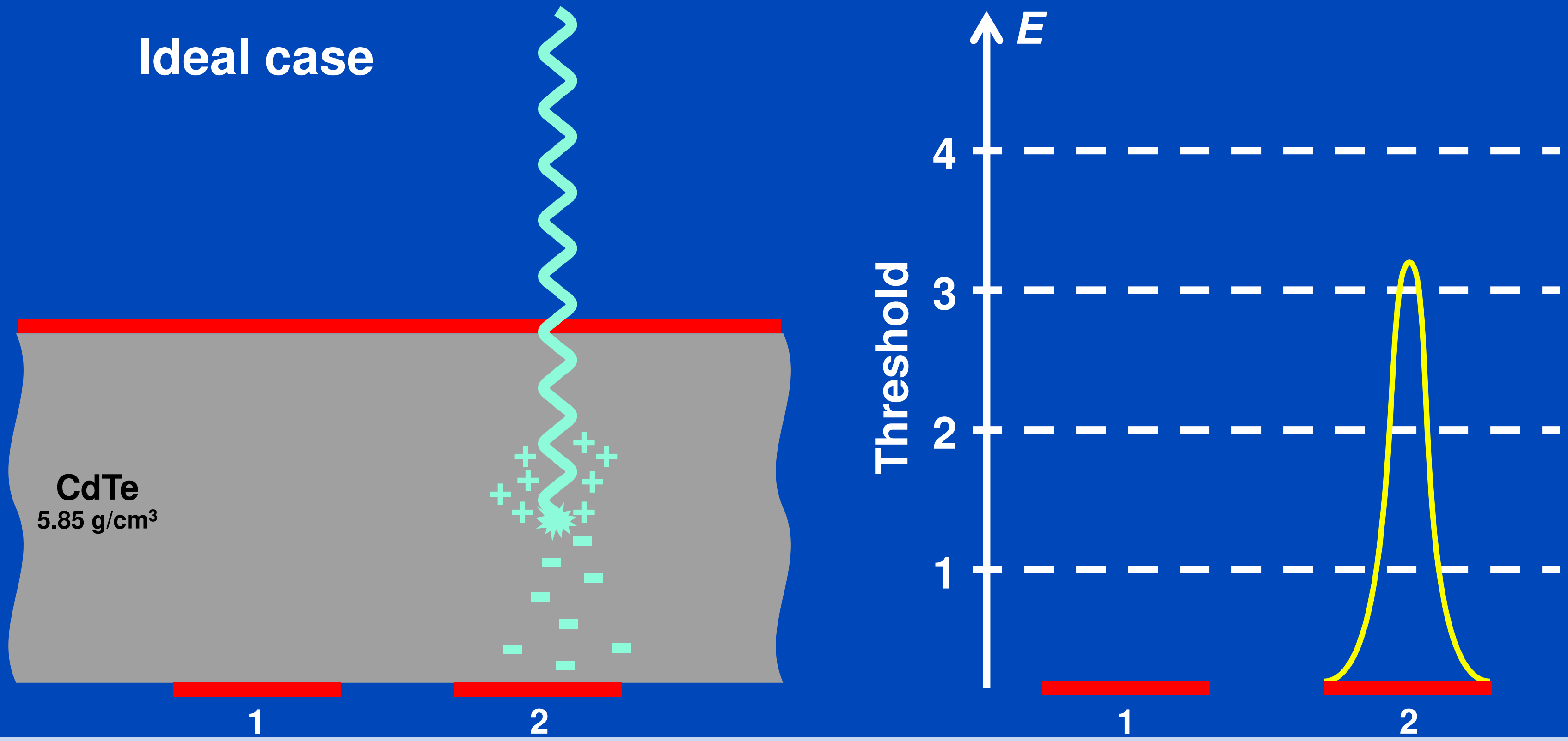

Photon Events

- Detection process in the sensor
- Photoelectric effect (e.g. 30 keV), charge sharing

Energy dispersion due to charge diffusion

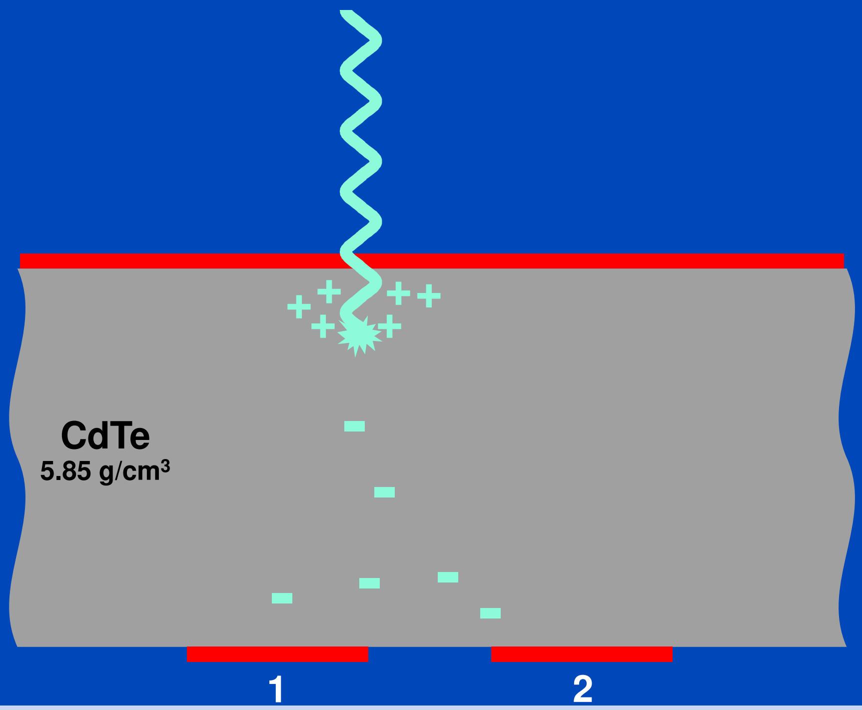

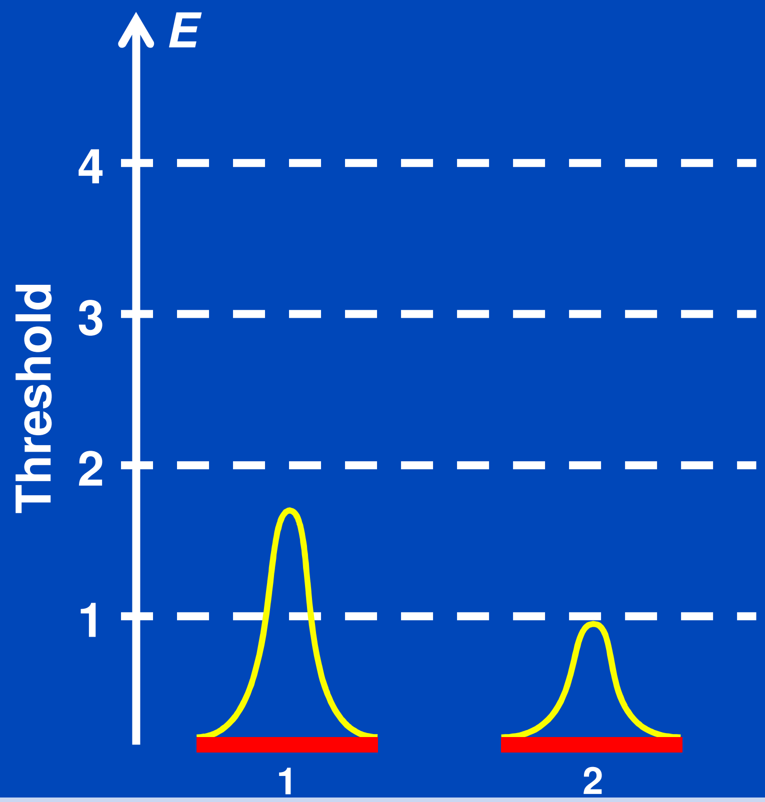

Clarification on the Escape Peaks

- **K-alpha escape peaks at energy $E_0 - E_{K\alpha}$**
  Incident photon energy E_0, K-alpha energy $E_{k\alpha}$ (which is 23.2 keV for Cd and 27.5 for Te)

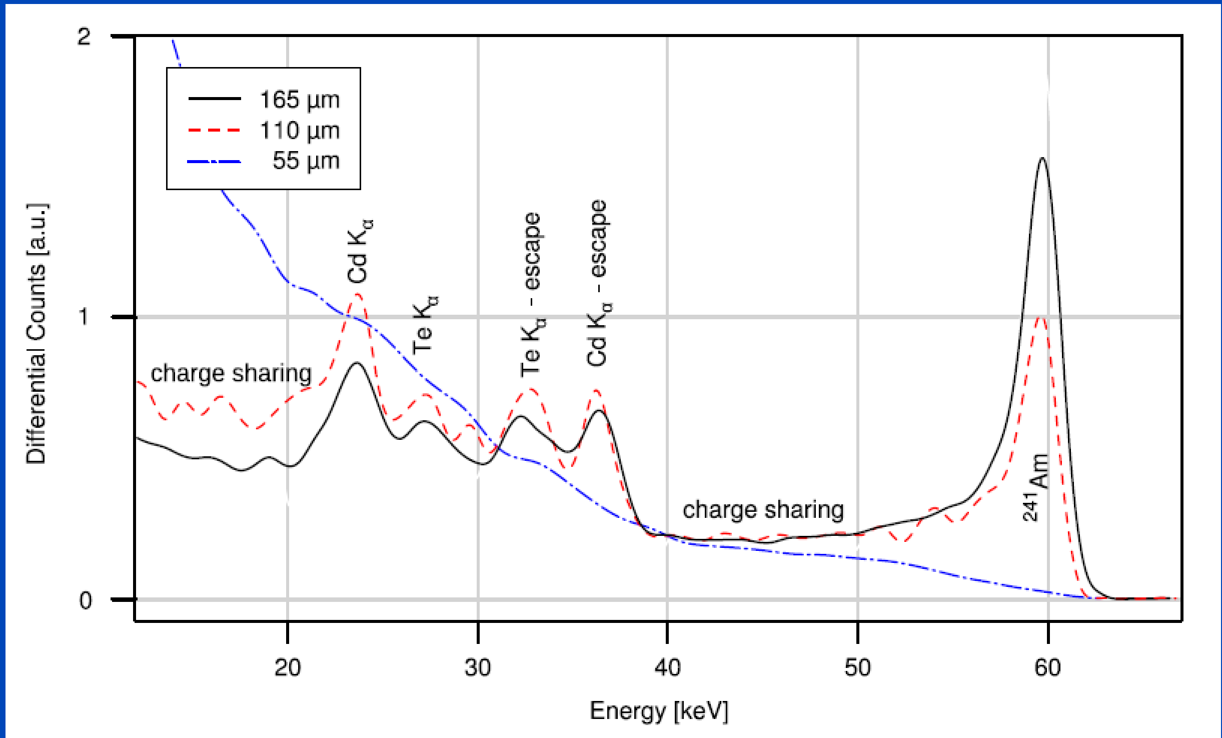

[T. Koenig et al., „Imaging properties of small-pixel spectroscopic x-ray detectors based on cadmium telluride sensors," Phys. Med. Biol. 57, 6743, 2012.]

Clarification on the Escape Peaks

- Incoming photon with E_0 interacts via photo effect and ejects electron with kinetic energy $E_0 – E_b$, i.e. E_0 reduced by the binding energy E_b of the K-shell electron
- Electron energy is registered by detector
- Empty shell positions are successively filled by electrons from higher shells emitting x-rays (mainly K_α and then, e.g., L_α)
- Only if all secondary x-rays are detected in the same pixel, the full energy E_0 will be measured
- K_α x-rays have highest energy and are likely to escape the detector or to be registered in a different pixel or not at all

[Diss. Martin Sedlmair, LMU München, 2009]

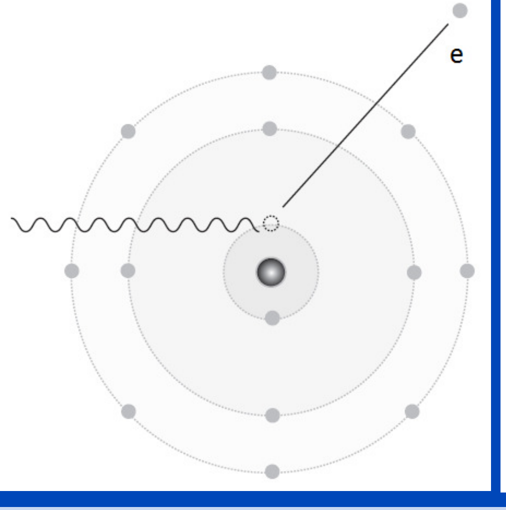

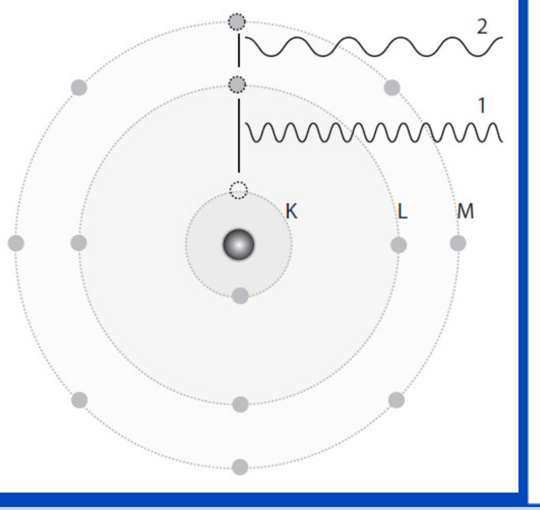

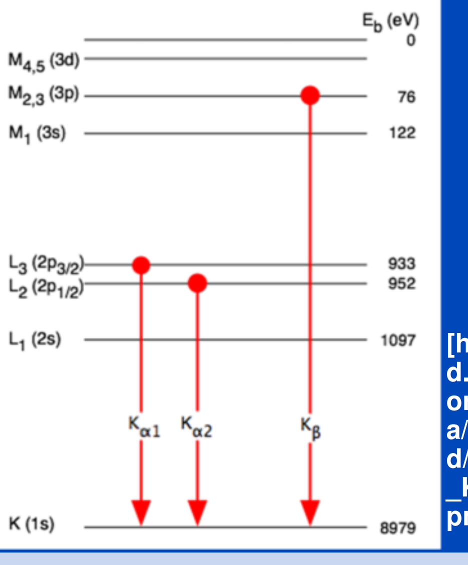

[http://upload.wikimedia.org/wikipedia/commons/d/d8/Copper_K_Rontgen.png]

Increment Matrices

$$I_{b,n}(u,v)$$

n = number of event type
= number of increment matrix set

Ideal case | **Realistic case**

Low energy bin | **High energy bin** | **Low energy bin** | **High energy bin**

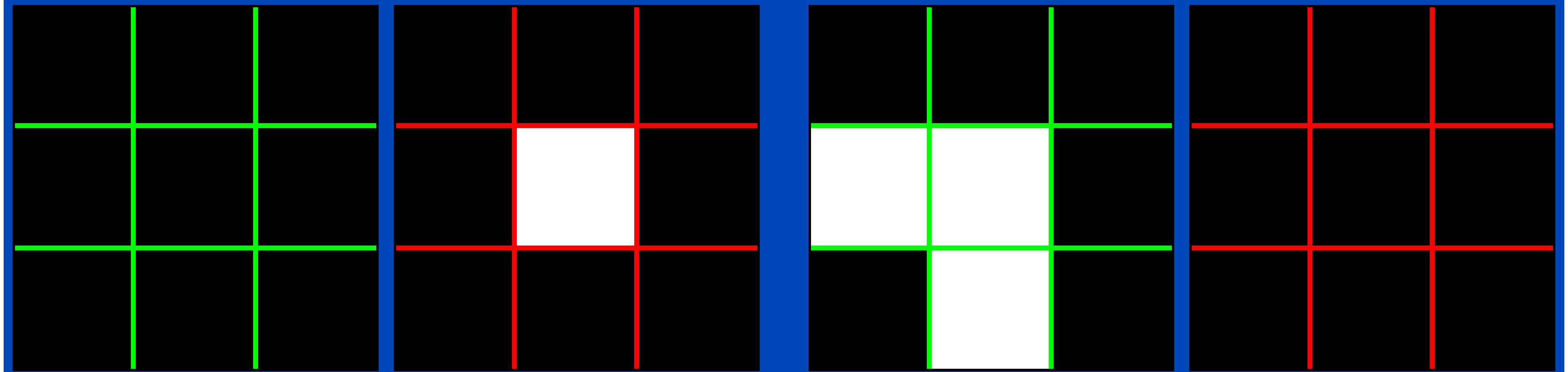

Example increment matrix set for a two energy bin system in an ideal (left) and a realistic case (right). It illustrates the detector response and the correct correlations resulting from a single photon incident off-center on the central pixel (black=0, white=1). The green and red lines separate the detector pixels only visually.

Increment Matrices

$$I_{b,n}(u,v)$$

n = number of event type
= number of increment matrix set

- 15 increment matrices for the low energy bin $b = 1$.
- More matrices can be generated by symmetry operations.
- At most four simultaneous counter increases are observed.

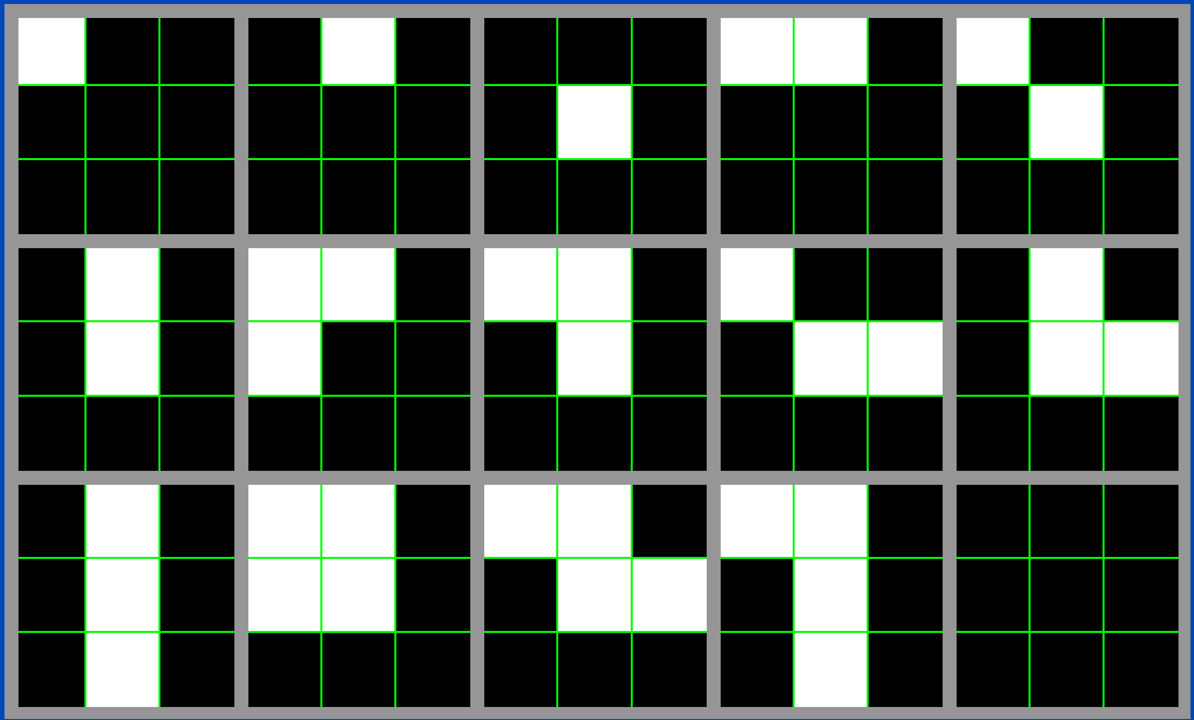

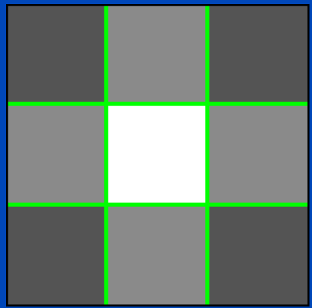

Average increment matrix of all occurring events. This kind of matrix is not able to correctly describe the resulting correlations since this would incorrectly correlate the whole 3×3 patch.

Photon Events – Increment Matrices

- Detection process in the sensor
- Photoelectric effect, e.g. 80 keV

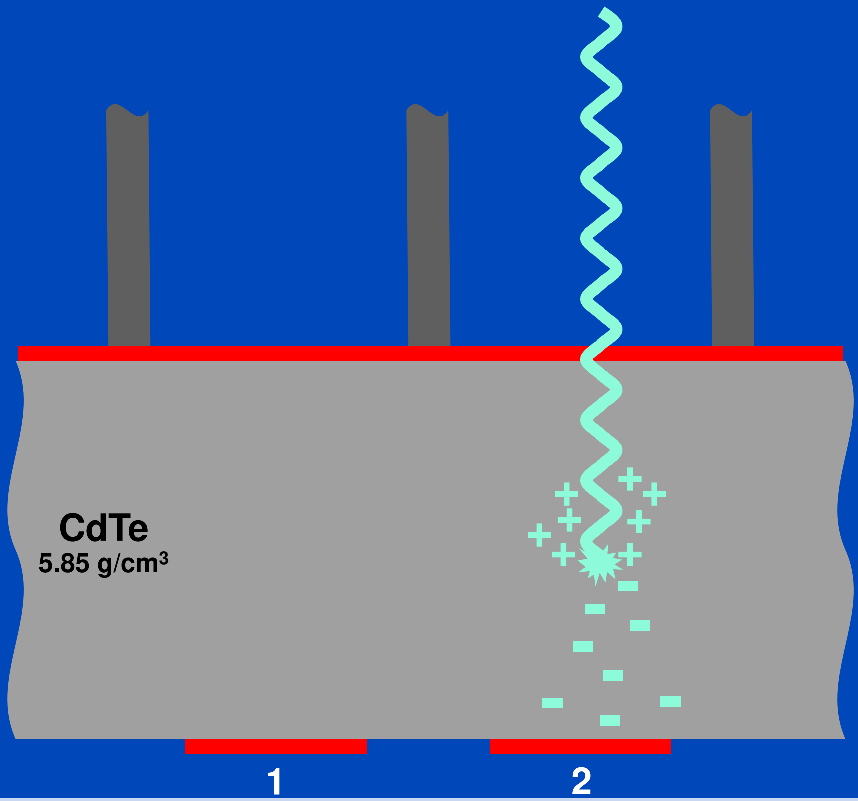

$$I_{4,n} = \begin{pmatrix} 0 & 0 & 0 \\ 0 & 0 & 0 \\ 0 & 0 & 0 \end{pmatrix}$$

$$I_{3,n} = \begin{pmatrix} 0 & 0 & 0 \\ 0 & 1 & 0 \\ 0 & 0 & 0 \end{pmatrix}$$

$$I_{2,n} = \begin{pmatrix} 0 & 0 & 0 \\ 0 & 0 & 0 \\ 0 & 0 & 0 \end{pmatrix}$$

$$I_{1,n} = \begin{pmatrix} 0 & 0 & 0 \\ 0 & 0 & 0 \\ 0 & 0 & 0 \end{pmatrix}$$

Increment matrix set for this event, say, $n = 1$

Photon Events – Increment Matrices

- Detection process in the sensor
- Compton scattering or K-fluorescence, e.g. 80 keV

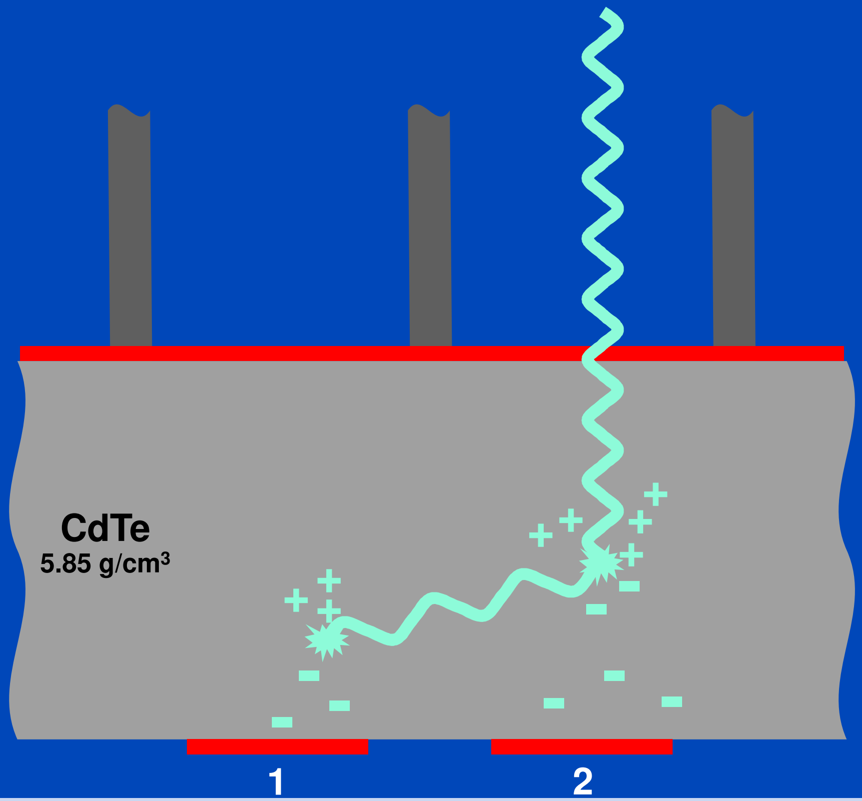

$$I_{4,n} = \begin{pmatrix} 0 & 0 & 0 \\ 0 & 0 & 0 \\ 0 & 0 & 0 \end{pmatrix}$$

$$I_{3,n} = \begin{pmatrix} 0 & 0 & 0 \\ 0 & 0 & 0 \\ 0 & 0 & 0 \end{pmatrix}$$

$$I_{2,n} = \begin{pmatrix} 0 & 0 & 0 \\ 0 & 1 & 0 \\ 0 & 0 & 0 \end{pmatrix}$$

$$I_{1,n} = \begin{pmatrix} 0 & 0 & 0 \\ 1 & 0 & 0 \\ 0 & 0 & 0 \end{pmatrix}$$

Increment matrix set for this event, say, $n = 2$

Photon Events – Increment Matrices

- Detection process in the sensor
- Photoelectric effect, low energy photon, e.g. 30 keV

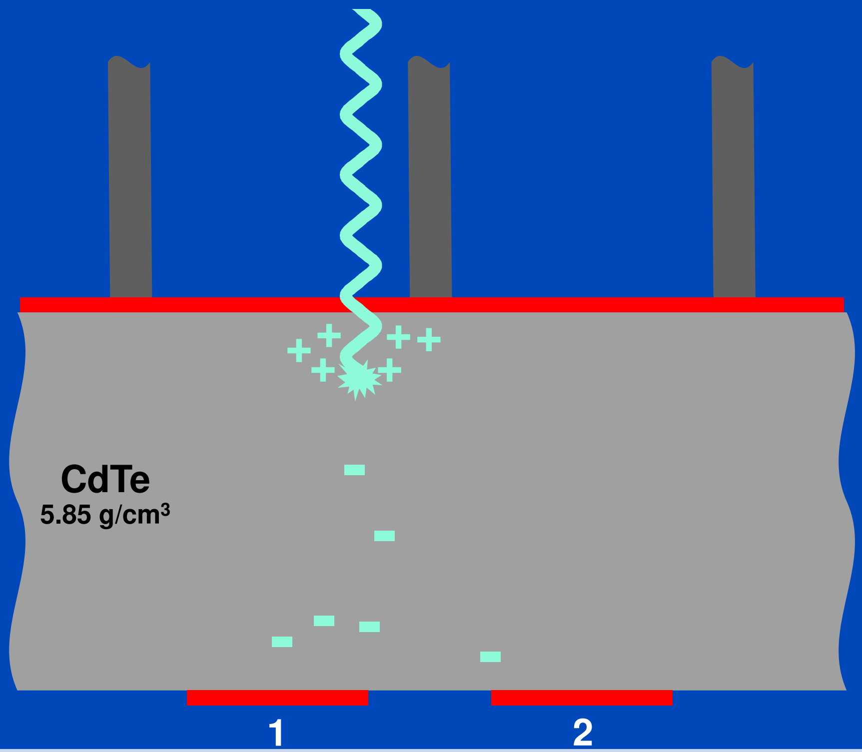

$$I_{4,n} = \begin{pmatrix} 0 & 0 & 0 \\ 0 & 0 & 0 \\ 0 & 0 & 0 \end{pmatrix}$$

$$I_{3,n} = \begin{pmatrix} 0 & 0 & 0 \\ 0 & 0 & 0 \\ 0 & 0 & 0 \end{pmatrix}$$

$$I_{2,n} = \begin{pmatrix} 0 & 0 & 0 \\ 0 & 0 & 0 \\ 0 & 0 & 0 \end{pmatrix}$$

$$I_{1,n} = \begin{pmatrix} 0 & 0 & 0 \\ 0 & 1 & 0 \\ 0 & 0 & 0 \end{pmatrix}$$

Increment matrix set for this event, say, $n = 3$

dkfz.

Noise Simulation

- **With the probability *P*(*n*, *E*) we can calculate photon numbers *N*(*n*, *u*, *v*) interacting via increment matrix set *n* with the detector:**

$$N(n,u,v) = \sum_E P(n,E)\eta(E)N(E,u,v)$$

- **Based on *N*(*n*, *u*, *v*) Poisson noise is generated. The resulting noisy photon numbers are marked with ~.**
- **The resulting detector signal for energy bin *b* is then given by the following convolution with the increment matrix sets:**

$$\tilde{S}_b(u,v) = \sum_n I_{b,n}(u,v) * \tilde{N}(n,u,v)$$

PC Detector Model

- Detector signal generation cascade

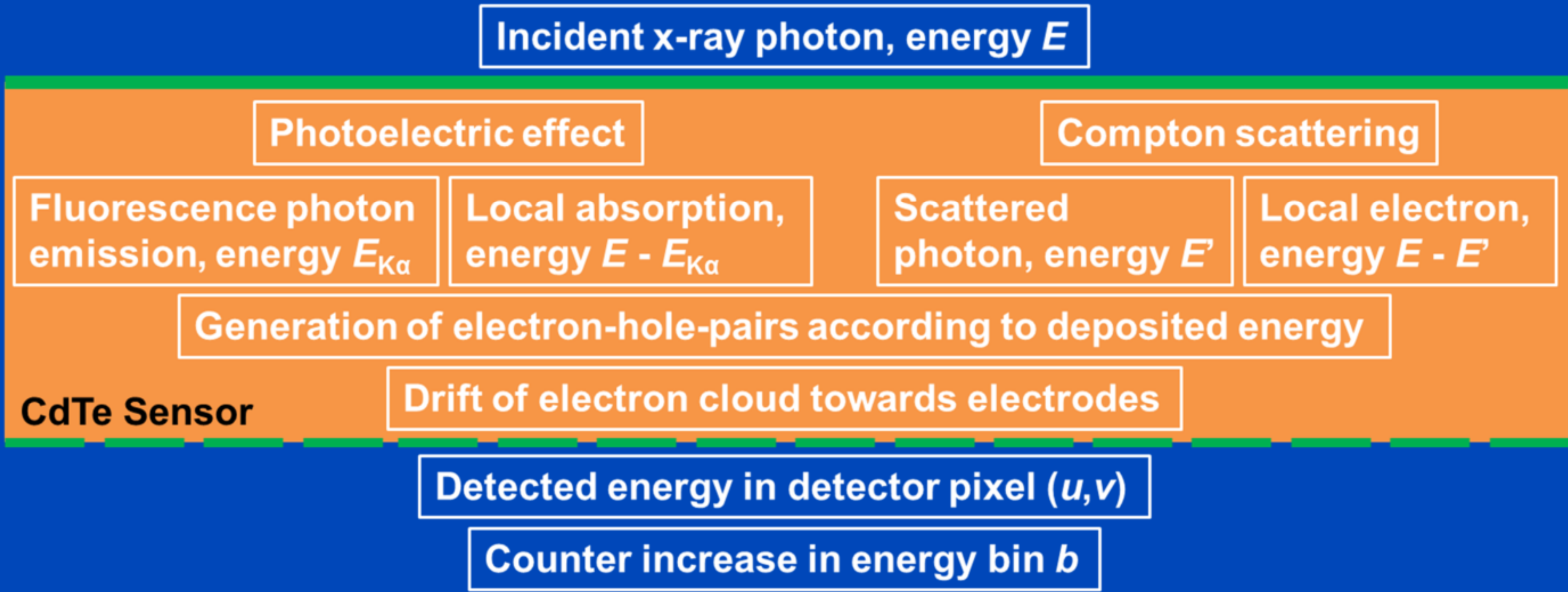

Event Probabilities

Absorption coefficient

$$\mu_{\mathrm{tot}}(E) = \mu_{\mathrm{PE}}(E) + \mu_{\mathrm{CS}}(E)$$

Detector absorption efficiency

$$\eta(E) = 1 - e^{-\mu_{\mathrm{tot}}(E) t_{\mathrm{Det}}}$$

Probability photoelectric effect

$$P_{\mathrm{PE}}(E) = \frac{\mu_{\mathrm{PE}}(E)}{\mu_{\mathrm{tot}}(E)}$$

Probability Compton scattering

$$P_{\mathrm{CS}}(E) = 1 - P_{\mathrm{PE}}(E)$$

$$E' = \frac{E}{1 + \frac{E}{m_e c^2}(1 - \cos(\phi))}$$

Probability K_α fluorescence

$$P^Z_{\mathrm{K}_\alpha}(E) = \omega^Z_{\mathrm{K}} f^Z_{\mathrm{K}} \Theta(E - E_{\mathrm{K}})$$

Probability K_α emission angle

$$P_\phi(\phi, E)\, d\phi = \mathrm{const}\, d\phi$$

Probability scattering angle

$$P_\phi(\phi, E)\, d\phi = \frac{1}{\sigma_e^{\mathrm{CS}}(E)} \times \left(\frac{r_e^2}{2}(1 + \cos^2\phi) F_{\mathrm{KN}}(\phi, E) \right) 2\pi \sin\phi\, d\phi$$

Sampling of the central detector pixel

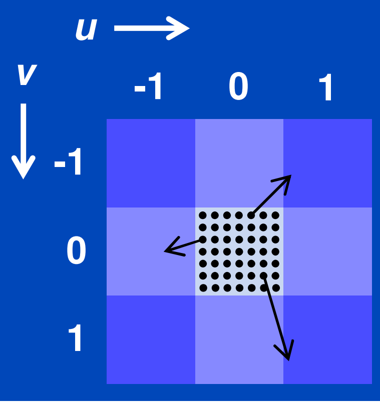

Spectral Response Functions

- Comparison with Yun *et al.*
- Thickness: 500 µm
- Pixel size: 100 µm
- 100 keV incident energy

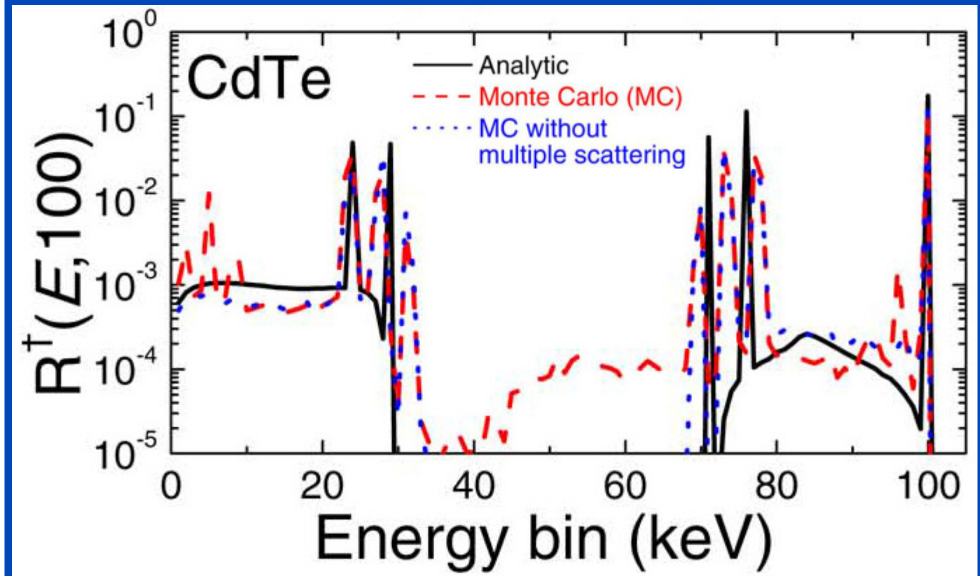

Spectral response:

$$R(E', E) = \frac{N(E')}{N(E)}$$

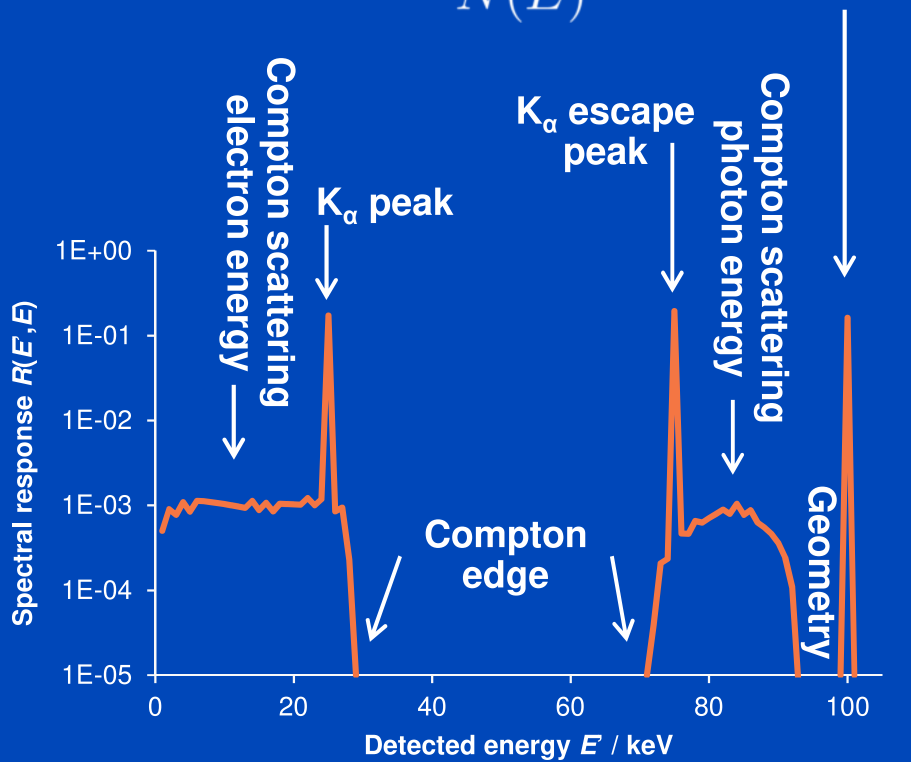

Yun, S., Kim, H. K., Youn, H., Tanguay, J., and Cunningham, I. A., "Analytic model of energy-absorption response functions in compound x-ray detector materials," IEEE TMI 32, 1819-1828 (2013).

Charge Cloud Drift

- **Comparing results from previous slides to measurements shows discrepancy**
  → Drift of charge cloud

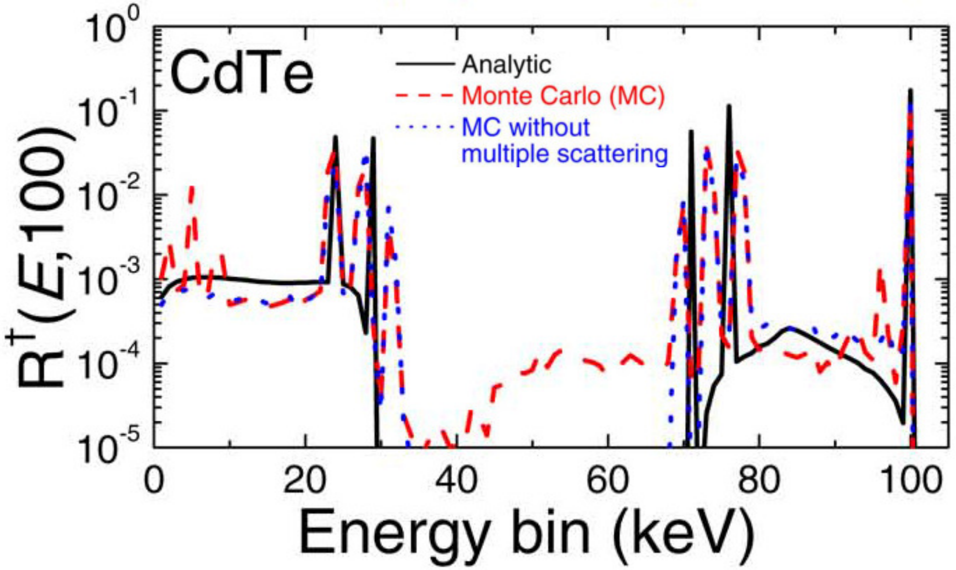

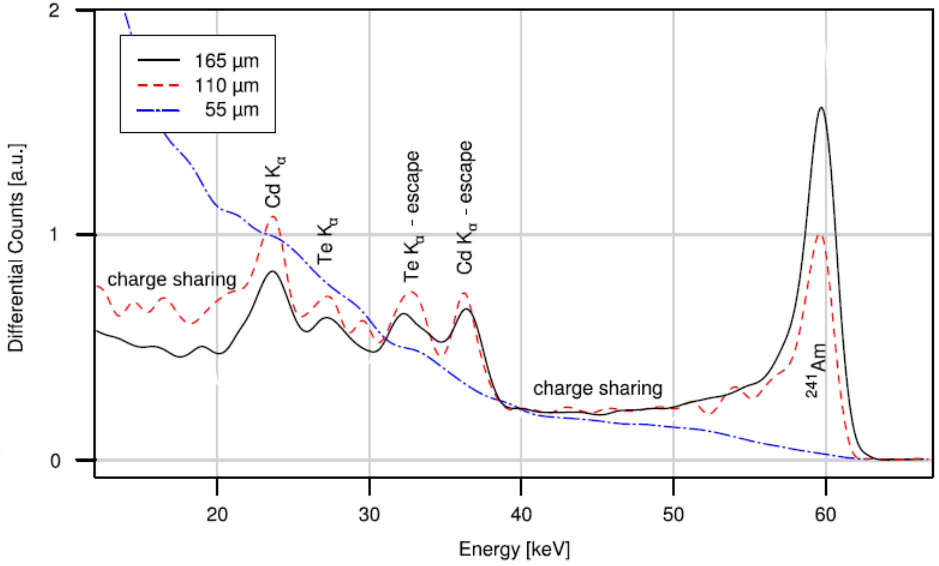

- **Compton scattering and fluorescence photons are not the only mechanisms leading to energy dispersion.**
- **Drifting charges seem to have a strong influence.**

Koenig, T., Schulze, J., Zuber, M., Rink, K., Butzer, J., Hamann, E., Cecilia, A., Zwerger, A., Fauler, A., Fiederle, M., and Oelfke, U., "Imaging properties of small-pixel spectroscopic x-ray detectors based on cadmium telluride sensors," PMB 57, 6743-6759 (2012).

dkfz.

Charge Cloud Drift

- **Influence of the charge cloud drift on the spectral response**

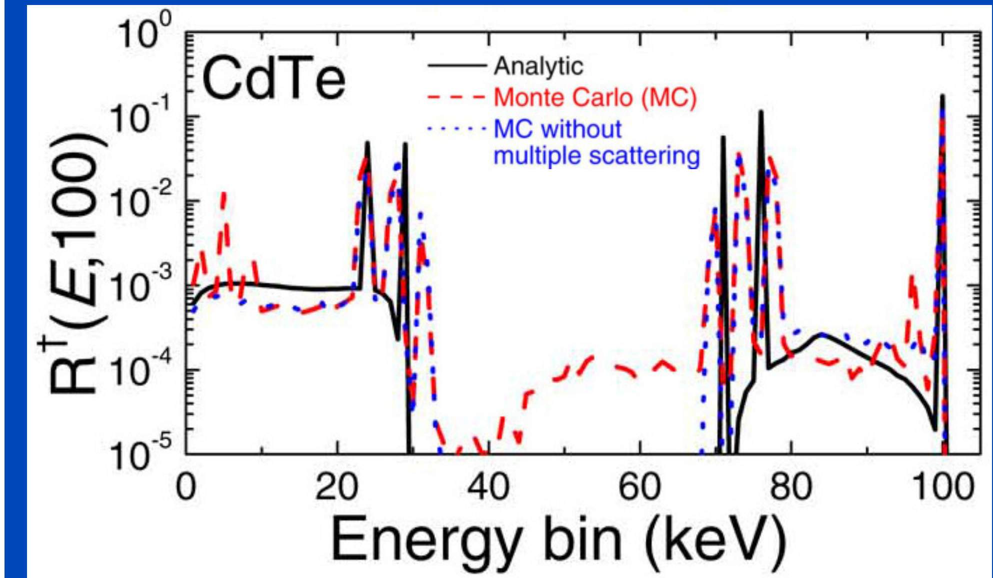

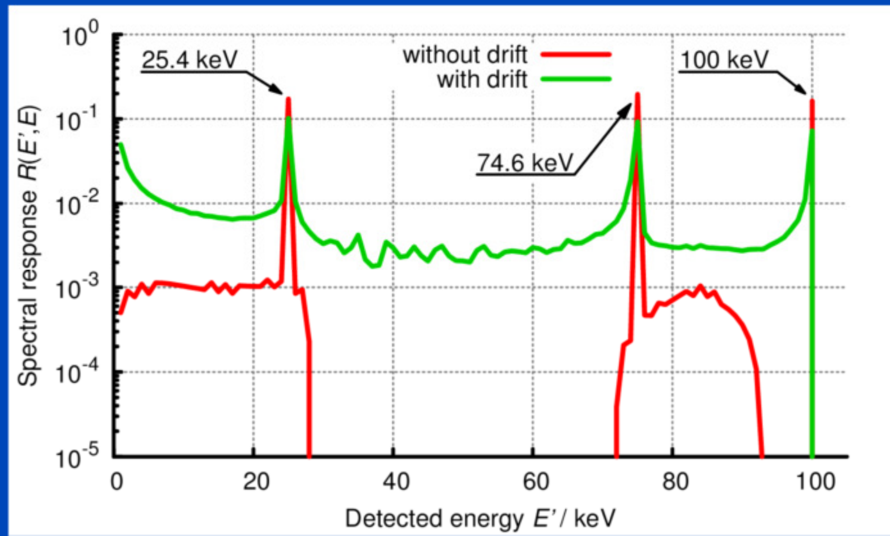

100 µm pixels, 0.5 mm CdTe, 500 V

Spectral response: $R(E', E) = \dfrac{N(E')}{N(E)}$

Yun, S., Kim, H. K., Youn, H., Tanguay, J., and Cunningham, I. A., "Analytic model of energy-absorption response functions in compound x-ray detector materials," IEEE TMI 32, 1819-1828 (2013).

Spectral Response

- **Comparison Koenig *et al*.**

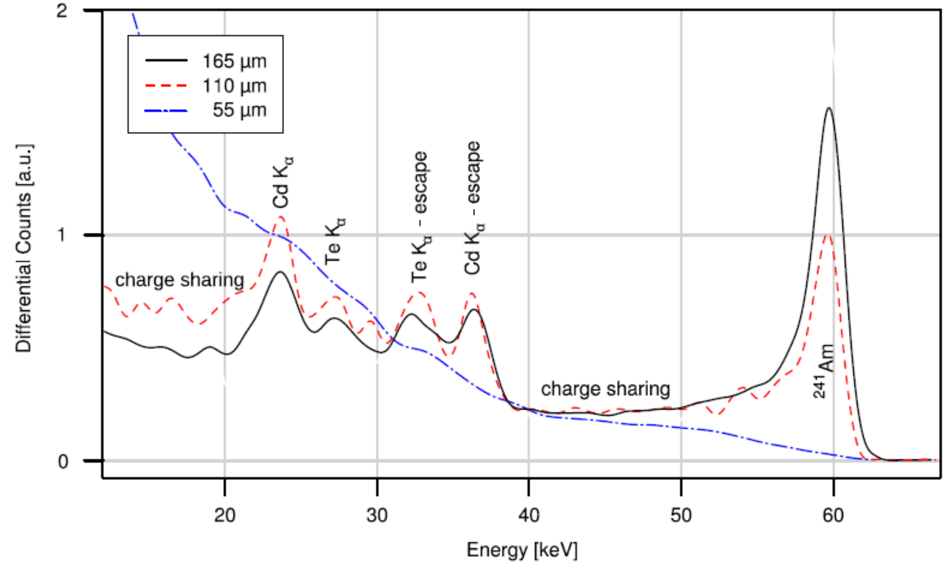

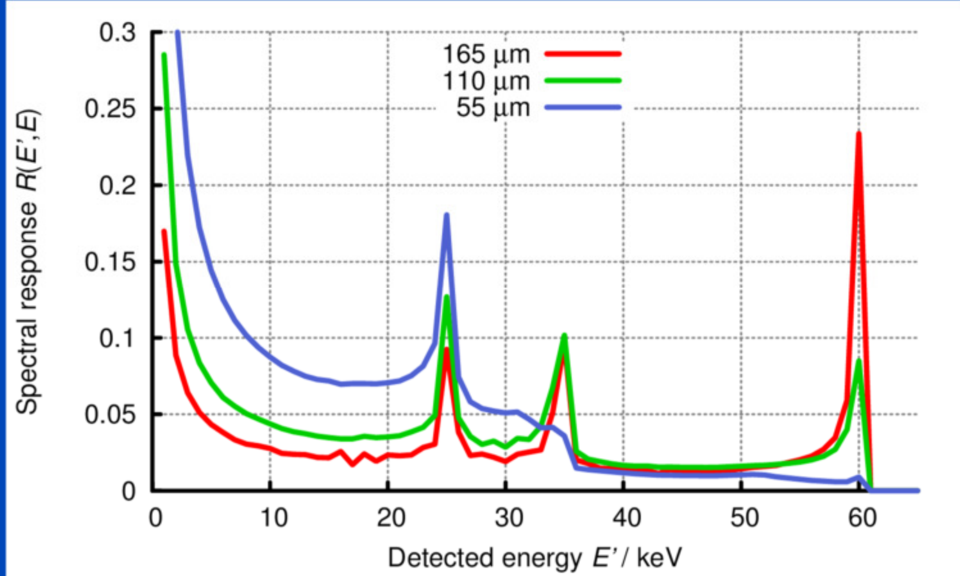

Different pixel sizes, 1 mm CdTe, 400 V

Spectral response: $R(E', E) = \dfrac{N(E')}{N(E)}$

Koenig, T., Schulze, J., Zuber, M., Rink, K., Butzer, J., Hamann, E., Cecilia, A., Zwerger, A., Fauler, A., Fiederle, M., and Oelfke, U., "Imaging properties of small-pixel spectroscopic x-ray detectors based on cadmium telluride sensors," PMB 57, 6743-6759 (2012).

Spectral Response

- **Comparison Schlomka *et al.***

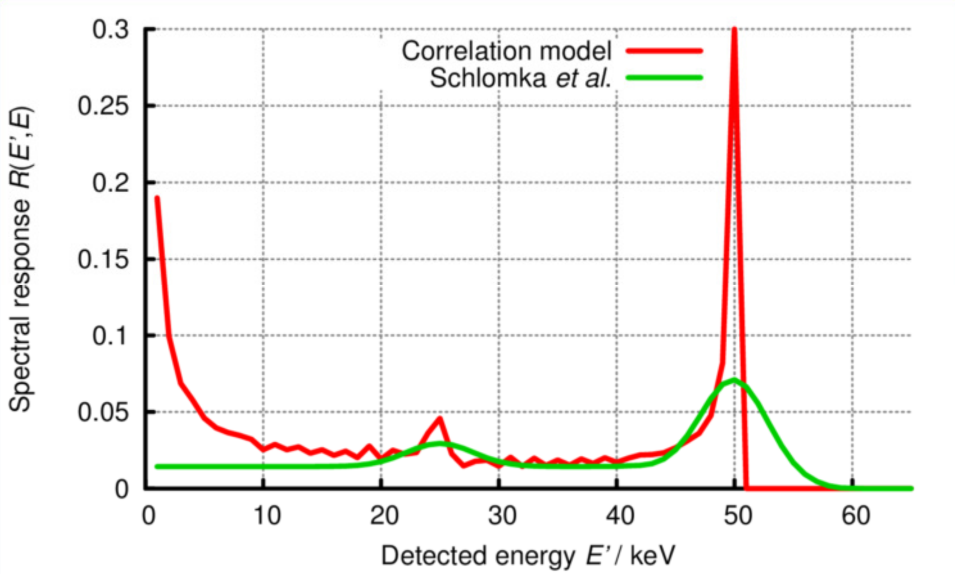

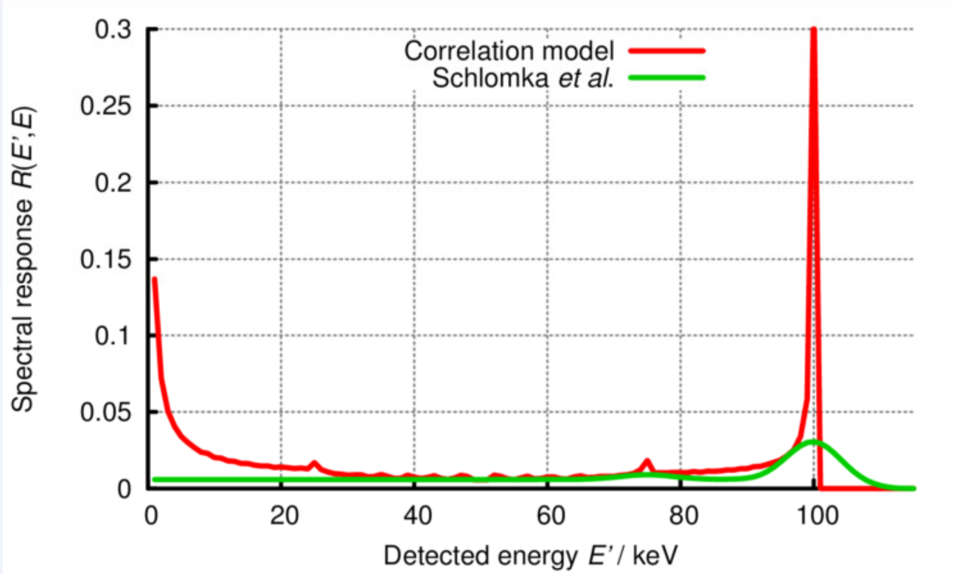

400 µm pixels, 3 mm CdTe, 500 V

Spectral response: $R(E',E) = \dfrac{N(E')}{N(E)}$

Schlomka, J. P., Roessl, E., Dorscheid, R., Dill, S., Martens, G., Istel, T., Bäumer, C., Herrmann, C., Steadman, R., Zeitler, G., Livne, A., and Proksa, R., "Experimental feasibility of multi-energy photon-counting K-edge imaging in pre-clinical computed tomography," PMB 53(15), 4031–4047 (2008).

dkfz.

Energy Bin Sensitivity

- **Energy bin sensitivity compared to Schlomka *et al.***

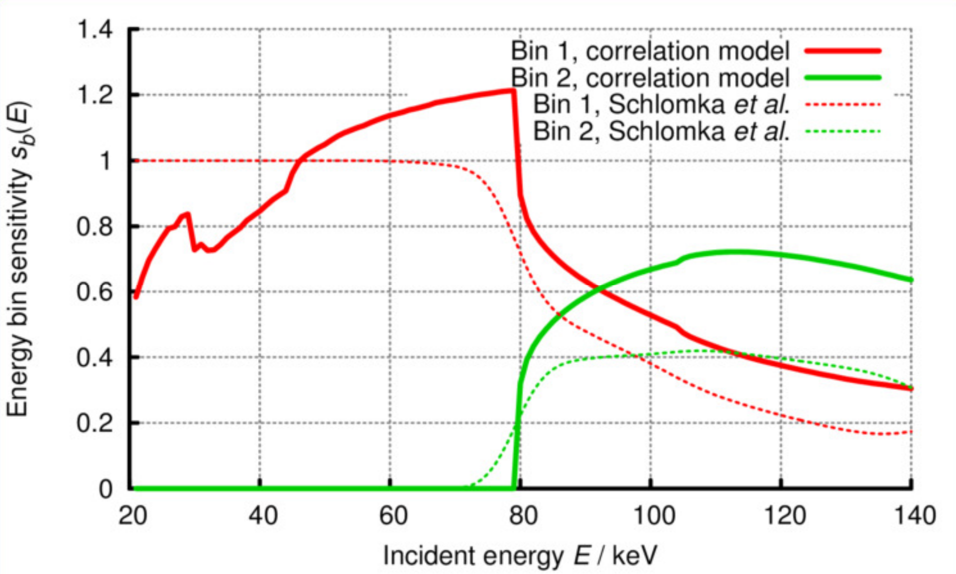

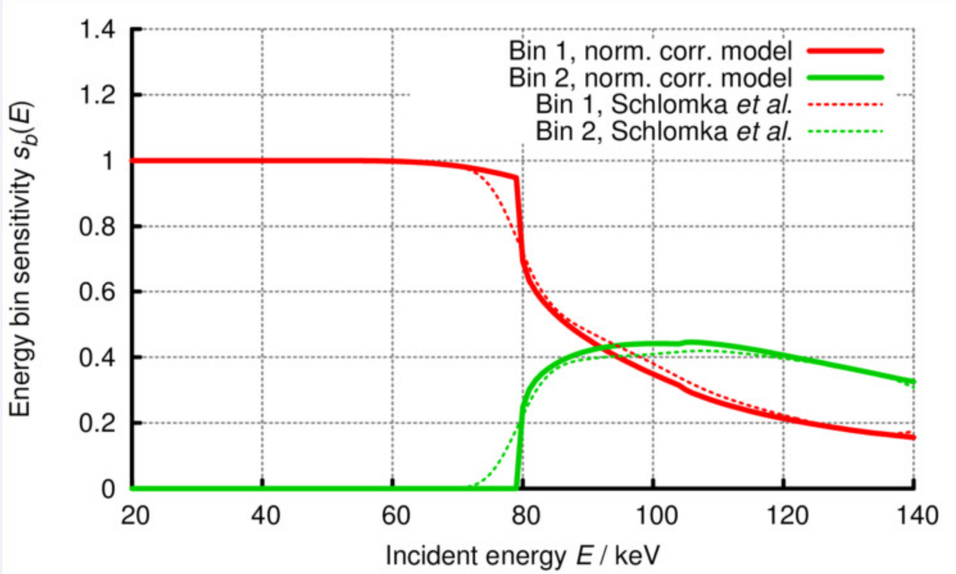

400 µm pixels, 3 mm CdTe, 500 V

Energy bin sensitivity: $s_b(E) = \int_{E_b}^{E_{b+1}} R(E', E)\, dE'$, with $E_{B+1} = \infty$

Covariance Matrix

- Covariance of reconstructed energy bin images measured over 50 independent noise realizations

Covariance matrix no correlations

	Bin 1	Bin 2
Bin 1	113.0%	0.1%
Bin 2	0.1%	268.8%

Covariance matrix correlations

	Bin 1	Bin 2
Bin 1	100.0%	-2.5%
Bin 2	-2.5%	268.3%

- The left matrix shows results for adding the noise to $S_b(u, v)$. The right matrix shows results for noise added to $N(n, u, v)$.

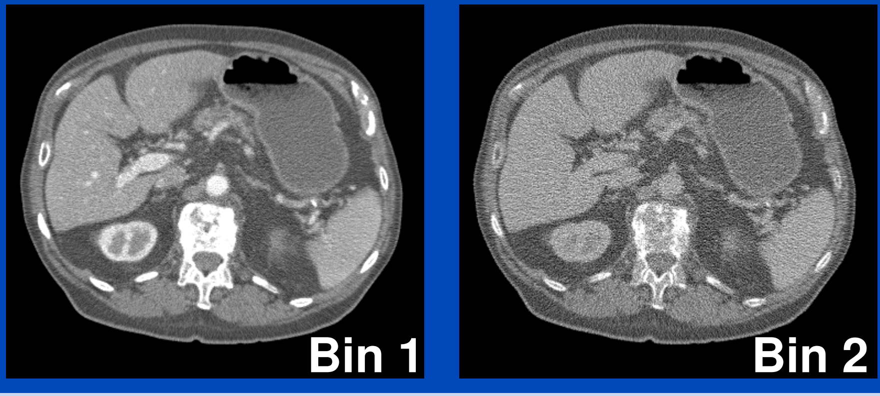

Thank You!

Parts of the reconstruction software were provided by RayConStruct® GmbH, Nürnberg, Germany.

This presentation will soon be available at www.dkfz.de/ct.

Job opportunities through DKFZ's international PhD or Postdoctoral Fellowship programs (marc.kachelriess@dkfz.de).